

## ABSTRACT

**Title of Document:** ROLE OF *Rv3167c* IN NECROSIS AND AUTOPHAGY INDUCTION BY AND IN VIRULENCE OF MYCOBACTERIUM TUBERCULOSIS

Lalitha Srinivasan, Doctor of Philosophy, 2015

**Directed by:** Dr. Volker Briken  
Associate Professor  
Cell Biology and Molecular Genetics

*Mycobacterium tuberculosis* (Mtb), an intracellular pathogen targeting lung phagocytes has been reported to manipulate apoptotic and necrotic host cell death. Mtb induces necrosis allowing for bacteria to escape from the host cell and infect naive cell populations. Mtb genes that influence host cell death responses as well as host cell pathways that are implicated in survival outcomes during mycobacterial infection represent interesting areas of investigation. In this study we identified the Mtb gene *Rv3167c* to be required for the inhibition of Mtb induced, caspase-independent necrotic cell death. The *Rv3167c* mutant strain ( $\Delta 3167c$ ) induced higher levels of necrosis in macrophages compared to Mtb or the complement strain. Using a combination of chemical inhibitors and bone marrow derived macrophages from different knock-out mice, we screened for host factors required for  $\Delta 3167c$  mediated cell death and were able

to eliminate involvement of known regulated necrosis pathways. Necrosis induction by  $\Delta 3167c$  was however found to be dependent on reactive oxygen species (ROS) generated by mitochondria and on inhibition of Akt activation. Apart from necrosis, *Rv3167c* was also found to be required for inhibition of host cell autophagy. Mitochondrial ROS, inhibition of Akt activation and upregulation of JNK activation were required for  $\Delta 3167c$ -induced autophagy. Recent studies on Mtb induced autophagy have shown that Mtb co-localizes with autophagosomes, leading to lysosomal mediated bacterial destruction. Surprisingly, we did not observe Mtb or  $\Delta 3167c$  co-localization with autophagosomes indicating Mtb has the ability to inhibit selective autophagy mediated killing. Deletion of *Rv3167c* results in an increase in Mtb virulence as demonstrated by the higher bacterial burden in the lungs and extra-pulmonary organs and the lower median survival time observed in  $\Delta 3167c$  infected mice compared to Mtb and complement strain infected control animals. In conclusion, this work indicates that Mtb utilizes *Rv3167c* to regulate necrosis and autophagy induction and to temper its own virulence.

ROLE OF *Rv3167c* IN NECROSIS AND AUTOPHAGY INDUCTION BY AND IN  
VIRULENCE OF MYCOBACTERIUM TUBERCULOSIS

By

Lalitha Srinivasan

Dissertation submitted to the Faculty of the Graduate School of the  
University of Maryland, College Park, in partial fulfillment  
of the requirements for the degree of  
Doctor of Philosophy  
2015

Advisory Committee:

Dr. Volker Briken, Ph.D., Chair

Dr. Kevin McIver, Ph.D.

Dr. Wenxia Song, Ph.D.

Dr. Xiaoping Zhu, D.V.M., Ph.D.

Dr. Philip DeShong, Sc.D., Dean's representative

© Copyright by

Lalitha Srinivasan

2015

## Dedication

I dedicate this dissertation to

My family

## Acknowledgements

First and foremost, I would like to thank my advisor Dr. Volker Briken for his guidance, support and encouragement throughout my graduate career. You have taught me to think critically, to think outside the box and to always keep the big picture in mind. Your enthusiasm for science helped me keep going even at the most bleak of times. I am also grateful to my committee members – Dr. Kevin McIver, Dr. Wenxia Song, Dr. Xiaopong Zhu and Dr. Phil DeShong for their feedback and comments on my work.

A big thank you to all my labmates for being a great sounding board for all my ideas, scientific and otherwise. Jeff, you have always asked me questions that have made me think and read more. Your easy attitude towards science and towards life in general is something that I hope to absorb more of. Plus, you have been a hoot with all your antics! Gaya, I will always miss our chats over coffee and our laughter sessions over silly things. You have been a great source of encouragement whenever I needed it. Swati, we have had a long journey in graduate school and have been through ups and downs together. Thank you for being a great support both inside and outside the lab. Sarah, you have boosted my morale many a time. Also, I have had a lot of fun pulling your leg. Thanks for being a good sport! Serdar, Amro - thank you for teaching me a lot of stuff when I first joined the lab and for introducing me to your native cuisines, never had better Turkish and Lebanese food anywhere else.

My friends and family has been an important part of this entire journey. Kanika, Divya – you lent an ear to all my vents and rants and gave me sage words of advice. Pubby, your layman questions about TB have helped me have a holistic perspective and to educate myself more. Amma, Appa and Chotu – thank you for always believing in me

and backing me in everything I did. Your confidence in me has always driven me to work hard and put in my best. Nitin – your love and support have been with me every step of the way, thank you for being there for me.

## TABLE OF CONTENTS

|  |      |
|--|------|
| Dedication .....   | ii   |
| Acknowledgements .....   | iii  |
| Table of contents .....  | v    |
| List of figures .....  | viii |
| List of tables .....   | x    |
| List of abbreviations .....  | xi   |
| <b>Chapter 1 Introduction</b>  |      |
| 1.1 Tuberculosis .....   | 1    |
| 1.1.1 Causative agent .....  | 1    |
| 1.1.2 Treatment and prevention .....   | 3    |
| 1.1.3 The disease and its progression .....  | 4    |
| 1.2 Innate immune response to Mtb .....  | 6    |
| 1.2.1 Pattern recognition receptors .....  | 6    |
| 1.2.2 Cytokines .....  | 8    |
| 1.3 Adaptive immune response to Mtb .....  | 9    |
| 1.4 Mtb mediated evasion of the immune response .....                                    | 10   |
| 1.5 Cell death – apoptosis and necrosis .....  | 12   |
| 1.5.1 Morphological and biochemical features of cell death – apoptosis vs necrosis ..... | 16   |
| 1.5.2 Signaling pathways leading to apoptosis .....                                      | 18   |
| 1.5.3 Regulated necrosis signaling pathways .....  | 20   |
| 1.5.4 Necrosis and Mtb pathogenesis .....  | 28   |
| 1.5.5 Mechanisms involved in Mtb induced necrotic cell death .....                       | 30   |
| 1.5.6 Mtb genes implicated in necrotic cell death induction .....                        | 33   |
| 1.6 Autophagy .....  | 35   |
| 1.6.1 Molecular machinery of macroautophagy .....  | 35   |
| 1.6.2 Molecular machinery of selective autophagy .....                                   | 39   |
| 1.6.3 Regulation of macroautophagy .....   | 40   |
| 1.6.4 Mtb and autophagy .....  | 43   |

|   |            |
|---|------------|
| 1.6.5 Mtb genes involved in autophagy modulation .....  | 46         |
| 1.6.6 Mechanisms involved in autophagy modulation by Mtb .....  | 47         |
| 1.7 Hypervirulence .....  | 51         |
| 1.7.1 Hypervirulence in Mtb .....   | 52         |
| 1.8 Summary .....   | 58         |
| <b>Chapter 2 <i>Rv3167c</i> is required for necrosis inhibition</b>                                     |            |
| <b>2.1 Introduction .....</b>   | <b>58</b>  |
| <b>2.2 Materials and Methods .....</b>  | <b>59</b>  |
| <b>2.3 Results and Discussion .....</b>   | <b>66</b>  |
| 2.3.1 Characterization of the <i>Rv3167c</i> mutant ( $\Delta 3167c$ ) .....                            | 66         |
| 2.3.2 $\Delta 3167c$ induces necrotic cell death .....  | 72         |
| 2.3.3 Molecular mechanisms of $\Delta 3167c$ induced necrosis .....                                     | 78         |
| 2.3.4 $\Delta 3167c$ induced necrosis is dependent on mitochondrial ROS .....                           | 92         |
| 2.3.5 Discussion .....  | 97         |
| <b>Chapter 3 <i>Rv3167c</i> is required for autophagy inhibition</b>                                    |            |
| <b>3.1 Introduction .....</b>   | <b>102</b> |
| <b>3.2 Materials and Methods .....</b>  | <b>103</b> |
| <b>3.3 Results and Discussion .....</b>   | <b>106</b> |
| 3.3.1 $\Delta 3167c$ induces autophagy .....  | 106        |
| 3.3.2 Molecular mechanisms of $\Delta 3167c$ induced autophagy .....                                    | 114        |
| 3.3.3 Crosstalk between $\Delta 3167c$ induced necrosis and autophagy .....                             | 120        |
| 3.3.4 Discussion .....  | 125        |
| <b>Chapter 4 <i>Rv3167c</i> manipulates Mtb virulence</b>   |            |
| <b>4.1 Introduction .....</b>   | <b>129</b> |
| <b>4.2 Materials and Methods .....</b>  | <b>130</b> |
| <b>4.3 Results and Discussion .....</b>   | <b>133</b> |
| 4.3.1 Higher bacterial burden is recovered from organs of $\Delta 3167c$ infected mice<br>.....         | 133        |
| 4.3.2 Increased cellular infiltration is observed in the lungs of $\Delta 3167c$ infected mice<br>..... | 135        |

|  |            |
|--|------------|
| 4.3.3 Increased levels of inflammatory cytokines and chemokines are detected in lung homogenates of $\Delta$ 3167c infected mice ..... | 137        |
| 4.3.4 $\Delta$ 3167c infected mice have lowered survival compared to those infected with Mtb .....                                     | 139        |
| 4.3.5 Discussion .....   | 141        |
| <b>Chapter 5 General Discussion and Significance .....</b>   | <b>142</b> |
| <b>APPENDIX A List of antibodies used in this study .....</b>  | <b>151</b> |
| <b>BIBLIOGRAPHY .....</b>  | <b>152</b> |

## LIST OF FIGURES

|  |       |
|--|-------|
| <b>Fig 1.</b> Possible outcomes of Mtb infection .....   | 5     |
| <b>Fig 2.</b> Integrated overview of regulated necrosis pathways .....   | 16    |
| <b>Fig 3.</b> Apoptotic signaling pathways .....   | 20    |
| <b>Fig 4.</b> Outcomes of RIPK1 and RIPK3 signaling .....  | 22    |
| <b>Fig 5.</b> Inflammasome mediated necrosis .....   | 25    |
| <b>Fig 6.</b> PARP1 & AIF mediated necrotic cell death .....   | 28    |
| <b>Fig 7.</b> Mechanisms of Mtb mediated necrosis induction .....  | 33    |
| <b>Fig 8.</b> Overview of non-selective and selective autophagy .....  | 36    |
| <b>Fig 9.</b> Molecular machinery of autophagy .....   | 38    |
| <b>Fig 10.</b> Regulation of macroautophagy .....  | 41    |
| <b>Fig 11.</b> Mechanisms involved in autophagy modulation by Mtb .....  | 50    |
| <b>Fig 12.</b> Deletion of <i>Rv3167c</i> does not affect <i>in vitro</i> growth of Mtb and Mtb uptake by macrophages .....        | 67    |
| <b>Fig 13.</b> $\Delta 3167c$ induces cell death in both cell lines and primary macrophages .....                                  | 69    |
| <b>Fig 14.</b> $\Delta 3167c$ strain replicates similar to Mtb <i>ex vivo</i> .....  | 71    |
| <b>Fig 15.</b> $\Delta 3167c$ infected cells lose plasma membrane integrity .....  | 73    |
| <b>Fig 16.</b> $\Delta 3167c$ induces non – apoptotic DNA fragmentation .....  | 75    |
| <b>Fig 17.</b> $\Delta 3167c$ induces caspase independent cell death .....   | 77    |
| <b>Fig 18.</b> $\Delta 3167c$ induced necrosis is independent of LXA <sub>4</sub> and PGE <sub>2</sub> .....                       | 80    |
| <b>Fig 19.</b> Cathepsin B, cathepsin D and lysosomal lipase activity is not required for $\Delta 3167c$ induced necrosis .....    | 82    |
| <b>Fig 20.</b> $\Delta 3167c$ induced necrosis is independent of RIPK1 and RIPK3 .....   | 84    |
| <b>Fig 21.</b> $\Delta 3167c$ induced necrosis is independent of PARP and AIF .....  | 86    |
| <b>Fig 22.</b> Necrosis induction by $\Delta 3167c$ is independent of inflammasomes .....  | 88    |
| <b>Fig 23.</b> Necrosis induction by $\Delta 3167c$ is independent of TNF, TLR and type I IFN signaling .....                      | 90-91 |
| <b>Fig 24.</b> $\Delta 3167c$ induces higher levels of cytosolic and mitochondrial ROS compared to Mtb and complement strain ..... | 94    |
| <b>Fig 25.</b> $\Delta 3167c$ induced necrosis is dependent on mitochondrial ROS .....   | 96    |

|  |     |
|--|-----|
| <b>Fig 26.</b> $\Delta 3167c$ induces autophagy .....  | 107 |
| <b>Fig 27.</b> $\Delta 3167c$ induces autophagy .....  | 108 |
| <b>Fig 28.</b> $\Delta 3167c$ does not mediate inhibition of autophagosome maturation .....                          | 111 |
| <b>Fig 29.</b> $\Delta 3167c$ mediated autophagy is independent of Eis .....   | 113 |
| <b>Fig 30.</b> Autophagy induction by $\Delta 3167c$ is dependent on JNK but not p38 MAPK activation .....           | 115 |
| <b>Fig 31.</b> Autophagy induction by $\Delta 3167c$ is independent of Beclin1 levels and Bcl2 phosphorylation ..... | 117 |
| <b>Fig 32.</b> Autophagy induction by $\Delta 3167c$ is dependent on inhibition of Akt activation .....              | 119 |
| <b>Fig 33.</b> Necrosis induction by $\Delta 3167c$ is dependent on Akt while autophagy induction requires ROS ..... | 121 |
| <b>Fig 34.</b> $\Delta 3167c$ induced autophagy does not result in necrosis .....                                    | 124 |
| <b>Fig 35.</b> Bacillary load in organs of C57Bl6 mice .....   | 134 |
| <b>Fig 36.</b> Appearance and histopathology of lungs harvested from infected mice .....                             | 136 |
| <b>Fig 37.</b> Lung homogenate cytokine analysis .....   | 138 |
| <b>Fig 38.</b> $\Delta 3167c$ infected mice have lower survival compared to Mtb .....                                | 140 |
| <b>Fig 39.</b> Model for <i>Rv3167c</i> dependent Mtb mediated necrosis and autophagy .....                          | 150 |

## LIST OF TABLES

|   |    |
|---|----|
| <b>Table 1.</b> Regulated cell death modes .....                      | 14 |
| <b>Table 2.</b> List of hypervirulent Mtb gene deletion mutants ..... | 56 |

## LIST OF ABBREVIATIONS

|                    |   |
|--------------------|---|
| 3-MA               | 3- methyladenine  |
| ABC                | ATP binding cassette  |
| AIF                | Apoptosis inducing factor   |
| AMPK               | Adenosine monophosphate activated protein kinase                                  |
| ASC                | Apoptosis associated speck like protein   |
| ATP                | Adenosine triphosphate  |
| BCG                | Bacille Calmette Guerin   |
| BMDM               | Bone marrow derived macrophage  |
| CaMKK              | Calcium/calmodulin dependent protein kinase kinase                                |
| CARD               | Caspase activation and recruitment domain   |
| CLR                | C-type lectin receptor  |
| CXCL1              | C-X-C motif ligand 1  |
| Cyt C              | Cytochrome C  |
| DC-SIGN            | Dendritic cell specific intracellular adhesion molecule 3 – grabbing non-integrin |
| DPI                | Diphenyleneiodonium   |
| DRAM1              | DNA damage regulated autophagy modulator  |
| Eis                | Enhanced intracellular survival   |
| FADD               | Fas associated death domain   |
| FAP                | Fibronectin attachment protein  |
| FIP200             | FAK family kinase-interacting protein of 200KDa                                   |
| GFP                | Green fluorescent protein   |
| HMGB1              | High mobility group protein B1  |
| Hpi                | Hours post infection  |
| HSP                | Heat shock protein  |
| HuMDM's            | Human monocyte derived macrophages  |
| IFN                | Interferon  |
| IL                 | Interleukin   |
| INH                | Isonizaid   |
| iNOS               | Inducible nitric oxide synthase   |
| JNK                | c-jun N terminal kinase   |
| <i>L.major</i>     | <i>Leishmania major</i>   |
| LAM                | Lipoarabinomannan   |
| LAMP               | Lysosome associated membrane protein  |
| LLO                | Listeriolysin O   |
| LTA4H              | Leukotriene A <sub>4</sub> hydrolase  |
| LXA <sub>4</sub>   | Lipoxin A <sub>4</sub>  |
| <i>M.fortuitum</i> | <i>Mycobacterium fortuitum</i>  |
| <i>M.marinum</i>   | <i>Mycobacterium marinum</i>  |
| <i>M.smegmatis</i> | <i>Mycobacterium smegmatis</i>  |
| ManLAM             | Mannosylated lipoarabinomannan  |
| MAPK               | Mitogen activated protein kinase  |
| <i>mce1</i>        | Mammalian cell entry 1  |
| MEF's              | Mouse embryonic fibroblasts   |

|                      |  |
|----------------------|--|
| MHC                  | Major histocompatibility complex               |
| MIC                  | Minimum inhibitory concentration               |
| MMR                  | Macrophage mannose receptor                    |
| MNNG                 | Methylnitronitrosoguanidine                    |
| MOI                  | Multiplicity of infection                      |
| MPTP                 | Mitochondrial permeability transition pore     |
| Mtb                  | <i>Mycobacterium tuberculosis</i>              |
| MTBC                 | <i>Mycobacterium tuberculosis</i> complex      |
| mTOR                 | Mammalian target of rapamycin                  |
| NBR1                 | Neighbor of BRCA1 gene 1                       |
| NDP52                | Nuclear dot protein 52KDa                      |
| Nec1                 | Necrostatin 1                                  |
| NLR                  | NOD like receptor                              |
| NOD                  | Nucleotide oligomerzation domain               |
| NOX2                 | NADPH oxidase 2                                |
| PAMP                 | Pathogen associated molecular protein          |
| PARP1                | Poly ADP ribose polymerase 1                   |
| PBMC                 | Peripheral blood monocytic cells               |
| PDIM                 | Pthiocerol dimycoserate                        |
| PE                   | Proline glutamatic acid                        |
| PE-PGRS              | PE-polymorphic guanine-cytosine-rich sequences |
| PGE <sub>2</sub>     | Prostaglandin E <sub>2</sub>                   |
| PGL                  | Phenolic glycolipid                            |
| PI                   | Propidium iodide                               |
| PI3K                 | Phosphatidyl inositol 3 kinase                 |
| PI3KR4               | Phosphoinositide 3-kinase regulatory subunit 4 |
| PI3P                 | Phosphatidyl inositol 3 phosphate              |
| PILAM                | Phosphatidylinositol capped lipoarabinomannan  |
| PIM                  | Phosphatidylinositol mannosides                |
| Pkn                  | Protein kinase                                 |
| PRR                  | Pattern recognition receptor                   |
| PTGES                | Prostaglandin E synthase                       |
| PZA                  | Pyrazinamide                                   |
| RIPK                 | Rest in peace kinase                           |
| RNI                  | Reactive nitrogen intermediates                |
| ROS                  | Reactive oxygen species                        |
| <i>S.flexneri</i>    | <i>Shigella flexneri</i>                       |
| <i>S.typhimurium</i> | <i>Salmonella typhimurium</i>                  |
| SCID                 | Severe combined immunodeficiency               |
| STPK                 | Serine threonine protein kinase                |
| <i>T.gondii</i>      | <i>Toxoplasma gondii</i>                       |
| TBK1                 | TANK binding kinase 1                          |
| TDM                  | Trehalose dimycolate                           |
| TEM                  | Transmission electron microscopy               |
| TLC                  | Thin layer chromatography                      |
| TLR                  | Toll like receptor                             |

|                          |                                       |
|--------------------------|---------------------------------------|
| TNF                      | Tumor necrosis factor                 |
| TNFR                     | Tumor necrosis factor receptor        |
| TRADD                    | TNF receptor associated death domain  |
| TRAF                     | TNF receptor associated factor        |
| TSC                      | Tuberous sclerosis complex            |
| ULK1                     | Unc-51-like-kinase1                   |
| <i>V.parahemolyticus</i> | <i>Vibrio parahemolyticus</i>         |
| VAMP8                    | Vesicle associated membrane protein 8 |
| VitD3                    | Vitamin D3                            |
| WHO                      | World Health Organization             |

## **CHAPTER 1 INTRODUCTION**

### **1.1 Tuberculosis**

Tuberculosis (TB) is an ancient disease – instances have been documented in ancient Chinese medical texts dating back to approximately 2700 B.C. (1). Studies using on archaeological remains further support the ancient association of TB with humanity, DNA from the *Mycobacterium tuberculosis* complex has been recovered from approximately 9000 year old neolithic remains (2). Also otherwise referred to as pthisis or the white plague, TB was the leading cause of death by an infectious agent throughout the 19<sup>th</sup> and the early 20<sup>th</sup> centuries in industrialized countries (3). Currently, most deaths on account of TB occur in low and middle-income countries where the disease is endemic. About one-third of the world's population is infected with Mtb and the World Health Organization (WHO) reported 9 million new cases and 1.5 million deaths in 2013 on account of TB (4). TB is second only to HIV in terms of mortality induced by an infectious disease.

#### **1.1.1 Causative agent**

Bacteria belonging to the genus *Mycobacterium* cause tuberculosis in humans and animals such as cattle and fish. The causative agent of human TB, *Mycobacterium tuberculosis* (Mtb), was discovered by Robert Koch in 1882 (5). Mtb belongs to a group of closely related members collectively referred to as the *Mycobacterium tuberculosis* complex (MTBC). Members of this complex include *Mycobacterium canetti* and *Mycobacterium africanum* that infect only humans and *Mycobacterium bovis* (*M.bovis*) that can infect both humans as well as cattle (6). *Mycobacterium marinum* (*M.marinum*) does not belong to the MTBC and causes a disseminated disease in its natural hosts

namely fish and frogs and a localized disease in the skin of immunocompetent human hosts (7). *M. marinum* infections in zebrafish have recently been used in several studies to model Mtb pathogenesis (8-11). *Mycobacterium avium* and *Mycobacterium kansasii* are facultative pathogens that cause infections in immunocompromised individuals (12). Mtb was thought to have arisen from a zoonotic transmission of *M. bovis* from cows to humans based on evidence that human tuberculosis was coincident with animal domestication around 10,000 years ago. However, more recent comparative genomic analysis studies indicate that Mtb arose approximately 70,000 years ago and co-evolved and dispersed along with humans (1).

Mycobacteria are characterized by the presence of a very complex, lipid rich cell wall comprising of an inner and an outer layer surrounding the plasma membrane. The inner layer contains peptidoglycan, arabinogalactan and mycolic acids covalently linked to one another. The outer layer includes lipid-linked polysaccharides – lipoarabinomannan (LAM), phthicerol dimycoserate (PDIM), dimycolyl trehalose, sulfolipids and phosphatidylinositol mannosides (PIM's). In virulent mycobacteria, LAM is capped by mannose residues (ManLAM) while in avirulent mycobacteria LAM is either uncapped or is capped with phosphatidylinositol (PILAM) (13,14). Due to their unique lipid rich cell wall architecture mycobacteria cannot be stained by Grams stain, a different staining procedure termed acid-fast staining or Ziehl-Neelsen's staining is used which is based on the ability of mycobacteria to retain carbol fuschin stain even in presence of decolorizing acid-alcohol (14).

### **1.1.2 Treatment and Prevention**

The first anti-mycobacterial drug, streptomycin was discovered by Selman Waksman during the Second World War (5). The current treatment regimen for TB was introduced in the 1970's and comprises of four first line drugs – isoniazid, rifampicin, pyrazinamide and ethambutol that need to be taken for six months. While isoniazid and ethambutol target the mycobacterial cell wall by inhibiting production of mycolic acid and arabinogalactan respectively, rifampicin and pyrazinamide target protein synthesis in the bacteria (15). The major issues with anti-TB therapy are the high toxicity of the drugs used and non-completion of the prolonged treatment regimen by patients leading to development of drug resistance (15,16). Multi-drug resistant Mtb (MDR-TB) refers to TB strains that are resistant to the first line drugs isoniazid and rifampicin. Patients infected with MDR-TB are treated with a combination of four second line drugs for at least eight months. Second line drugs against TB include aminoglycosides and fluoroquinolones. Extremely drug resistant TB strains (XDR TB) are defined by their resistance to isoniazid, pyrazinamide and to atleast two of the second line drugs (17). While third line drugs are available that can be used against XDR-TB, these drugs are expensive and associated with more side effects than both the first and second line treatments (15). More recently, totally drug resistant TB (TDR-TB) strains resistant to all available first and second line drugs have been reported in Iran and India (18). Given the rise of drug resistant strains of Mtb, efforts are on to discover new anti-TB drugs and four drugs are in Phase III clinical testing at present (15).

Currently, there is only vaccine in use against TB, the Bacille Calmette Guerin (BCG) vaccine. BCG is a live attenuated vaccine and was generated by Albert Calmette

and Camille Guerin in 1919 at the Pasteur Institute in France by the repeated subculturing of *M.bovis in vitro* (19). BCG is one of the most widely administered vaccines in the world (5). However, BCG is most useful in preventing TB only in young children, it fails to prevent TB in adults. The lower efficacy of the vaccine in adults has been attributed to the waning of the cellular immune response elicited by the vaccine along with age. As BCG is ineffective in individuals who have been previously exposed to mycobacteria for example environmental mycobacteria or by prior vaccination, booster doses cannot be administered to improve upon the waning immune response (17). With the emergence of HIV, another issue that has arisen is the increased risk of HIV positive children developing disseminated disease following BCG vaccination (5). Current efforts in research and development of new TB vaccines focus on two strategies – first to replace BCG with improved recombinant BCG or with attenuated Mtb strains and second to supplement BCG with subunit vaccines (5,17).

### **1.1.3 The disease and its progression**

Mtb is spread from one human host to another via the aerosol route. Following inhalation of infectious aerosol droplets, the pathogen gains access to the distal parts of the lung where it is taken up by phagocytes. The infectious dose has been estimated to be as low as a single bacterium (20). Alveolar macrophages were considered to be the predominant lung cell population initially infected by Mtb. However a recent study reported that monocyte derived macrophages and dendritic cells were also targeted by the bacteria in the murine lung (21). There are three possible outcomes following Mtb infection. First, the pathogen can be eliminated early on by the innate immune response and the exposed individuals exhibit no symptoms of infection nor do they develop an

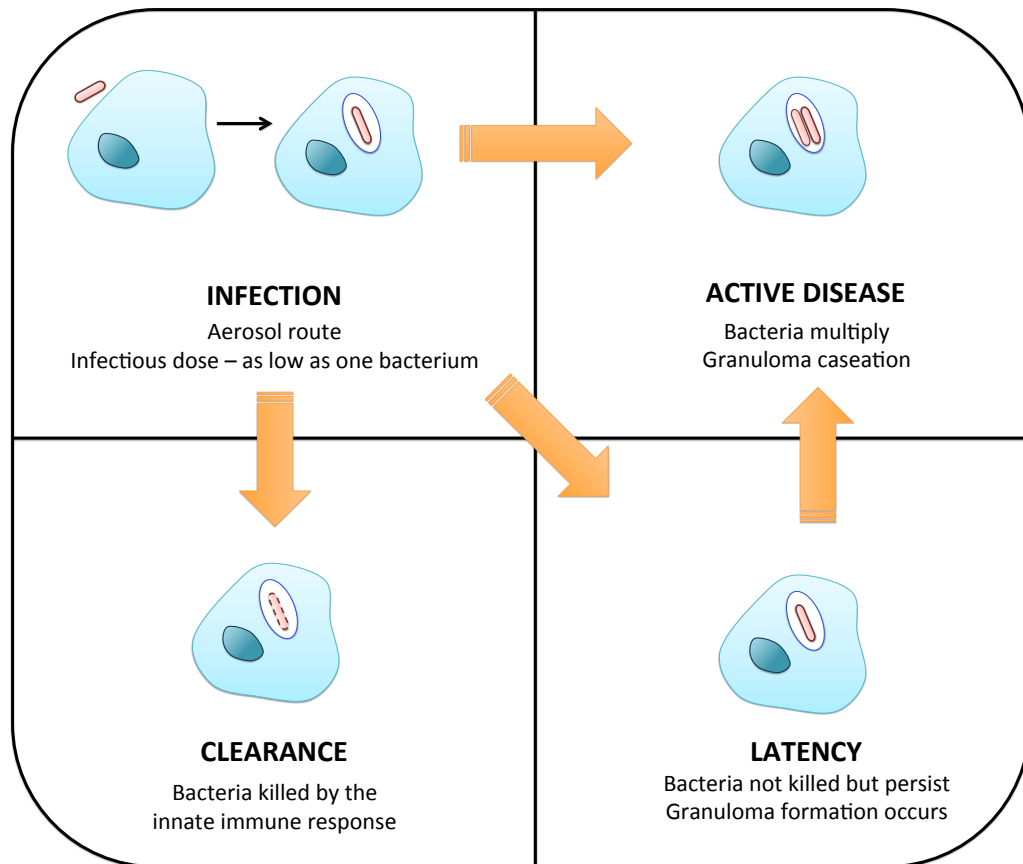


**Fig 1. Possible outcomes of Mtb infection**

Three possible outcomes may follow infection of the host by Mtb. In some cases, the innate immune response may successfully eliminate the pathogen leading to clearance of infection. More commonly, the bacteria multiply within the host cells leading to development of a localized inflammatory response, immune cell recruitment and eventually activation of the adaptive immune response. These events lead to formation of the granuloma comprising of infected macrophages at the centre, surrounded by foamy macrophages and other phagocytes and lymphocytes at the periphery. Bacteria located within the granuloma enter into a persistent state and a latent, asymptomatic infection develops. In about 5-10% of latently infected individuals disease reactivation occurs characterized by multiplication of bacteria located within the granuloma and tissue necrosis. Individuals with active disease are symptomatic and infectious. Under some conditions (eg: immunodeficiency), active disease may develop immediately after infection bypassing the latent stage.

Adapted from (17).

adaptive immune response. Second, a latent form of the disease develops in infected individuals when the innate immune response is unable to eliminate Mtb. Infected macrophages induce a localized inflammatory response that recruits immune cells to the site of infection and leads to the activation of the adaptive immune response. This results in formation of the granuloma, the signature feature of tuberculosis infection. The granuloma comprises of the central core of infected macrophages surrounded lipid rich foamy macrophages and other phagocytes. Lymphocytes are seen at the granuloma periphery and a fibrous cuff delineates the structure. Within the granuloma the bacteria enter a state of persistence. Latency is the most common outcome of the disease and affected individuals do not exhibit any overt symptoms nor do they shed bacteria. Third, in a small percentage of the infected population (about 5-10% of latently infected individuals), the disease is reactivated. In this state, bacteria located within the granuloma start multiplying and induce tissue necrosis leading to granuloma caseation. Individuals with active disease exhibit symptoms and are infectious. Development of the active disease is associated with conditions changing the immune status of the host – old age, malnutrition and HIV infection are some factors associated with development of active TB disease (Fig 1) (17,20,22,23).

## **1.2 Innate immune response to Mtb**

### **1.2.1 Pattern recognition receptors (PRR's)**

Toll like receptors (TLR's), C-type lectin receptors (CLR's) and NOD like receptors (NLR's) are involved in the recognition of Mtb. The Mtb ligands heat shock protein 65KDa (Hsp65), 19KDa lipoprotein and LAM are recognized by TLR2 present on macrophage surface. TLR2 mediated recognition of Mtb leads to the production of

pro-inflammatory cytokines such as tumor necrosis factor (TNF) and IL6. Additionally, TLR2 signaling is required for the generation of the cathelicidin LL-37 that has anti-mycobacterial activity (24). The intracellular TLR9 is involved in recognition of Mtb genomic DNA and contributes to TLR2 mediated responses (25). TLR2/TLR9 double knockout mice are more susceptible to Mtb infection compared to wild type mice. Mice deficient in the downstream signaling adaptor MyD88 exhibit an even higher susceptibility to Mtb infection compared to the TLR2/TLR9 double knockout mice (23). CLR's implicated in Mtb recognition include the macrophage mannose receptor (MMR) and the dendritic cell specific intracellular adhesion molecule 3 – grabbing non-integrin (DC-SIGN) which recognize ManLAM, Dectin-1 that recognizes lipoglycans and Mincle that recognizes trehalose dimycolate (TDM). While MMR, Dectin-1 and Mincle signaling contribute to pro-inflammatory cytokine production, DC-SIGN activation leads to synthesis of the anti-inflammatory cytokine IL10 (22),(25). The adaptor protein caspase recruitment domain containing protein 9 (CARD9) is involved in signaling events downstream of CLR's. CARD9 deficient mice are extremely susceptible to Mtb and succumb within four weeks of aerosol Mtb infection (26). The cytoplasmic PRR nucleotide oligomerization domain 2 (NOD2) recognizes the N-glycosylated muramyl dipeptide and is required for the optimal production of TNF, IL6 and IL12p40 (22). Production of active IL1 $\beta$  and IL18 requires cleavage of pro-forms of these cytokines by activated caspase 1. NLR's form part of complexes termed as inflammasomes assembled in response to detection of pathogen associated molecular patterns (PAMP's) and danger associated molecular patterns (DAMP's) that are needed for caspase 1 activation. IL1 $\beta$  production in response to Mtb infection requires the NLRP3 inflammasome (27).

However, mice deficient in NLRP3 do not exhibit increased susceptibility to Mtb compared to wild type mice. Rather, mice deficient in the adaptor protein ASC that is part of several NLR inflammasomes are highly susceptible to Mtb infection (23). The increased susceptibilities of mouse strains lacking adaptors compared to those lacking PRR's to Mtb infection indicates the co-operative and redundant roles these PRR's play in generating immune responses to the pathogen.

### **1.2.2 Cytokines**

Several cytokines are produced in response to Mtb infection and they play an important role both in the early and late stages of infection. The most important cytokines in Mtb control include TNF, IL12, IL1 $\beta$  and interferon  $\gamma$  (IFN $\gamma$ ). The role of TNF in controlling Mtb infections has been well documented in both animal models and humans. Compared to wild type mice, animals deficient in TNF exhibit increased mortality to Mtb infection (28). TNF is required for the recruitment of cells to the granuloma as mice and zebrafish deficient in TNF do not form granulomas in response to Mtb and *M.marinum* infection respectively (28,29). Therapeutic interventions targeted at TNF for treatment of rheumatoid arthritis was associated with increased susceptibility to Mtb (25). TNF mediated control of Mtb infection is also be associated with its ability to induce apoptosis (30). While requirement of TNF for Mtb control is well established, a recent study using zebrafish larval infections with *M.marinum* demonstrated that while excessive TNF production was successful at reducing bacterial burden, it was detrimental to the host due to the induction of uncontrolled necrotic cell death (9). IL12 p80 is required for the migration of infected dendritic cells to the lymphnodes to initiate the adaptive immune

response. IL12p70 production within the lymphnodes is required for the optimal induction of IFN $\gamma$  production (31).

Both macrophages and dendritic cells produce IL1 $\beta$  in response to Mtb infection (32,33). Both *Il1r1*<sup>-/-</sup> and *IL1 $\beta$* <sup>-/-</sup> mice are extremely susceptible to Mtb and die within 40 days of infection compared to infected wild type controls that survive for more than a year (34). The exact mechanism by which IL1 $\beta$  exerts a strong anti-mycobacterial effect is still not clear. IL1 $\beta$  has been shown to potentiate TNF mediated apoptotic cell death (35). Lungs from Mtb infected *Il1r1*<sup>-/-</sup> mice exhibit profound necrosis compared to organs obtained from wild type controls (31). These two studies point to a role for IL1 $\beta$  in modulating host cell death following Mtb infection. Susceptibility of *Il1r1*<sup>-/-</sup> mice to Mtb infection can also be attributed to IL1 $\alpha$ , indeed IL1 $\alpha$  deficient mice also exhibit severe susceptibility to Mtb (34). Role of IFN $\gamma$  is described in more detail in section 1.3.

### **1.3 Adaptive immune response to Mtb**

The adaptive immune response against Mtb is driven mainly by T-lymphocytes. Both CD4<sup>+</sup> helper T cells and CD8<sup>+</sup> cytotoxic T cells are involved in the control of Mtb infection, deficiency of either of the cell types results in an increased mortality of infected mice (22,23). CD8<sup>+</sup> T cell deficient mice succumb earlier than the wild type controls but later than the CD4<sup>+</sup> T cell deficient mice in response to Mtb infection (36). Studies reveal that the rate of progression of TB disease from latent to active state increases by 5 to 10 fold following HIV infection (23). The cytokine response elicited by Mtb shapes the adaptive immune response against the pathogen. Following antigen presentation in association with Class II MHC molecules, CD4<sup>+</sup> T cells can acquire a Th1 or a Th2 phenotype. IL12p70 produced by the innate immune cells during Mtb

infection drives the development of a Th1 response (31). Both CD4<sup>+</sup> and CD8<sup>+</sup> cells migrate to the lungs and produce the cytokine IFN $\gamma$ . IFN $\gamma$  activates the infected macrophages leading to increased killing of phagocytosed mycobacteria. This is achieved by upregulating expression of the enzyme inducible nitric oxide synthase (iNOS) and increasing generation of reactive nitrogen intermediates (RNI) in the infected macrophages. IFN $\gamma$  can also route endosomal compartments containing mycobacteria to fuse with lysosomes by inducing autophagy in infected cells. Antigen presentation by infected cells is also enhanced following exposure to IFN $\gamma$  as it upregulates expression of MHC genes (20,22,23,37). CD8<sup>+</sup> T cells may also exert direct cytotoxic effects on infected macrophages (36).

#### **1.4 Mtb mediated evasion of the immune response**

Mtb has several ways by which it can inhibit host immune responses. A recent study has shown that following inhalation via aerosol droplets, Mtb utilizes PDIM present in its cell wall to avoid phagocytic uptake in the upper airways of the lung. Using co-infection models of *M.marinum* together with the *S.aureus* and *P.aeruginosa*, this work demonstrated that the presence of commensals and environmental microbes in the upper airways leads to the recruitment of microbicidal macrophages with increased iNOS activity, avoiding these macrophages is beneficial to mycobacteria. In contrast, more permissive macrophages are recruited actively by mycobacteria in the distal regions of the lungs using a different surface lipid, phenolic glycolipid (PGL) (8). Following uptake by phagocytic cells, Mtb resides in a compartment that resembles the early endosome. Mtb mediated phagosomal arrest is dependent on inhibition of Rab7 recruitment and phosphatidyl inositol 3 phosphate (PI3P) generation. The secreted Mtb effectors PtpA

and Ndk prevent Rab7 activation and convert active GTP bound Rab7 to its inactive GDP bound form respectively. ManLAM present on Mtb surface prevents generation of PI3P while another effector SapM is required for PI3P degradation (22,23,38). Recruitment of the host protein coronin 1 to live Mtb containing phagosomes is also implicated in inhibition of phagosome fusion with lysosomes (39). Other bacterial factors such as PknG and zmp1 are also involved in preventing phagosome-lysosome fusion via unknown mechanisms (38). Mtb also inhibits acidification of the compartment that it is present in by preventing recruitment of the proton ATPase and mycobacterial PtpA is involved in this process as well. While classical literature supported the view that Mtb remained within the modified early endosome like compartment at all times, more recently reports have emerged demonstrating that Mtb eventually escapes from the phagosome to the cytosol (40). Cytosolic translocation has been found to depend on the Mtb protein EsxA secreted via the type VII secretion system ESX1 (41-43).

During phagocytosis of Mtb, the NADPH oxidase complex 2 (NOX2) is assembled on the phagosomal membrane and it generates reactive oxygen species (ROS) within the phagosomal compartment by transferring electrons from NADPH to molecular oxygen (44). Mtb produces antioxidants such as superoxide dismutases SodA and SodC and the catalase KatG that help neutralize phagosomal ROS. The Mtb gene *nuoG* encodes for a type I NADH dehydrogenase that inhibits NOX2 derived ROS production in infected cells by uncharacterized mechanisms (45). ROS may exert direct microbicidal effects and are required for TNF mediated apoptotic cell death of Mtb infected macrophages (45). ROS are also required for the generation of inflammatory responses downstream to TLR2 recognition of Mtb (24,46). Thus by controlling ROS generation,

Mtb inhibits apoptotic cell death and regulates TLR2 driven cytokine production. Another example of Mtb mediated control of cytokine generation is in the case of IL1 $\beta$ . Mtb mediates NLRP3 inflammasome dependent IL1 $\beta$  production but at the same time also inhibits IL1 $\beta$  production by the AIM2 inflammasome (47). Type I IFN's elicited by Mtb also dampen IL1 $\beta$  production (48). While Mtb mediated TNF production of infected macrophages, the secreted TNF was less bioactive as Mtb also mediated an IL10 dependent release of TNF receptor 2 (TNFR2) which bound to and neutralized TNF (30).

Elimination of infected host cells by apoptosis is yet another innate immune mechanism that Mtb interferes with. Mtb inhibits cell death via apoptosis to avoid both direct bactericidal effects of the process and via uptake of dying cells by neighboring phagocytes. Additionally, uptake of Mtb antigens via phagocytosis of apoptotic bodies by dendritic cells allowed for the presentation of extracellular antigens to CD8<sup>+</sup> T cells, a process termed cross-presentation that led to a more robust CD8<sup>+</sup> T cell response (49). While it inhibits apoptosis, Mtb induces cell death via necrosis. A more detailed description of Mtb mediated necrosis – genes and mechanisms involved and the consequences of the phenomenon are described in Section 1.5. Autophagy is an innate immune mechanism that exerts direct mycobactericidal effects as well controls the host inflammatory response. Mtb mediated modulation of autophagy has been discussed in Section 1.6.

### **1.5 Cell death – Apoptosis and Necrosis**

The earliest classification of cell death was based on morphology and three types of cell death were identified – type I, type II and type III which today are referred to as apoptosis, autophagy associated cell death and necrosis respectively (50,51). Historically,

apoptosis was considered to be the only regulated cell death mechanism while necrosis was thought to be an accidental form of cell death. However, the discovery that TNF can induce either apoptotic or necrotic cell death in different cell types raised doubts on necrosis being an unregulated process (50). The most recent classification of cell death modalities proposed by the Nomenclature Committee on Cell Death (NCCD) is based on biochemical parameters and five categories of cell death are recognized – extrinsic apoptosis, intrinsic apoptosis, regulated necrosis, autophagic cell death and mitotic catastrophe (Table 1) (52).

Regulated necrosis is defined as a genetically controlled cell death form that results in loss of cellular integrity and release of cytoplasmic contents (51,52). Recent research has unveiled several examples of necrosis occurring in a controlled, regulated fashion in response to death receptors, immune receptors, physico-chemical insults and bacterial and viral pathogens (50,53). These triggers initiate specific signaling modules that via different mediators lead to activation of executioner mechanisms and cell demise (Fig 2) (50,52). As the study of regulated necrosis has evolved, different names have been used to refer to specific forms of cell death (necroptosis – RIPK1 and RIPK3 mediated cell death, pyroptosis – inflammasome mediated cell death, parthanatos – PARP1 mediated cell death), the usage of general terms that describe functional connotations has been recommended by the NCCD.

| Alternate names                   |              | Caspase requirement | Biochemical features   |
|-----------------------------------|--------------|---------------------|--|
| Extrinsic apoptosis               |              | +                   | Death receptor signaling, activation of caspases 3,6,7,8   |
| Intrinsic apoptosis               |              | +                   | MOMP, activation of caspase 3,6,7,9  |
| Autophagic cell death             |              | -                   | Accompanies autophagy, LC3 lipidation  |
| Mitotic catastrophe               |              | -                   | Mitotic arrest, caspase 2 activation in some cases   |
| <b>Regulated necrosis</b>         |              |                     |  |
| RIPK1 and RIPK3 dependent         | Necroptosis  | -                   | RIPK1 & RIPK3 phosphorylation and activation.  |
| Inflammasome dependent cell death | Pyroptosis   | +                   | Caspase 1 activation, accompanied by IL1 $\beta$ and IL18 secretion  |
| Inflammasome dependent cell death | Pyronecrosis | -                   | Dependent on cathepsin activity and activation of inflammasomes but independent of caspase 1 activity, accompanied by IL1 $\beta$ and IL18 secretion                                     |
| PARP1 dependent cell death        | Parthanatos  | -                   | PARP1 activation, PAR generation, Translocation of mitochondrial AIF to nucleus  |
| NETosis                           |              | -                   | NADPH oxidase activation, release of extracellular traps composed of histones and chromatin  |
| Ferroptosis                       |              | -                   | Reported to occur in tumor cells via inhibition of Cys/Glu antiporter, dependent on decreasing concentration of glutathione and ROS generated by Fenton reactions occurring in lysosomes |
| Oxytosis                          |              | -                   | Reported to occur in neurons via inhibition of Cys/Glu antiporter, dependent on glutathione and mitochondrial ROS  |
| CypD dependent                    | necrosis     | -                   | Dependent on CypD mediated opening of MPTP, loss of mitochondrial membrane potential   |
| Entosis                           |              | -                   | RHO and ROCK activation  |

**Table 1. Regulated cell death modes**

Adapted from (51,52).

Abbreviations: MOMP- mitochondrial outer membrane permeabilization; RIPK – rest in peace kinase; PARP1 – poly ADP ribose polymerase 1; PAR – poly ADP ribose; AIF – apoptosis inducing factor; CypD – cyclophilin D; MPTP – mitochondrial permeability transition pore; ROCK1 – RHO associated coiled coiled containing protein kinase

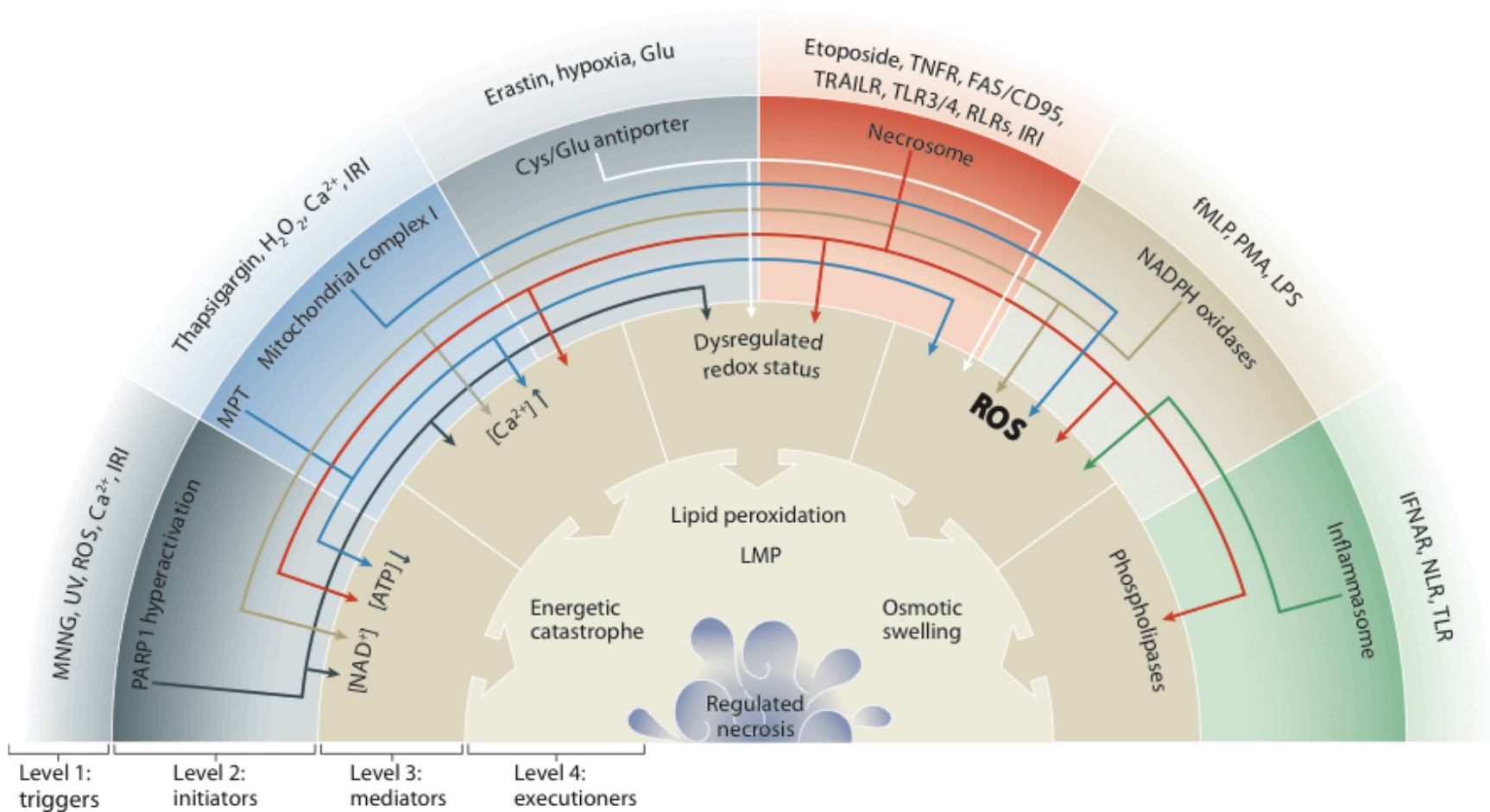


**Fig 2. Integrated overview of regulated necrosis pathways**

Various stimuli initiate specific signaling modules that via different mediators activate executioner mechanisms. These regulated signaling pathways lead to cell death with characteristic necrotic features.

Adapted from (51).

### **1.5.1 Morphological and biochemical features of cell death – apoptosis vs necrosis**

While apoptotic cells have been associated with distinct morphological features, necrosis is identified by the absence of these features. Nuclei of apoptotic cells undergo condensation and fragmentation. During apoptosis, genomic DNA is fragmented between nucleosomes to generate fragments that are multiples of 180-200 base pairs in size (54). Apoptotic cells shrink and plasma membrane blebbing is observed, however plasma membrane integrity is not affected. Apoptotic bodies enclosing the contents of the dying cell are released that are engulfed by neighboring phagocytes. Apoptosis is considered to be immunologically silent, as cellular contents are not spilled into the extracellular milieu (55,56). In contrast to apoptotic cells, nuclei of necrotic cells remain mostly unchanged. Transmission electron microscopy (TEM) studies show minor chromatin condensation to small irregular patches in necrotic cells while in case of apoptotic cells complete condensation to crescent shaped forms is observed. Plasma membrane integrity of necrotic cells is compromised and intracellular contents are released from the dying cell (55,56).

The characteristic morphological features of apoptosis are dependent on the activity of cysteinyl aspartate-specific proteases (caspases). Caspases target several proteins downstream of their activation leading to the characteristic features of apoptosis. For instance, caspases cleave and inactivate the inhibitor of caspase activated DNase (iCAD). This in turn leads to CAD activation and fragmentation of genomic DNA into oligonucleosomal fragments characteristic of apoptotic cells (54). Another characteristic biochemical feature of apoptosis is the exposure of phosphatidyl serine (PS) normally present in the inner leaflet of the plasma membrane on the dying cell surface. Necrosis

induction is independent of caspase activation and PS is not detected on surface of necrotic cells (56).

Distinguishing apoptosis from necrosis based on morphological and biochemical features is challenging. Apoptotic cells if not phagocytosed go on to acquire features of necrotic cells, an event termed as secondary necrosis (56,57). Cells undergoing secondary necrosis have permeabilized plasma membranes and could be mistaken for primary necrotic cells. A study comparing kinetics of subcellular events in cells dying by primary necrosis and secondary necrosis, showed similar sequence of lysosomal membrane permeabilization, oxidative burst and plasma membrane permeabilization in both cases (57). Cells undergoing primary necrosis may exhibit features of apoptosis as well. For instance, monocytes treated with TNF and cycloheximide in presence of the pan caspase inhibitor zVAD-fmk undergo RIPK1 dependent necrosis but expose PS on their surface prior to losing plasma membrane integrity (58). A similar observation was also made in IFN $\gamma$  treated, *M.bovis* infected necrotic cells and in cells treated with alkylating DNA damage inducing agents causing PARP1 and AIF dependent necrosis (59,60). The terminal deoxynucleotidyl transferase dUTP nick end labeling (TUNEL stain) labels 3'OH ends of DNA fragments and is used frequently for apoptotic cell death detection. *S.typhimurium* infected cells undergoing necrotic cell death however have been shown to stain with TUNEL as well (61). Examination of multiple morphological and biochemical features of dying cells using different approaches is needed for the proper identification of apoptotic and necrotic cells.

### **1.5.2 Signaling pathways leading to apoptosis**

Apoptosis pathways can be classified into two categories – extrinsic and intrinsic. Extrinsic apoptotic pathways are initiated in response to interaction of death receptors belonging to the TNF receptor superfamily with their cognate ligands. Intrinsic apoptotic pathways are activated in response to changes in the equilibrium between pro and anti-apoptotic members of the Bcl2 family induced by stimuli such as oxidative stress, genotoxic stress, UV light etc. Both pathways lead to the activation of initiator caspases. In the extrinsic pathway, a death inducing signaling complex (DISC) is formed that recruits the initiator caspase 8 leading to its oligomerization, autoprocessing and activation. In the intrinsic pathway, the preponderance of pro-apoptotic Bcl2 family members leads to mitochondrial outer membrane permeabilization (MOMP) and release of cytochrome C (CytC) from the mitochondrial intermembrane space to the cytosol. CytC associates with apoptosis activating factor 1 (Apaf-1) and provides a platform for the oligomerization, auto-cleavage and activation of caspase 9. Activated initiator caspases lead to the cleavage and activation of the effector caspases 3, 6 and 7 that target a vast array of proteins and lead to execution of apoptosis (49,52,55). (Fig 3).

The two pathways of apoptosis are not mutually exclusive and activated caspase 8 can cleave the pro-apoptotic Bcl2 family member Bid to generate tBid (truncated Bid), which in turn induces MOMP and activates the intrinsic apoptotic pathway (49).

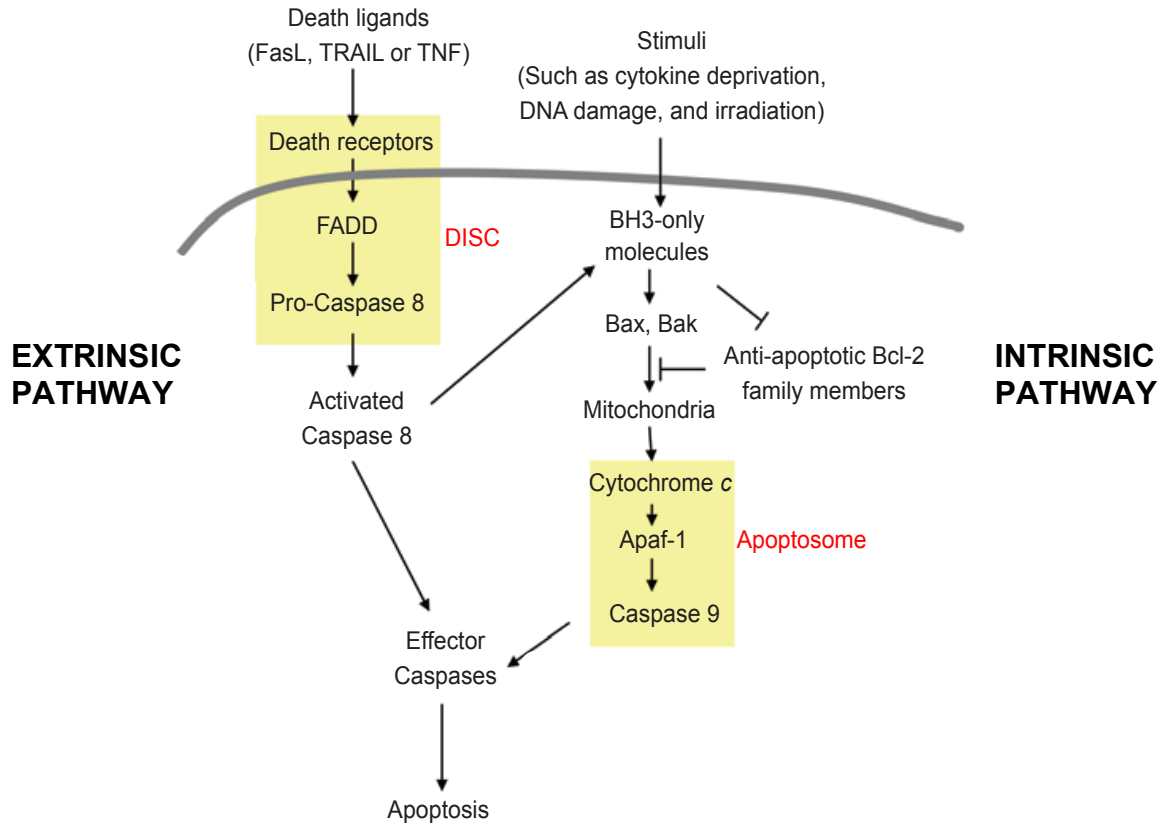


**Fig 3. Apoptotic signaling pathways**

The extrinsic apoptotic pathway is activated following recognition of death ligands by their cognate receptors. This results in formation of DISC and cleavage and activation of the initiator caspase 8. The intrinsic apoptotic pathway is activated in response to stimuli that lead to a preponderance of the pro-apoptotic Bcl2 family members (BH3-only molecules). This leads to cytochrome C leakage from mitochondria, formation of apoptosome complex in the cytosol and cleavage and activation of the initiator caspase 9. Activated initiator caspases cleave and activate the effector caspases 3,6 and 7 that in turn target different host molecules and lead to development of characteristic features of apoptotic cell death.

Abbreviations: FasL – fas ligand; TRAIL – TNF related apoptosis inducing ligand; DISC – death inducing signaling complex; FADD – Fas associated death domain, Apaf1 – apoptosis associated factor 1

Adapted from (235).

### **1.5.3 Regulated necrosis signaling pathways**

Several signaling modules leading to necrotic cell death have emerged in recent years with some signaling pathways being initiated in response to specific stimuli in specific cell types. Described below are three major pathways of necrotic cell death that have been extensively studied in recent years.

#### **1.5.3.1 RIPK1 and RIPK3 mediated cell death**

The regulated necrosis pathway dependent on RIPK1 (rest in peace kinase 1) and/or RIPK3 (rest in peace kinase 3) has been reported to be induced in response to signaling by death receptors, pattern recognition receptors as well in response to viral infections and was labeled necroptosis (50,53). Signaling events leading to RIPK1 and RIPK3 dependent cell death have been best described downstream of TNF binding to TNFR1. Following TNF binding, the cytosolic portion of TNFR1 recruits TRADD (TNF receptor associated death domain), RIPK1, TNF receptor associated factor (TRAF 2 and 5) and cellular inhibitor of apoptosis 1 and 2 (cIAP1 and 2). RIP1 is ubiquitinated by the activity of TRAF 2 and 5 and recruits the transforming growth factor  $\beta$  activated kinase 1 complex (TAK1) leading to NF $\kappa$ B activation and expression of pro-survival factors. Eventually, TNF bound TNFR1 is internalized and a DISC is formed comprising of TRADD, Fas associated death domain (FADD), deubiquitinated RIPK1, RIPK3 and caspase 8. RIPK1 and RIPK3 can also form a TRADD independent cytosolic complex termed ripoptosome with FADD and caspase 8. DISC and ripoptosome act as platforms for caspase 8 cleavage and activation leading to apoptosis induction (Fig 4) (50-52,62).

In conditions where caspase 8 expression and activity is inhibited, RIPK1 and RIPK3 associate in complexes termed as necrosomes where they autophosphorylate and

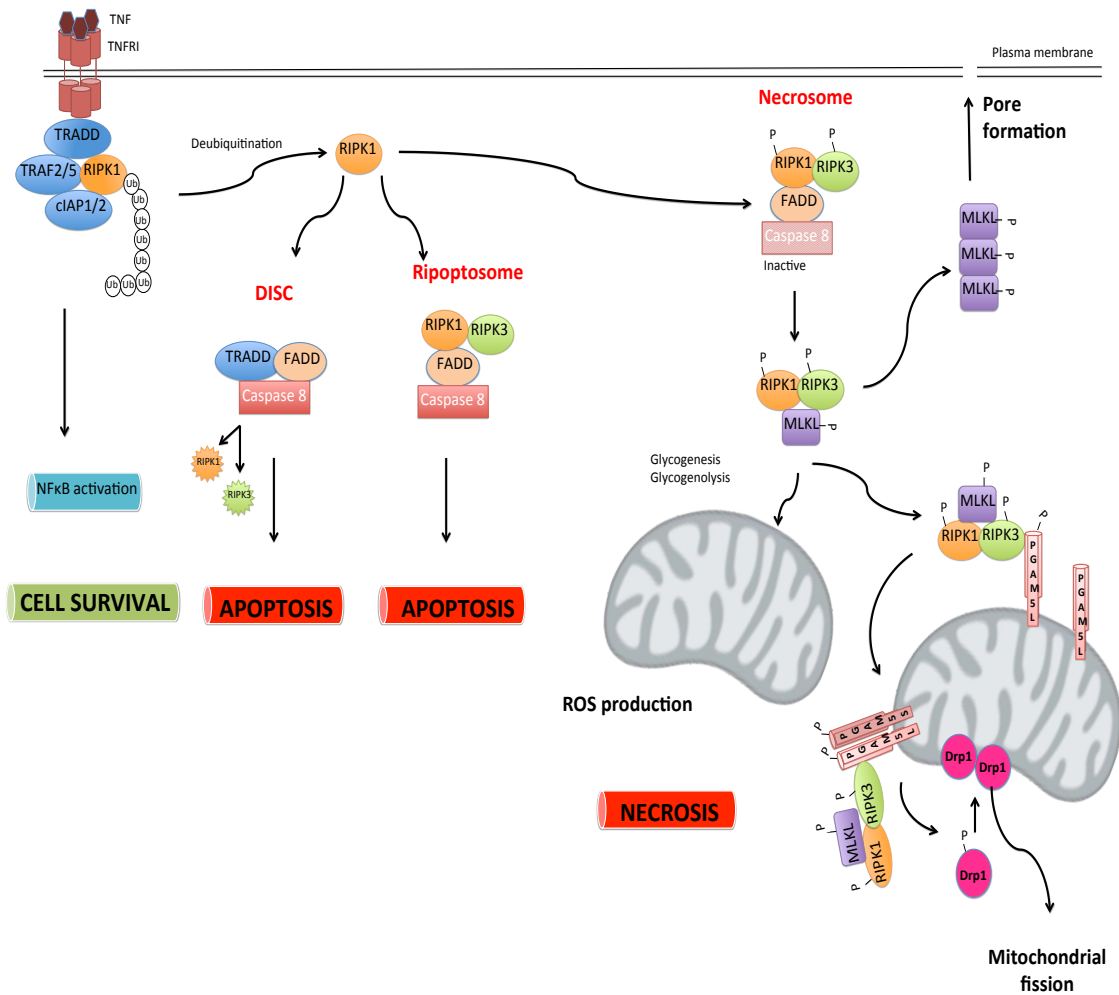


**Fig 4. Outcomes of RIPK1 and RIPK3 signaling**

When recruited to TNF bound TNFR1 present at the cell surface, RIPK1 is ubiquitinated and contributes to NFκB activation and survival. Following endocytosis, the death inducing signaling complex (DISC) is formed which leads to caspase 8 activation and degradation of RIPK1 and RIPK3. Alternatively, RIPK1 and RIPK3 may form part of another apoptosis inducing complex, the ripoptosome. In situations where caspase 8 expression and activation is inhibited, RIPK1 and RIPK3 form a complex where they autophosphorylate and transphosphorylate each other and lead to necrotic cell death via different mechanisms. Upregulation of mitochondrial ROS generation, promoting mitochondrial fission and plasma membrane pore formation contribute to necrosis downstream of the necrosome.

Abbreviations: TRADD – TNF receptor associated death domain; FADD – Fas associated death domain; TRAF- TNF receptor associated factor; cIAP1/2 – cellular inhibitor of apoptosis 1/2; RIPK1/3 – Rest in peace kinase1/3; MLKL – mixed lineage kinase domain like; PGAM5 – phosphoglycerate mutase family member 5; Drp1 – dynamin related protein 1

transphosphorylate each other. Phosphorylated RIPK3 recruits and phosphorylates MLKL (mixed lineage kinase domain like protein) (63). Inhibition of RIP1 kinase activity by necrostatin-1 (Nec1), silencing RIPK3 and MLKL inhibition using necrosulfonamide (NSA) repressed necrosis induction in cells treated with TNF and cycloheximide in presence of the pan-caspase inhibitor zVAD-fmk (63,64). Thus RIPK1 can mediate survival, apoptosis and necrosis in response to TNF. RIPK3 is required only for TNF mediated apoptosis and necrosis (Fig 4).

Multiple mechanisms have been attributed to necrosis induction downstream of necrosome formation. RIPK3 has been shown to interact with and activate enzymes participating in glycogenolysis and glutaminolysis thereby leading to an increase in cellular metabolic activity and consequent mitochondrial ROS generation (50,62). RIPK1 activity has also been linked to ceramide generation. Both ROS and ceramide can cause lysosomal membrane permeabilization leading to cell death. The mitochondrial protein phosphatase phosphoglycerate mutase family member 5 (PGAM5) has been identified as a downstream effector of MLKL and RIPK3 (65). The PGAM5 splice variant PGAM5L is recruited to the necrosome and is required for the RIPK3 mediated phosphorylation of PGAM5S present on the mitochondrial surface. This in turn leads to dephosphorylation and activation of Drp1 (dynamin related protein 1), a GTPase crucial for mitochondrial fission and downstream necrosis induction (66). More recently MLKL has been shown to form trimers that translocate to the plasma membrane leading to an increase in  $Ca^{2+}$  influx and subsequent necrosis (67). Another study suggested that insertion of the MLKL trimers induced pore formation in the plasma membrane leading to necrosis (68) (Fig 4).

### 1.5.3.2 Inflammasome mediated cell death

Inflammasome mediated death shares both apoptotic and necrotic features with death dependent on caspase 1 activity and the dying cells exhibiting DNA fragmentation (apoptotic feature) as well as cell membrane rupture (necrotic feature) and is referred to as pyroptosis (Fig 5A) (69,70). Inflammasomes are cytosolic multi-protein complexes assembled in response to pathogens, toxins and danger associated molecular patterns (DAMP's) and comprise of pattern recognition receptors (PRR's) belonging to the NOD-like receptor (NLR) and the PYHIN families and in some cases the adaptor protein ASC (apoptosis associated speck like protein) (33). Recruitment of pro-caspase 1 by inflammasomes leads to their oligomerization and auto-proteolysis generating activated caspase 1 (69). In case of ASC independent inflammasome NLRC4, pyroptosis induction has been shown to occur in the absence of caspase 1 autoproteolysis in response to *S.typhimurium* infection (71). Apart from cell death induction, caspase 1 activation is also required for the cleavage and secretion of the pro-inflammatory cytokines IL1 $\beta$  and IL18 (69,70). Cell death has also been reported to occur in a NLRP3 and ASC dependent but caspase 1 independent manner in *S.flexneri* and *N.gonorrhoeae* infected macrophages (72,73). This form of cell death was termed pyronecrosis to reflect dependence on inflammsome components but not caspase 1 and it required cathepsin B for its execution (Fig 5B) (72). In anthrax lethal toxin treated cells, cathepsins are required upstream of Nalp1b inflammasome for both caspase 1 activation and induction of cell death (74).

Mechanisms involved in cell death induction downstream of caspase 1 are not well defined (69). Using a diagonal gel proteomics approach, 41 caspase 1 substrates

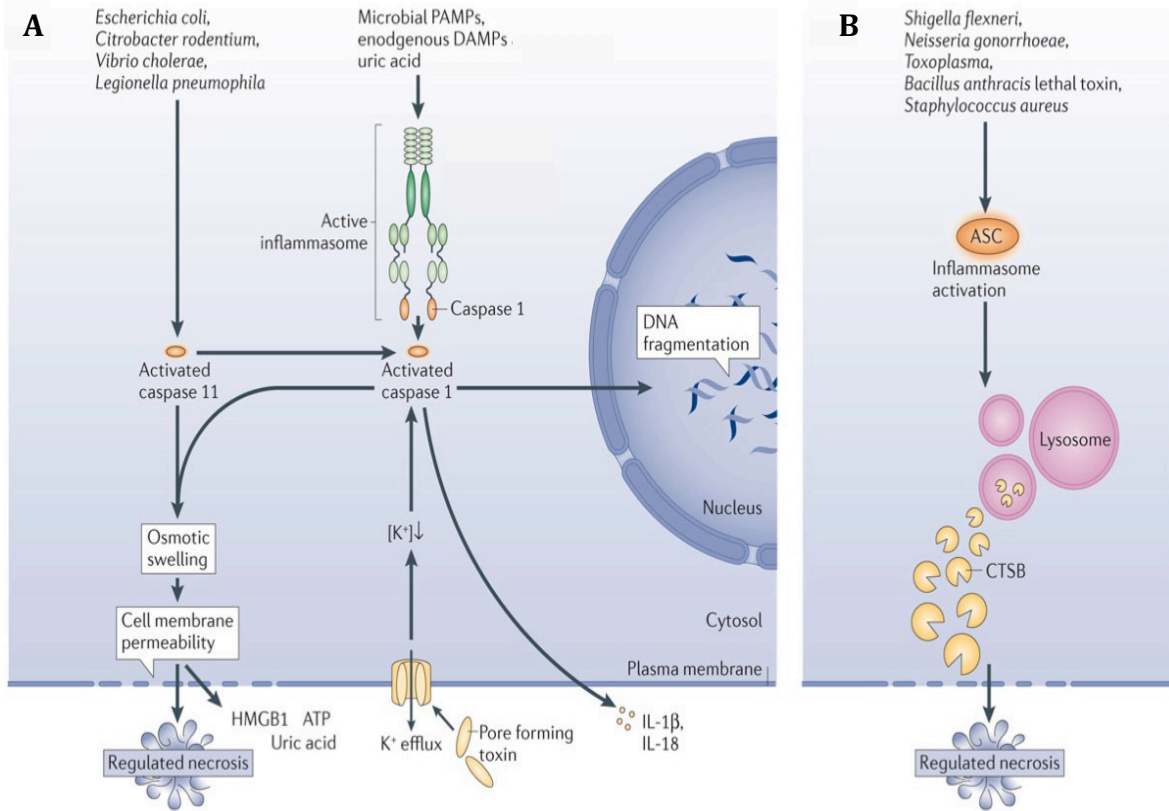


### Fig 5. Inflammasome mediated necrosis

(A) Exposure to PAMP's and DAMP's leads to inflammasome assembly and caspase 1 activation, which leads to release of IL1 $\beta$  and IL18 as well as cell death characterized by large scale DNA fragmentation and plasma membrane permeabilization. Gram negative bacteria activate caspase 11 that potentiates caspase 1 mediated cytokine processing and release and induces caspase 1 independent cell death.

(B) Necrosis induction downstream of inflammasome activation can also be executed by cathepsin B instead of caspase 1.

Adapted from (51).

were identified including glycolytic pathway enzymes and a lower glycolytic rate was detected in *S.typhimurium* infected wild type macrophages compared to caspase 1 deficient cells (75). This points towards a possible perturbation of bioenergetic pathways in caspase 1 mediated cell death. Another possible mechanism of caspase 1 mediated cell death could be the formation of plasma membrane pores. Infection with *S.typhimurium* led to the formation of plasma membrane pores that rendered macrophages permeable to ethidium bromide but not the larger ethidium homodimer 2. Size exclusion studies using osmoprotectants determined the pore size to range between 1.1-2.4nm in diameter (76).

Macrophage treatment with LPS and infection with Gram negative bacterial pathogens (*E.coli*, *C.rodentium*, *S.typhimurium*, *B.pseudomallei*, *L.pneumophila*) leads to cell death dependent on the pro-inflammatory caspase 11 (Fig 5A) (77-82). Caspase 11 is transcriptionally upregulated downstream of TLR signaling and its activation has been shown to depend on IFN $\beta$  signaling (78,79,81). While caspase 11 potentiates caspase 1 mediated proIL1 $\beta$  cleavage, caspase 11 mediated cell death has been shown to be independent of caspase 1 activity (78,79,81,82). Mechanisms leading to cell death downstream of caspase 11 activation have not been elucidated.

### **1.5.3.3 PARP1 and AIF mediated cell death**

PARP1 (Poly ADP ribose polymerase 1) is a nuclear enzyme that catalyzes the generation of poly ADP ribose (PAR) polymers from NAD<sup>+</sup>. Although required for DNA repair, PARP1 has been implicated and its role extensively investigated in cell death induction in response to DNA damaging agents and excitotoxic stimuli (83-86). PARP1 mediated cell death is referred to as parthanatos in literature and it is characterized by both apoptotic and necrotic features. PS exposure on the plasma membrane outer leaflet,

chromatin condensation and DNA fragmentation (albeit large scale) are apoptotic characteristics while caspase independence and loss of membrane permeability are necrotic qualities of PARP1 mediated cell death (87).

PARP1 is activated in response to DNA damage and synthesizes linear and branched PAR polymer chains that are covalently attached to acceptor proteins such as histones and to PARP1 itself (87-89). The negatively charged PAR polymers accumulated near the DNA damage site act as a scaffold for the recruitment of proteins involved in single strand break repair. Following completion of repair, the enzyme poly ADP ribose glycohydrolase (PARG) degrades the PAR polymers, leading to PARP1 release (87,88). During apoptotic cell death, PARP1 is cleaved and rendered inactive.

Execution of cell death downstream of PARP activation can occur via two mechanisms – ATP depletion and nuclear translocation of apoptosis inducing factor (AIF) from the mitochondria. PARP1 over-activation results in  $\text{NAD}^+$  usage and eventual depletion of cellular  $\text{NAD}^+$  and ATP levels. This bioenergetic catastrophe could account for PARP1 mediated cell death (87,89). AIF is a 62KDa mitochondrial inner membrane anchored protein with its N-terminus exposed to the matrix and the C-terminus facing the intermembrane space (IMS). A small pool of unbound AIF was also shown to exist in the IMS (87,90). AIF contains FAD and NADH binding domains and participates in oxidative phosphorylation (87,90). Studies show that PARP1 mediated cell death is inhibited in AIF deficient cells or cells treated with an AIF antibody (83-85). In response to excitotoxic stimuli, nuclear PAR generation and eventual translocation to the mitochondria was observed and delivery of purified PAR induced translocation of full

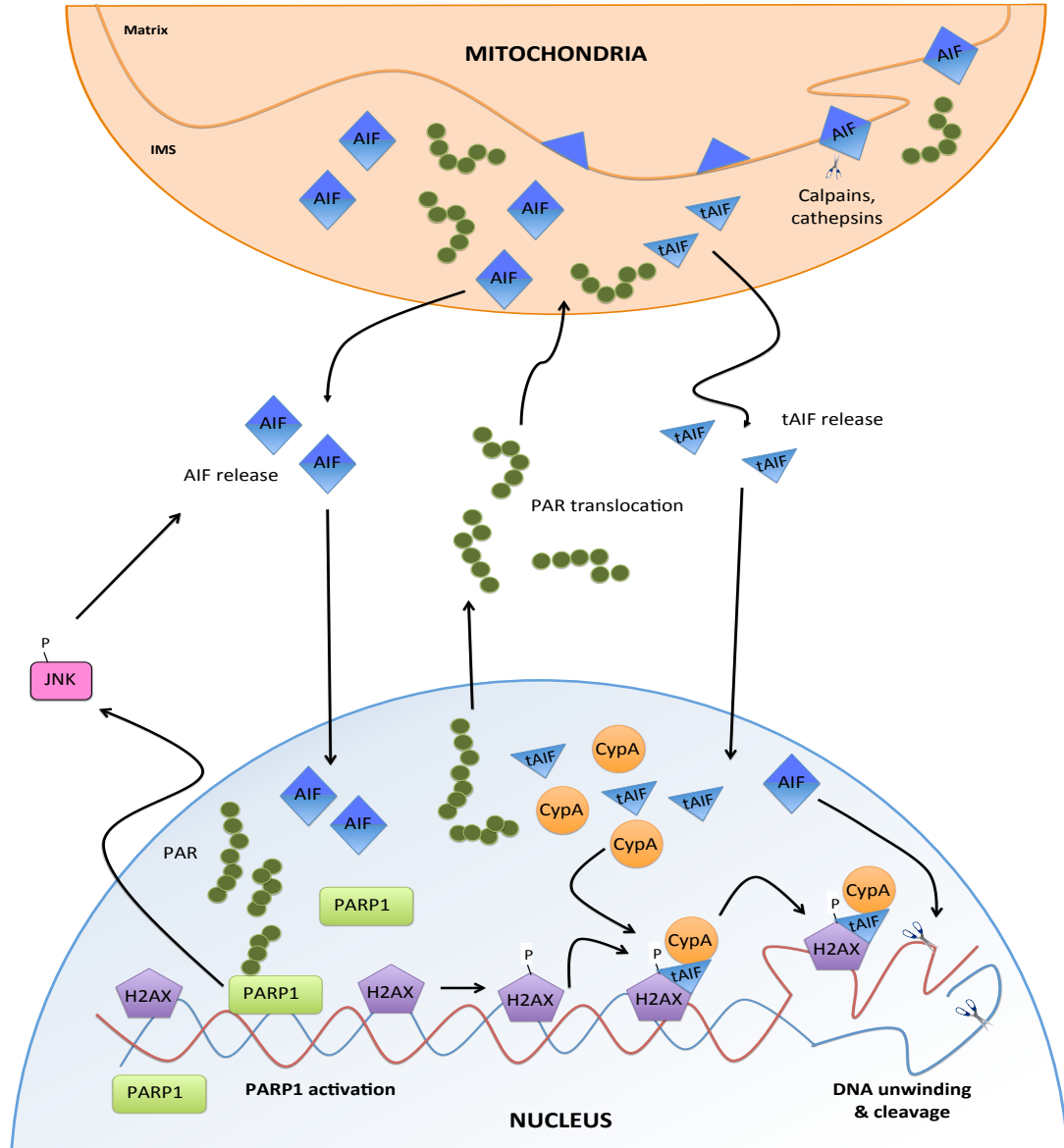


**Fig 6. PARP1 & AIF mediated necrotic cell death**

PARP1 is activated in response to DNA damage to generate PAR polymers that translocate to the mitochondria and cause AIF present in the IMS to translocate to the nucleus. Alternatively, truncated AIF generated either by cathepsins or calpains translocates to the nucleus where it associates with CypA and phosphorylated H2AX. This complex results in DNA unwinding and fragmentation. Mechanisms involved in DNA fragmentation downstream of full length AIF are unknown.

Abbreviations: IMS – intermembrane space; AIF – apoptosis inducing factor; tAIF – truncated AIF; PARP1 – poly ADP ribose polymerase 1; PAR – poly ADP ribose; CypA – cyclophilin A; H2AX – histone H2AX

length AIF (possibly from the IMS pool) to the nucleus (84,85). PARP1 mediated cell death in response to alkylating DNA damage agents and enterovirus 71 infection was found to require calpain dependent cleavage of mitochondrial AIF to a 57KDa form prior to nuclear translocation (86,91). Cathepsins have also been implicated in AIF cleavage (92). JNK phosphorylation and activation was also shown to be required for PARP1 mediated AIF nuclear translocation, AIF cleavage was not addressed in this study (93,94). Following translocation to the nucleus, truncated AIF associates with cyclophilin A (CypA) and phosphorylated histone H2AX to form a DNA degrading complex leading to DNA fragmentation (Fig 6) (60). Mechanisms involved in full length AIF mediated chromatinolysis are unknown.

#### **1.5.4 Necrosis and Mtb pathogenesis**

Apoptosis induction is associated with a decrease in Mtb viability either via direct bacterial killing or by the uptake of bacteria contained within apoptotic cells by bystander macrophages and neutrophils and Mtb has adopted different mechanism to inhibit apoptotic host cell death (49). However, cell death by necrosis does not affect Mtb viability. No changes in Mtb recovery from infected macrophages was observed following treatment with the necrosis inducer hydrogen peroxide while apoptosis induction with ATP lead to loss of bacterial viability (95). Similarly, reduction in cytosolic  $Ca^{2+}$  levels achieved by addition of ruthenium red (a mitochondrial  $Ca^{2+}$  uniporter inhibitor) lead to an increase in necrosis of Mtb infected cells but had no effects on bacterial survival (96). Addition of uninfected macrophages to *M.avium* infected apoptotic cells reduced bacterial survival while a analogous treatment of infected cells rendered necrotic by sonication did not have a similar effect (97). A comparative study

of Mtb clinical strains with the reference strain H37Rv showed that the clinical isolates which grew better than H37Rv *ex vivo* also induced higher levels of necrosis (98).

Studies on susceptibility to Mtb of mouse mutants that lack genes contributing to necrosis induction or inhibition also indicate that necrosis induction is beneficial for the pathogen rather than the host. The *sst1* (super-susceptibility to tuberculosis 1) locus has been associated with the varying susceptibility of different mice strains to Mtb infection and the *ipr1* (intracellular pathogen resistance 1) gene encoded within this locus was identified to mediate this effect (99). Mice deficient in *ipr1* were found to be more susceptible to Mtb. *ipr1*<sup>-/-</sup> BMDM's underwent necrosis in *ex vivo* infections compared to cells from control mice in which the cell death mode was determined to be apoptotic (99). Mtb mediated necrosis has been shown to be dependent on production of the lipid mediator lipoxin A<sub>4</sub> (LXA<sub>4</sub>) and consequent inhibition of prostaglandin E<sub>2</sub> (PGE<sub>2</sub>) in infected macrophages (100). Lipoxins and prostanoids can be generated from arachidonic acid by the action of lipoxygenases and cyclooxygenases respectively (100). Mice deficient in 5-lipoxygenase (5-LO) and subsequently in LXA<sub>4</sub> production were found to be more resistant to Mtb infection. Conversely deficiency in prostaglandin E synthase (PTGES) and in PGE<sub>2</sub> rendered the mice more susceptible to Mtb infection (101,102). Leukotriene A<sub>4</sub> hydrolase (LTA4H) is required for the production of leukotriene B<sub>4</sub> from arachidonic acid and absence of LTA4H led to an increased production of LXA<sub>4</sub> in zebrafish larvae (103). LTA4H morphant zebrafish larvae had lower TNF, increased bacterial burdens and higher susceptibility to *M.marinum* infection compared to WT controls. This was attributed to increased production of LXA<sub>4</sub> and necrosis induction in the morphant zebrafish larvae (10). Interestingly, LTA4H high

zebrafish larvae (generated by introduction of LTA4H mRNA) were also found to be hypersusceptible to *M. marinum* infection and this phenotype was attributable to increased TNF production resulting in mitochondrial ROS, RIPK1 and RIPK3 dependent necrosis induction (9,103). LTA4H polymorphisms were found to be associated with susceptibility to TB in humans as well (10).

### **1.5.5 Mechanisms involved in Mtb induced necrotic cell death**

The first insight into the mechanisms of Mtb mediated necrosis induction came from a study comparing the effects of virulent Mtb strain H37Rv and attenuated Mtb strain H37Ra infection on host cell mitochondrial function. H37Rv induced necrosis was found to be dependent on increased loss of mitochondrial membrane potential in infected cells and could be inhibited by cyclosporine A (CsA), an inhibitor of mitochondrial permeability transition pore (MPTP) formation and by decreasing mitochondrial  $Ca^{2+}$  levels (104). Mitochondrial outer membrane permeabilization (MOMP) and CytC translocation to cytosol was associated with H37Ra induced apoptosis (104).

Modulation of eicosanoid production by Mtb leads to necrosis via three mechanisms – loss of mitochondrial membrane potential, inhibition of plasma membrane repair and inhibition of apoptotic envelope formation. Mtb infection resulted in production of LXA<sub>4</sub> that inhibits expression of cyclooxygenase 2 (COX2) enzyme required for synthesis of PGE<sub>2</sub>. PGE<sub>2</sub> signaling via its G-protein coupled prostanoid receptor 2 (EP2) and consequent activation of protein kinase A (PKA) was required to prevent loss of mitochondrial membrane potential and necrosis (105). PGE<sub>2</sub> also upregulates expression of the lysosomal  $Ca^{2+}$  sensor Syt7 which is required for the recruitment of lysosomal vesicles to the plasma membrane for repair of microdisruptions

failing which necrosis occurs (102). LXA<sub>4</sub> downregulates expression of the serpin protease inhibitor plasminogen activator inhibitor type 2 (PAI2), an inhibitor of annexin-1 cleavage. Annexin-1 is recruited to the surface of apoptotic cells and is crosslinked to form the apoptotic envelope, which prevents loss of plasma membrane integrity. Truncated annexin cannot be crosslinked and thus Mtb infected cells die via necrosis (Fig 7) (106).

Macrophage necrosis induction was also found to occur in response to high bacillary load (MOI 25-50) of Mtb (107-109). Based on assessment of plasma membrane permeability and nuclear fragmentation and condensation, cell death induction by high MOI of Mtb was found to have both apoptotic and necrotic features (107). This was eventually confirmed by electron microscopy studies (108). While loss of mitochondrial membrane potential was observed, it was found to be independent of MPT pore (MPTP) formation (108). Calcium chelation, TLR and TNF signaling and caspase 3 activity were also found to be dispensable for high MOI Mtb induced cell death (107,109). High MOI Mtb infection was found to induce lysosomal membrane permeabilization and loss of mitochondrial membrane potential and necrosis induction was attributed to the activity of lysosomal lipase but not cathepsins (Fig 7) (108). High intracellular bacillary load was found to lead to necrosis of lung monocytic cells and neutrophils in *in vivo* mouse infections as well and the burst size was estimated to be between 20-40 bacilli (21).

Infection with Mtb leads to inflammasome activation and IL1 $\beta$  release (27). Mtb mediated necrosis was found to be independent of caspase 1 and cathepsin activity, excluding the role of both pyroptosis and pyronecrosis (32,108,109). The inflammasome component NLRP3 however has been demonstrated to be required for Mtb mediated

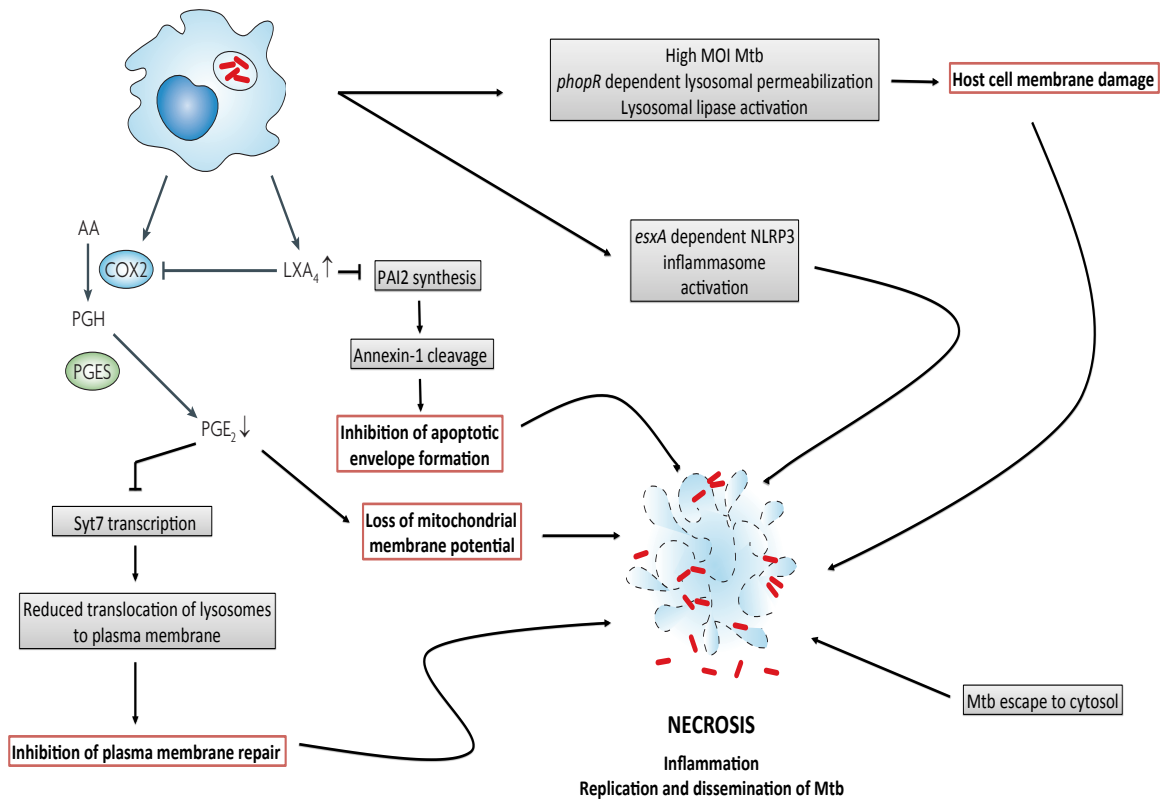


**Fig 7. Mechanisms of Mtb mediated necrosis induction**

Mtb infection upregulates production of the eicosanoid LXA<sub>4</sub> that leads to increased annexin-1 cleavage and inhibition of apoptotic envelope formation. LXA<sub>4</sub> represses production of the eicosanoid PGE<sub>2</sub> resulting in loss of mitochondrial membrane potential and inhibition of plasma membrane repair. These events lead to death of infected cells by necrosis. A high load of Mtb in host cells was found to result in necrotic cell death by activation of lysosomal lipases and resultant host cell membrane damage. Mtb mediated NLRP3 inflammasome activation and bacterial escape from the phagosome to the cytosol are also associated with induction of host cell necrosis.

Abbreviations: AA – arachidonic acid; COX2 – cyclooxygenase ; PGH – prostaglandin H; PGES – prostaglandin E<sub>2</sub> synthase; PGE<sub>2</sub> - prostaglandin E<sub>2</sub>; LXA<sub>4</sub> – lipoxin A<sub>4</sub>

necrosis (Fig 7) (32). The study identified Mtb mediated phagosomal damage and activation of the tyrosine kinase Syk upstream of NLRP3 activation, mediators downstream of NLRP3 contributing to cell death were not identified (32).

Following entry into a macrophage, Mtb arrests phagosome-lysosome fusion and has been found to remain within compartments resembling the early endosome. However, studies have reported that Mtb eventually escapes from the phagosome to the cytosol (41-43,110,111). Necrotic cell death was found to closely follow Mtb escape to the cytosol (42). Mechanisms underlying necrosis induction following Mtb escape have not been investigated.

#### **1.5.6 Mtb genes implicated in necrotic cell death induction**

Mtb has two specialized secretion systems encoded by the ESX loci - ESX1 and ESX5 - in order to transport proteins across its cell wall. The EsxA protein encoded by the *esxA* gene located in the ESX1 locus has been shown to form pores in artificial lipid bilayers as well in RBC membranes resulting in hemolysis (112-114). Both ESX1 and *esxA* mutant strains has been shown to induce much lower levels of necrosis in infected macrophages compared to the wild type Mtb strain (32,42,109,115,116). Conflicting reports exist regarding the role of EsxA in high MOI Mtb induced cell death with one report attributing this phenotype to the *phoPR* two component regulatory system (108,109). EsxA has also been implicated in apoptosis induction in other studies and the difference in cell death modality could be attributed to the different cell types as well as cell death detection techniques used in these studies (33,117,118). It must be noted that EsxA is required for the secretion of other ESX1 substrates as well. Therefore, it is difficult to determine the contribution of EsxA itself in Mtb mediated necrosis.

The ESX5 locus is required for the transport of PE-PPE proteins and an Mtb ESX5 mutant strain was found to be deficient in necrosis induction. The ESX5 locus induced necrosis was found to be dependent on cathepsin B (116). The requirement of the ESX5 locus to induce necrosis could possibly be due to its role in the secretion of the PE25/PPE41 complex as macrophages treated with the recombinant protein complex undergo necrosis (119). Ectopic expression of PE-PGRS33 protein in mammalian cells led to mitochondrial localization of the protein and induction of necrosis (120).

Mtb mediated inhibition of the eicosanoid PGE<sub>2</sub> contributes to necrotic cell death via loss of mitochondrial membrane potential and inhibition of plasma membrane repair mechanisms and a recent study implicated Mtb phospholipase (PLC) genes to influence PGE<sub>2</sub> production (102,104,106,121). Mtb encodes for four PLC genes (*plc A,B,C,D*). A comparative study of two clinical strains of Mtb showed that the strain 97-1200 in which all the *plc* genes were deleted induced lower levels of necrosis, higher COX2 mRNA expression and increased PGE<sub>2</sub> production in infected alveolar macrophages compared to the 97-1505 strain in which *plcA* and *plcB* were expressed (121). A recent study has implicated the Mtb CpnT (channel protein with necrosis inducing toxin) protein encoded by *Rv3903c* in necrosis induction, decreased necrosis was observed in macrophages infected with the *cpnT* mutant compared with Mtb infected cells. Increased levels of caspase 1, caspase 3 and RIPK1 independent cell death was observed in Jurkat T cells overexpressing the C terminal fragment of CpnT compared to control cells (122). Another Mtb gene implicated in regulation of necrosis is *Rv3364c*, which contributes to inhibition of caspase 1 activation and necrosis induction in infected macrophages (123).

## **1.6 Autophagy**

Autophagy is an evolutionarily conserved catabolic process that involves sequestration of cytosolic contents into *de novo* generated double membrane vesicles termed as autophagosomes. Subsequent fusion of autophagosomes with lysosomes leads to degradation of autophagosomal contents (139,140). Autophagy induction is achieved by both intracellular and extracellular stresses such as amino acid starvation, growth factor deprivation, reduced ATP levels, ER stress, hypoxia, oxidative stresses and microbial invasion (141). Autophagy can be non-selective i.e. random areas of the cytosol are engulfed within the autophagosome, this process is termed macroautophagy. Alternatively, cargo may be specifically targeted to the autophagosomes in selective autophagy (Fig 8). Based on the cargo, selective autophagy may be of different types – mitophagy (mitochondria), reticulophagy (ER membranes), xenophagy (micro-organisms) (142).

Apart from directly killing micro-organisms by directing them to lysosomal compartments, autophagy also serves to deliver cytosolic PAMP's to endosomes harboring cytosolic PRR's resulting in generation of innate immune responses (37). Autophagy also negatively regulates inflammasome activation by eliminating PAMP's and by targeting ubiquitinated inflammasome complexes for destruction (143).

### **1.6.1 Molecular machinery of macroautophagy**

There are 5 distinct stages in autophagy – induction, membrane nucleation, vesicle expansion, lysosomal fusion and degradation of autophagosomal contents.

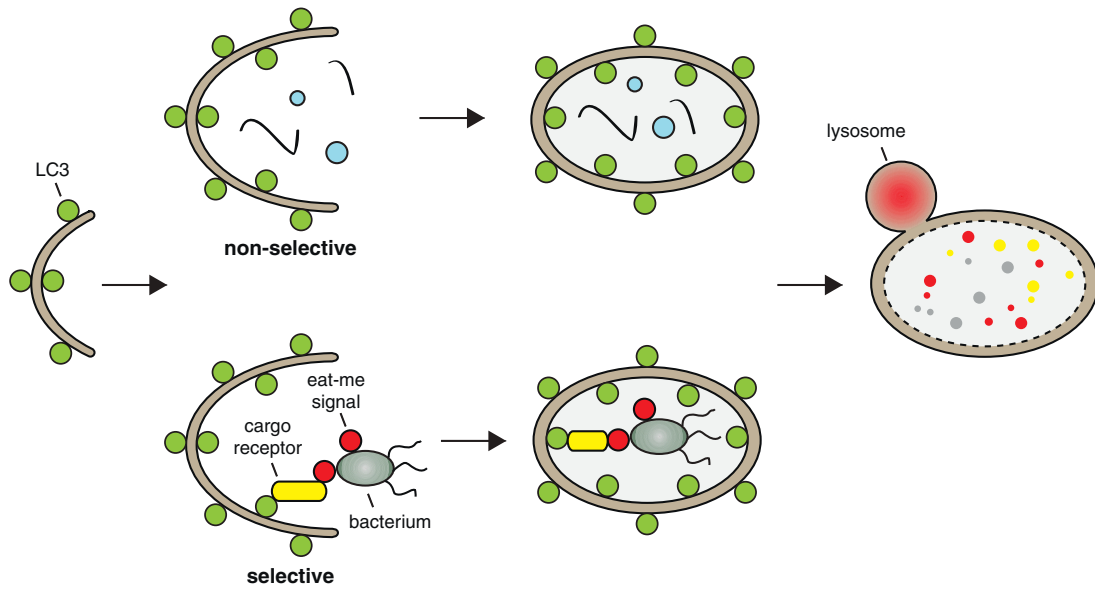


**Fig 8. Overview of non-selective and selective autophagy**

Cytosolic material is captured in a non-specific manner in non-selective or macroautophagy. Specific cargo receptors are involved in selective autophagy with xenophagy of a bacterium being depicted in this image. The captured material is encapsulated in a double membrane autophagosome that eventually fuses with a lysosome leading to degradation of autophagosomal contents.

Adapted from (142).

Execution of these stages requires the participation of both Atg (Autophagy Related Genes) and non-Atg proteins (139,144,145).

Autophagy induction is characterized by the formation of ULK1 complex consisting of Unc-51-like-kinase1 (ULK1), Atg13 and FAK family kinase-interacting protein of 200KDa (FIP200). Formation of the ULK1 complex is required for the recruitment of Beclin1, Atg14L (ATG14-like) and PI3KR4 (phosphoinositide 3-kinase regulatory subunit 4) proteins to the assembly site. These proteins initiate membrane nucleation by recruiting the class III PI3K Vps34 to the assembly site that results in the production of PI3P (phosphatidylinositol 3-phosphate) and phagophore formation at the assembly site. Elongation of the phagophore is achieved by the action of two ubiquitin like conjugation systems. First, Atg12 is conjugated to Atg5 via the activity of Atg7 and Atg10. The Atg12-Atg5 conjugate binds to Atg16 and the entire complex is attached to the phagophore. The Atg12-Atg5-Atg16 complex conjugates phosphatidylethanolamine (PE) to Atg8 via an amide bond. Atg7 and Atg3 are also involved in this process (139,141,146). Conversion of soluble Atg8 (LC3I) to membrane bound Atg8-PE (LC3II) is monitored to study autophagy induction (147,148).

Once vesicle formation is complete, the Atg12-Atg5-Atg16 complex is released from the autophagosomal membrane. A proportion of LC3II is also deconjugated from the autophagosomal membrane by the action of the cysteine protease Atg4b thus recycling LC3 for new autophagosome formation. The fusion of the autophagosome with lysosomes ensues; this requires the small GTPase Rab7, the autophagosomal syntaxin7

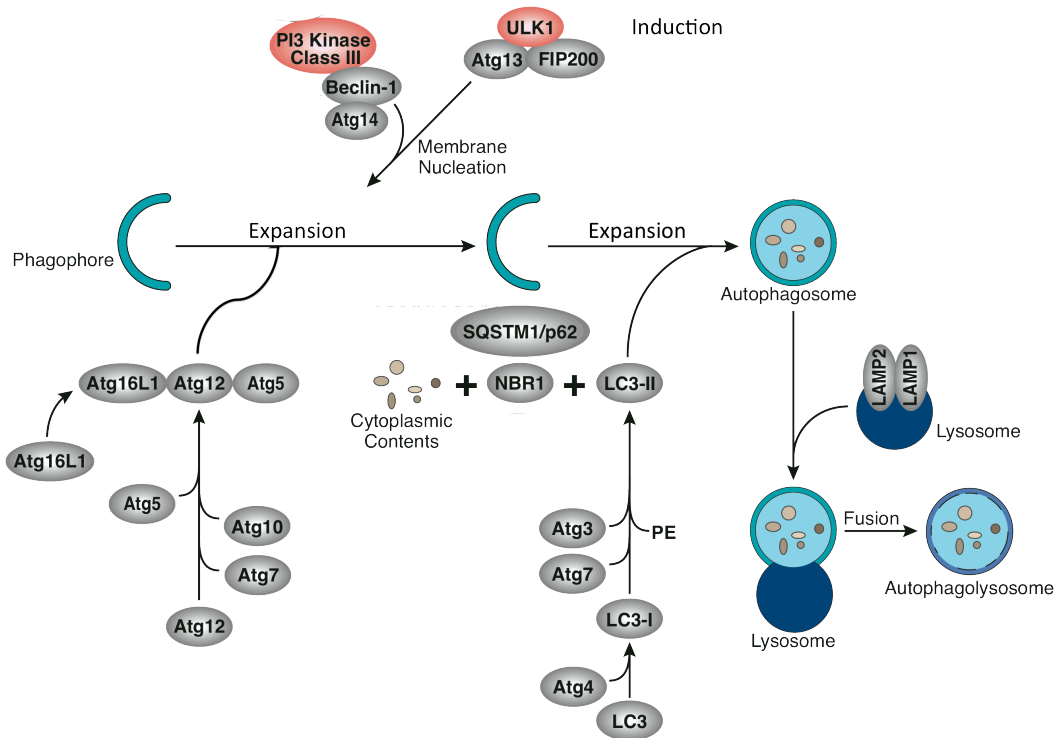


**Fig 9. Molecular machinery of autophagy**

There are 5 distinct stages in autophagy – induction, membrane nucleation, expansion, fusion with lysosome and degradation of autophagolysosomal contents. Each stage involves formation of protein complexes as described in the text. SQSTM1/p62, and NBR1 are examples of cargo receptors involved in selective autophagy.

Adapted from Cell Signaling website  
<http://media.cellsignal.com/www/pdfs/science/pathways/Autophagy.pdf>

and the VAMP8 (vesicle associated membrane protein 8) and LAMP2 (lysosomal associated membrane glycoprotein 2) proteins on the lysosomal membrane (139) . Destruction of the autophagosomal contents occurs via activity of lysosomal proteases and hydrolases (Fig 9).

More recently studies have emerged describing non-canonical autophagy pathways which exclude some of the core autophagic machinery components (140). Glucose starvation mediated autophagy has been shown to be independent of initiating ULK1 while Beclin1-independent autophagy has been reported to occur in response to treatment with apoptosis inducers. (139,140). Atg5 independent autophagy has been reported to be involved in mitochondrial clearance in erythrocytes (140). Another form of non- canonical autophagy involves the recruitment of a subset of autophagy components to phagosomal compartments. For example, LC3 is recruited to *S.typhimurium* containing phagosomes, a phenomenon referred to as LC3 associated phagocytosis (LAP) (149). Both canonical and non-canonical autophagy share a common outcome i.e. destruction of sequestered cargo.

### **1.6.2 Molecular machinery of selective autophagy**

Execution of selective autophagy occurs via similar mechanisms as macroautophagy with one important addition – recognition of substrates and their tethering to Atg8 either directly or via cargo receptor proteins. Currently four cargo receptor proteins are known to exist – p62/SQSTM1 (sequestome 1), NBR1 (neighbor of BRCA1 gene 1), Optineurin and NDP52 (nuclear dot protein 52KDa). All of these receptors possess short LC3 interacting regions (LIR's) and ubiquitin recognition domains while NDP52 has an additional galectin 8 interacting region (142). Ubiquitin has

been shown to coat intracellular pathogens such as *S.typhimurium* and Mtb allowing for their recognition by the autophagic machinery via the cargo receptors (142,150,151). Damage to the Salmonella containing vacuole (SCV) leads to exposure of previously hidden membrane glycans and binding by galectins. Of these, galectin 8 is recognized by NDP52, which then recruits the SCV and its contents to autophagosomes (139,142).

### **1.6.3 Regulation of macroautophagy**

A central regulator of autophagy in response to various stimuli is the serine threonine kinase mTOR (mammalian target of rapamycin). mTOR is required for the assembly of the ULK1 complex most likely via phosphorylation of ULK1. mTOR exists in 2 complexes – mTORC1 (consisting of mTOR, mLST8/GβL, RAPTOR) and mTORC2 (consisting of mTOR, mLST8/GβL and RICTOR) (152). Exposure to insulin and growth factors leads to Akt phosphorylation and activation, which in turn phosphorylates TSC2 (tuberous sclerosis complex 2). This results in inhibition of TSC2 interaction with TSC1 (TSC - tuberous sclerosis complex). The TSC1-TSC2 complex inhibits the conversion of the Ras family small GTPase Rheb (Ras homolog enriched in brain) from its GDP bound form to a GTP bound form. GTP bound Rheb is required for the activation of mTOR. The active mTORC1 complex inhibits autophagy induction by preventing the formation of the ULK1 complex. Low cellular energy and high intracellular  $Ca^{2+}$  levels lead to TSC1-TSC2 complex formation through AMPK (adenosine monophosphate activated protein kinase) and CaMKK (calcium/calmodulin dependent protein kinase kinase) activation and thus feed into mTORC1 inhibition and autophagy induction. Amino acid deprivation prevents translocation of mTOR to

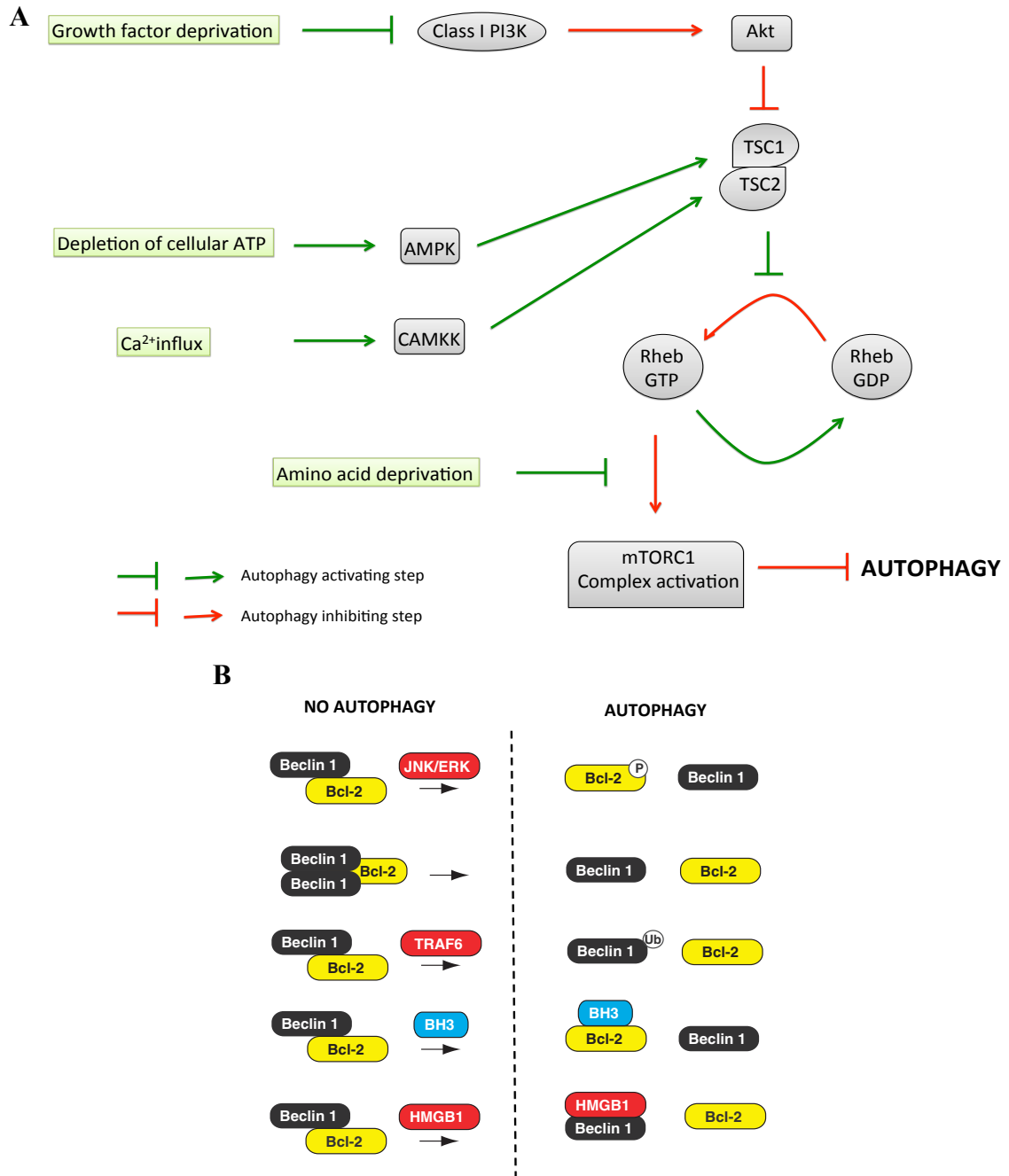


**Fig 10. Regulation of macroautophagy**

(A) Pathways involved in macroautophagy induction in response to different stimuli.

(B) Possible modes of Beclin1-Bcl2 complex dissociation required for autophagy induction. Adapted from (146).

compartments containing GTP bound Rheb and thus inhibits mTOR activation (Fig 10A) (141,153).

Macroautophagy is also regulated at the membrane nucleation step via Beclin1 availability. Beclin1 has 3 structural domains – a coiled- coiled domain (utilized for self oligomerization), an evolutionarily conserved domain (required for interaction with other membrane nucleation proteins) and a BH3 domain (152). In healthy cells, Beclin1 (using its BH3 domain) forms a complex with the anti apoptotic Bcl2 protein, thereby rendering Beclin1 unavailable to participate in macroautophagy. However, following exposure to autophagy inducing signals, Bcl2 is phosphorylated and dissociates from Beclin1. The MAPK JNK has been implicated in Bcl2 phosphorylation in response to starvation, ER stress and hypoxic conditions (141,154). Dissociation of Beclin1-Bcl2 complex may also result from Beclin1 modifications such as oligomer formation, ubiquitination, displacement of Beclin1 following interaction of Bcl2 with BH3 containing proapoptotic proteins such as Bad and displacement of Bcl2 by Beclin1 binding proteins such as high mobility group protein B1 (HMGB1) (Fig 10B) (146).

Transcriptional regulation of proteins involved in autophagy has been described in response to nutrient stresses and cytokine signaling (155-157). IL6 has been found to inhibit autophagy induction by IFN $\gamma$  in Mtb infected THP1 cells and this is thought to be due to the repression of Atg7 expression and subsequent inhibition of the Atg12-Atg5 complex (158). Similarly the Th2 cytokines IL4 and IL13 inhibit autophagy of IFN $\gamma$  treated, Mtb infected macrophages in a Stat6 dependent manner. Stat6 is linked to increased expression of Bcl2 which inhibits autophagy via Beclin1 binding (159). The

cathelicidin LL37 which induces mycobacterial killing in human macrophages via autophagy also upregulates Beclin1 and Atg5 expression (160).

#### **1.6.4 Mtb and autophagy**

Initial studies on Mtb and autophagy focused on the effect of physiological, pharmacological and immunological autophagy inducers on mycobacteria infected cells. Incubation of BCG infected macrophages under serum and amino acid starvation conditions or treatment with the mTOR inhibitor rapamycin led to autophagy activation and colocalization of bacteria with LC3 and with lysosomal markers (lysotracker, LAMP1, cathepsin D, CD63) (158, 161). A similar effect was seen following IFN $\gamma$  treatment of BCG-infected macrophages and the IFN $\gamma$  inducible GTPase LRG47 was found to be responsible (161,162). More recently a novel STAT1 independent, p38 MAPK and PI3K dependent pathway has been implicated in autophagy induction by IFN $\gamma$  (163). IL6, IL4 and IL13 were found to inhibit IFN $\gamma$  induced autophagy (158,159). IL1 $\beta$  treatment of macrophages induced autophagy and inhibited mycobacterial survival in a TBK1 dependent manner (164). Low serum levels of calcidiol, a precursor of 1,25 dihydroxy vitaminD3 (VitD3) is associated with susceptibility to tuberculosis (145). Increased colocalization of Mtb with autophagosomes was observed in human macrophages following VitD3 treatment and this was found to be dependent on increased expression of the cathelicidin LL37 (160). ATP signaling through the P2X7 receptor and LPS signaling via TLR4 were also found to promote localization of mycobacteria with autophagosomes (165,166).

More recently studies have shown that Mtb in the absence of other stimuli induces autophagy. A comparative study of autophagy induction by mycobacterial species

demonstrated an inverse relationship between autophagy induction and bacterial virulence in macrophages (167). Co-localization of Mtb with ubiquitin, the autophagy adaptors p62 and NDP52 and LC3 was found to be dependent on pore formation in phagosomal membranes by the ESX1 secreted protein EsxA (150). Ubiquitin and p62 were also recruited to LC3 positive, Mtb containing compartments in dendritic cells (168). While about 30% of intracellular Mtb were directed to autophagosomes in macrophages at 4hpi, in dendritic cells only about 10% of bacteria were LC3 positive at 24hpi (150,168).

Autophagy induction is associated with anti-mycobacterial effects. Treatment of infected macrophages with additional stimuli (starvation, rapamycin, IFN $\gamma$ , ATP, VitD3) results in increased killing of mycobacteria *ex vivo* as demonstrated by decreased CFU obtained compared to untreated infected cells (160,161,165). Treatment of Mtb infected cells with autophagy inhibitors (PI3K inhibitors 3-methyladenine (3-MA) and wortmannin) and silencing of autophagy genes reversed the decrease in mycobacterial viability. First line drugs used in TB treatment, isoniazid (INH) and pyrazinamide (PZA), were also found to induce autophagy in Mtb infected macrophages in a ROS, Ca<sup>2+</sup> and AMPK dependent manner. Silencing of Beclin1 or Atg5 was found to inhibit mycobacterial killing in infected cells treated with INH and PZA indicating that autophagy induction contributed to their optimal antibacterial activity (169). The ability of autophagy to overcome the phagolysosome biogenesis block exerted by Mtb and to deliver bacteria to the lysosomal compartments is thought to underly the mycobactericidal effects of autophagy (161,167). Addition of lysosomal fractions obtained from starved or IFN $\gamma$  treated autophagic macrophages were found to result in

reduced recovery of mycobacteria from infected cells. This was linked to increased generation of ubiquitin derived peptides in autophagic cells (170). Apart from mediating VitD3 induced autophagy, the cathelicidin LL37 was also found to colocalize with LC3 positive compartments (160). LL37 has been shown to reduce mycobacterial survival *in vitro* (171). It is therefore possible that cathelicidin might exert direct anti-mycobacterial effects *ex vivo* as well.

The role of autophagy as an anti-mycobacterial mechanism is further strengthened by evidence provided by *in vivo* studies. Two studies demonstrated that autophagy deficient  $Atg5^{\text{flox/flox}}$  Lys- Cre<sup>-</sup> mice infected via the aerosol route with a low dose of Mtb were extremely susceptible to infection, with mice succumbing within 4 weeks post infection compared to wild type controls. Increased bacterial loads were recovered from the lungs, liver and spleen of autophagy deficient mice and lungs from these mice showed abscess formation unlike the WT controls (150),(172). In addition to effects on bacterial load, the lung cytokine environment in Mtb infected autophagy deficient mice was found to be significantly pro-inflammatory with increased levels of cytokines such as IL1 $\alpha$ , IL1 $\beta$  and chemokines such as CCL5 and CXCL1 present compared to control mice. No differences were observed in levels of IFN $\gamma$  (150,172). Apart from the innate immune response, adaptive immune responses could also be modulated by autophagy. In dendritic cells, 30% of p62 and ubiquitin positive Mtb were found to colocalize with class II MHC suggesting that autophagy could promote presentation of mycobacterial peptides to CD4<sup>+</sup> T cells (168). Autophagy induction via starvation, rapamycin or IFN $\gamma$  treatment enhanced presentation of Ag85B by Mtb infected macrophages and dendritic cells *ex vivo*. These results translated *in vivo* as well with mice immunized with rapamycin treated, BCG

infected dendritic cells exhibiting better protection following challenge with Mtb compared to mice immunized with untreated, BCG infected dendritic cells (173).

### **1.6.5 Mtb genes involved in autophagy modulation**

The *esxA* gene product, EsxA is associated with the ability of Mtb to manipulate innate immune responses such as inflammasome activation, TLR signaling and cytokine production and host cell death. Additionally, EsxA is also associated with pore formation and phagosomal membrane damage (38). The ability of Mtb to induce autophagy in macrophages was linked to EsxA production; a lower percentage of *esxA* mutant bacteria colocalized with LC3 and Atg12 compared to the wild type Mtb control. Autophagy induction by EsxA was linked to its ability to induce phagosomal membrane damage as colocalization with LC3 was partially restored for an *esxA* mutant strain secreting the auto-activated form of the pore forming toxin listeriolysin O (LLO) (150). Pore formation by EsxA facilitated the exposure of Mtb extracellular DNA to STING, a component of the cytosolic DNA pathway, leading to autophagy and induction of type I IFN response (150,174).

The 19KDa mycobacterial lipoprotein LpqH has been implicated in Mtb mediated autophagy induction in human macrophages. Treatment of macrophages with recombinant LpqH led to TLR1/2/CD14 dependent increase in intracellular  $Ca^{2+}$  levels and AMPK activation, leading to downstream activation of p38 MAPK. These signaling pathways lead to an increase in the conversion of vitamin D3 to its active form (175). Active VitD3 induces autophagy by upregulating expression of the cathelicidin LL37 (160,175).

While evidence exists demonstrating that Mtb induces selective autophagy, there are reports that indicate that the pathogen possesses the ability to inhibit autophagy. The *eis* (enhanced intracellular survival) gene encodes for an aminoacyltransferase that acetylates the JNK specific phosphatase MKP7 (176). The Mtb *eis* mutant induces higher levels of autophagy compared to the WT control in a ROS and JNK dependent manner demonstrating that *eis* has an anti-autophagic function (177). Lipoarabinomannan (LAM) is a mycobacterial lipoglycan capped with mannose residues in pathogenic Mtb (ManLAM) compared to phosphatidyl-myo-inositol (PILAM) in non-pathogenic *M.smegmatis*. Latex beads coated with ManLAM did not co-localize with LC3 compared to PILAM coated beads indicating that ManLAM plays a role in autophagy inhibition by Mtb (178). While Watson *et al* determined EsxA to be required for Mtb mediated autophagy in macrophages, another study in dendritic cells indicated that Mtb induced autophagy was independent of EsxA, rather EsxA was required for inhibition of autophagosome fusion with lysosomes (179).

#### **1.6.6 Mechanisms involved in autophagy modulation by Mtb**

Data for the involvement of mTOR in Mtb mediated autophagy is ambivalent. Both pathogenic and non-pathogenic mycobacterial species were found to induce autophagy in an mTOR independent fashion in macrophages. Concomitant with autophagy induction, increased levels of phosphorylated ribosomal S6 kinase, a downstream target of mTOR, was detected in Mtb infected cells compared to uninfected controls indicating that the bacteria induced mTOR activation (167). However, another study showed that Mtb upregulates microRNA-155 levels in both lungs of mice and in BMDM's *ex vivo* which in turn post-transcriptionally inhibits expression of Rheb, an

activator of mTOR and a negative regulator of autophagy (180). Mtb mediated autophagy induction and delivery to lysosomes was shown to require phosphorylation of TBK1 in response to detection of bacterial DNA by STING adaptor protein (150). TBK1 induces selective autophagy by phosphorylating p62 at Ser403, this was previously demonstrated to increase affinity of p62 for ubiquitin, and is also needed for autophagosome maturation (142),(164) . The DNA damage regulated autophagy modulator DRAM1 was found to co-localize with *Mtb* in primary human macrophages in a MyD88 dependent manner and was demonstrated to be required for p62 mediated autophagic clearance of *M.marinum* in zebrafish embryos (181). Ubiquitination of Mtb and its localization with autophagic markers was shown to require the ubiquitin ligase Parkin, which is required for mitophagy as well (151). Using a digitonin based selective membrane permeabilization protocol, Manzanillo *et al* demonstrated that ubiquitin co-localizes to bacteria present within intact phagosomes (151).

Just as Mtb possesses both pro and anti autophagic genes, studies have described mechanisms employed by Mtb to avoid autophagic degradation. Macrophages infected with the non-pathogenic *M.smegmatis* and *M.fortuitum* showed increased accumulation of LC3 positive vesicles compared to those infected with Mtb (167). Phagosomes containing live Mtb recruit the host protein coronin-1a unlike those containing heat killed bacteria and silencing of coronin-1a was found to inhibit Mtb survival (39). Coronin-1a was found to be required for inhibition of autophagy by Mtb in macrophages and activation of p38 MAPK was found to be essential to this process (182). Alteration of host lipid metabolism by the virulent Mtb strain H37Rv resulting in increased accumulation of triacylglycerides and lipid body formation compared to the avirulent

H37Ra was associated with decreased autophagy induction. Pharmacological inhibition of lipid body formation increased co-localization of Mtb with LC3 and lysotracker positive compartments and decreased bacterial survival in macrophages (Fig 11) (183).

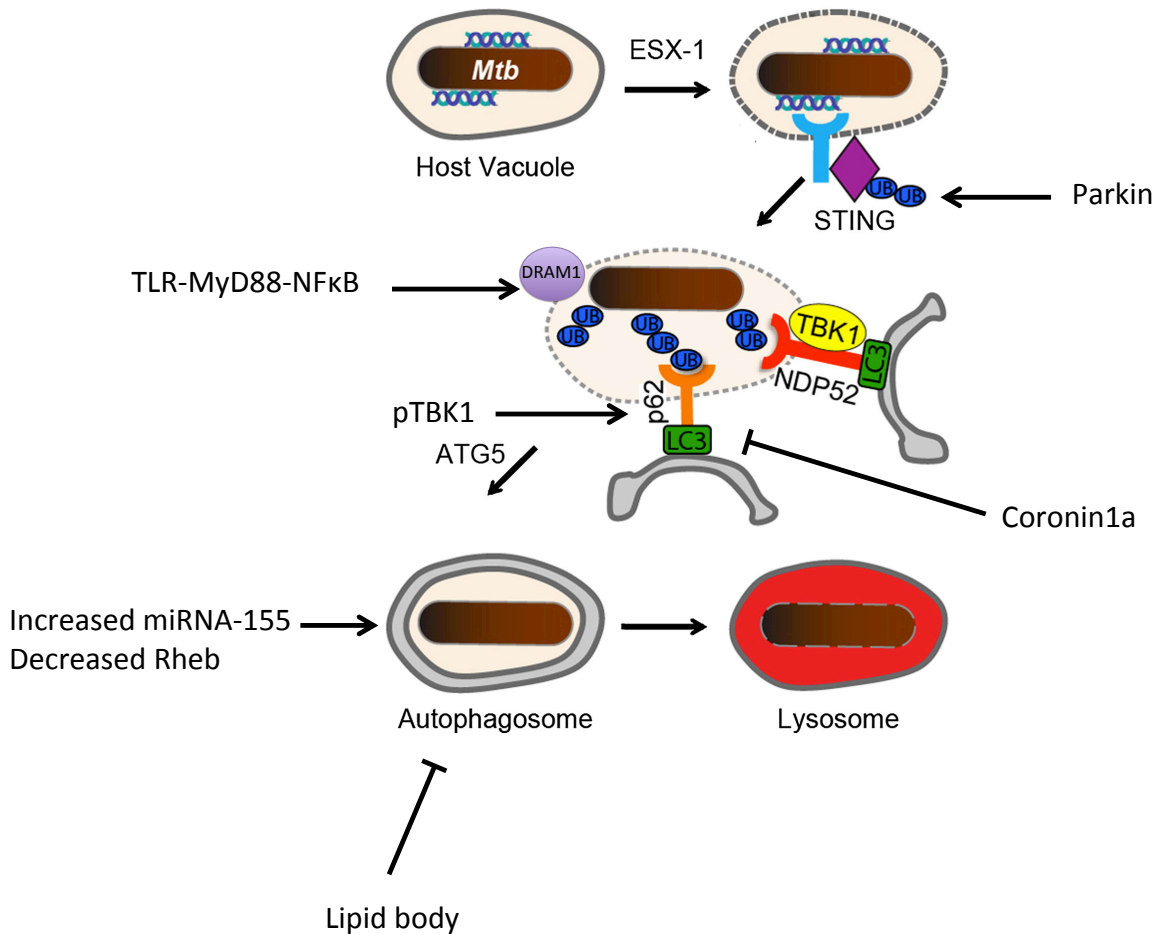


**Fig 11. Mechanisms involved in autophagy modulation by *Mtb***

Within the infected macrophage, *Mtb* induces phagosomal membrane damage in an ESX-1 dependent manner. This leads to recognition of *Mtb* extracellular DNA by the cytosolic receptor STING and the downstream phosphorylation and activation of TBK1. Phosphorylated TBK1 in turn phosphorylates the selective autophagy adaptor p62 and increases its affinity for ubiquitin that colocalize with the bacteria. Activation of the TLR-MyD88-NFκB axis by mycobacteria leads to DRAM1 recruitment to the phagosome that also contributes to p62 mediated autophagic clearance. TBK1 was also found to participate in recruitment of another selective autophagy adaptor NDP52. The ubiquitin ligase Parkin is required for the ubiquitination and targeting of *Mtb* to the autophagosome. *Mtb* infection also upregulates miRNA155 levels in the host cell which downregulate expression of Rheb, a negative regulator of autophagy. Atleast two mechanisms are employed by *Mtb* to negatively regulate autophagy induction. Recruitment of coronin1a to the *Mtb* containing phagosome limits LC3 accumulation. Alteration of host lipid metabolism by *Mtb* in an ESX1 dependent manner leads to lipid body accumulation that is associated with decreased autophagy induction.

Adapted from (150).

## 1.7 Hypervirulence

Virulence is defined as the ability of a pathogen to cause morbidity and mortality in the host. Pathogens possess a wide variety of genes that contribute to virulence - deletion/disruption of these virulence genes leads to attenuation. However, there are numerous reports in literature of “anti-virulence genes” whose deletion or disruption enhances the ability of the pathogen to cause disease and results in hypervirulence as measured by lower infectious dose, reduced clearance and decreased host survival time.

Retention of anti-virulence genes by pathogens indicates possible benefits of moderating virulence. Two hypotheses have been proposed (204). First, genes involved in restraining virulence may offer a survival advantage in environmental niches or specific hosts in case of pathogens with complex lifecycles. For instance, the *S.typhimurium* *pcgL* mutant is hypervirulent in mice. However *pcgL*, a D-Ala-D-Ala dipeptidase, allows the pathogen to utilize D-Ala-D-Ala released during peptidoglycan turnover as a sole carbon source and possibly provides a survival advantage in nutrient limiting non-host environments (205). Second, virulence moderation may allow prolonged host survival and thus maximize transmission. *Leishmania major* (*L.major*) cycles between amastigote forms in the human host and the highly infectious promastigote forms in the sandfly vector. *L.major ptr1* mutants exhibit elevated differentiation to promastigote forms and were found to be hypervirulent in mice. Retention of the *ptr1* gene may allow host survival and thus maximize transmission to the sandfly vector and augment spread of the pathogen (204).

### 1.7.1 Hypervirulence in Mtb

Hypervirulence in Mtb has been reported in clinical strains as well as in defined gene mutants. The main parameters of determining hypervirulence in Mtb are bacterial load in the lungs and median survival time of infected mice.

#### 1.7.1.1 Hypervirulent clinical Mtb strains

Mtb strains belonging to the Beijing genotype family represent approximately 50% of the strains prevalent in southeast and east Asia and 13% of the strains present worldwide (206). A Beijing strain HN878 was found to be more virulent than another member of the same family (NHN5) in immunocompetent mice, with higher bacterial burden in the lungs and shorter median survival times. HN878 suppressed the *in vivo* pro-inflammatory cytokine response, infected mice however were found to express higher levels of IFN $\alpha$  and intranasal administration of recombinant IFN $\alpha/\beta$  worsened the survival outcome (207). Increased *in vivo* type I IFN production has also been reported for another Beijing strain W4 (208). The hypervirulence of HN878 was linked to the presence of an intact *pks1-15* gene and the production of phenolic glycolipids (PGL) by the bacteria. Mice infected with the *pks1-15* mutant had a longer median survival time compared to HN878 infected animals (209). While PGL production is characteristic of the HN878 strain only, several members of the Beijing family were found to overproduce triglycerides compared to Mtb strains from other lineages and the laboratory strain H37Rv (210). A more recent study implicated the purinergic receptor P2X7R mediated macrophage necrosis in the increased virulence of the Beijing strain 1471 compared to H37Rv. Beijing 1471 induced higher levels of IL1 $\beta$  and IFN $\gamma$  in macrophages *ex vivo* and increased mortality in immunocompetent mice (211).

### 1.7.1.2 Hypervirulence in defined Mtb gene mutants

The mammalian cell entry 1 (*mce1*) operon is one of the first reported anti-virulence Mtb genes. The *mce1* operon comprises of 13 genes (*Rv0166-Rv0178*) and is thought to encode for an ATP binding cassette (ABC) transporter (212). Deletion of either *Rv0168* (*yrbE1B*) or *Rv0169* (*mce1A*) leads to disruption of the entire operon (213). The *mce1* operon mutant was found to be hypervirulent in immunocompetent BALB/c mice with increased lung bacterial burden and mortality observed compared to mice infected with Mtb (213). Another study performed in C57Bl6 mice demonstrated increased mortality of *mce1* mutant infected mice compared to Mtb infected control animals as well, however no differences were detected in the lung bacterial burdens (212). Contrary to the well defined nodular lesions observed in lungs of Mtb infected mice at 10-12 weeks post infection, lungs from *mce1* mutant infected mice exhibited poorly organized lesions (212,213). In *ex vivo* macrophage infections, the *mce1* mutant was found to inhibit TNF, IL6, MCP-1 and nitrite production compared to Mtb (213). Phylogenomic analysis revealed the presence of operons similar to *mce1* in the *Actinomycetales* family encoding for ABC transporters involved in lipid import. Using thin layer chromatography (TLC) and mass spectrometry approaches, the *mce1* mutant strain was found to accumulate an excess of free mycolic acids in the cell wall compared to either Mtb or complemented strains (214). Accumulation of mycolic acids in the cell wall could improve fitness of the bacteria against host generated toxic molecules (ROS, RNS) as well as modulate the host immune response. The *mce1* operon is negatively regulated in *ex vivo* macrophage infections (but not *in vitro* in liquid culture) by *mce1R* located immediately upstream of the operon (215). Paradoxically, the *mce1R* mutant was

also found to be hypervirulent in BALB/c mice. Histopathological examination of the lungs revealed that unlike the aberrant granulomatous response observed in *mce1* mutant infected mice, the lungs of *mce1R* mutant infected mice exhibited an enhanced granulomatous response (216). The contrasting pathology of mice infected with the *mce1* operon mutant and the *mce1R* mutant illustrate the delicate balance of interactions between Mtb and the host required for successful infection.

The two component response regulator *dosRS* is involved in the induction of approximately 50 genes in response to hypoxia and nitrogen stress, with *hspX* being the most prominently up-regulated gene. Deletion of *dosR* rendered Mtb hypervirulent both in SCID mice and immunocompetent DBA/2 mice (217). Deletion of *hspX* also rendered the bacteria hypervirulent in BALB/c mice with increased bacterial burdens being recovered from the mutant infected animals compared to those infected with Mtb. However no differences in lung pathology or lung cytokine profiles were observed. Overexpression of *hspX* completely reduced *dosR* mutant growth to WT levels *ex vivo* indicating that at least under these conditions lack of *hspX* accounts for the enhanced growth of the *dosR* mutant (218). Deletion of three other two component systems (*kdpDE*, *trcXY*, *trcRS*) has also been found to render Mtb hypervirulent (219).

Mtb also possesses 11 serine threonine protein kinases (STPK's) to help respond to extracellular stimuli. Of these, deletion of three STPK's (*pknH*, *pknE*, *pknI*) rendered the bacteria hypervirulent. Higher bacterial loads were recovered from lungs and spleen of BALB/c mice infected with the *pknH* mutant strain compared to organs from Mtb or complement infected mice during the chronic phase of infection. *pknH* regulates expression of *embAB* operon encoding for arabinosyl transferases required for

arabinogalactan and lipoarabinomannan synthesis and results in a high lipoarabinomannan/lipomannan (LAM/LM) ratio in the cell wall (220). A low LAM/LM ratio could possibly lead to a proinflammatory response during infection with the *pknH* mutant as lipomannan is known to provoke inflammatory cytokine production. The *pknH* mutant was also found to grow better *in vitro* in response to nitric oxide indicating that the gene possibly controls bacterial growth after the onset of the adaptive immune response (220). Similar to the *pknH* mutant, the *pknE* mutant strain is also more resistant to nitrogen stress *in vitro* and is hypervirulent with increased bacillary loads observed in infected guinea pig lungs (221). The *pknE* mutant was also found to be pro-apoptotic and anti-necrotic in *ex vivo* macrophage infections (222). The *pknI* mutant was found to be hypervirulent in SCID mouse survival studies (223). Aside from studies performed on defined Mtb mutants, hypervirulent Mtb mutants have also been reported from two different transposon library screens (217).

Several genes from different classes thus are reported to be involved in Mtb hypervirulence. Alteration of the mycobacterial cell wall appears to be a common theme underlying several hypervirulent mutants. Interestingly, a wide array of immunopathological responses to hypervirulent Mtb mutants is observed and this highlights the complex relationship that exists between Mtb and the host that allows for the establishment of a persistent infection.

| Gene name          | Gene number                       | Measure of virulence  |
|--------------------|-----------------------------------|---|
| <i>mce1</i> operon | <i>Rv0166-Rv0178</i>              | Increased lung bacterial burden; reduced MST in i.v. infected Balb/C mice               |
| <i>mce1R</i>       | <i>Rv0165c</i>                    | Increased lung bacterial burden; reduced MST in i.v. infected Balb/C mice               |
| <i>dosR</i>        | <i>Rv3133c</i>                    | Increased lung bacterial burden in i.v. infected DBA/2 mice                             |
| <i>hspX</i>        | <i>Rv2031c</i>                    | Increased lung CFU in i.v. infected Balb/C mice   |
| <i>kdpDE</i>       | <i>Rv1027c</i> and <i>Rv1028c</i> | Increase lung CFU in i.v. infected DBA/2 mice; Decreased MST in i.v. infected SCID mice |
| <i>trcXY</i>       | <i>Rv3765c</i> and <i>Rv3764c</i> | Increase lung CFU in i.v. infected DBA/2 mice; Decreased MST in i.v. infected SCID mice |
| <i>trcRS</i>       | <i>Rv1032c</i>                    | Increase lung CFU in i.v. infected DBA/2 mice; Decreased MST in i.v. infected SCID mice |
| <i>pknH</i>        | <i>Rv1266c</i>                    | Increased lung CFU in i.v. infected Balb/C mice   |
| <i>pknE</i>        | <i>Rv1743</i>                     | Increased lung CFU in subcutaneously infected guinea pigs                               |
| <i>pknI</i>        | <i>Rv2914c</i>                    | Reduced MST in i.v. infected SCID mice  |

**Table 2. List of hypervirulent *Mtb* gene deletion mutants**

Abbreviations: CFU – colony forming units; i.v. – intravenous; MST – median survival time; SCID – severe combined immunodeficiency

## 1.8 Summary

Mtb possesses several strategies to avoid the innate immune response of the host, one such strategy is modulation of cell death outcomes. The focus of research in our lab is to understand mechanisms by which Mtb manipulates host cell death. A screen for anti-apoptotic genes in Mtb led to the identification of *Rv3167c*, an annotated TetR like transcriptional regulator (unpublished data, work done by Jessica Miller and Serdar Gurses). The goal of this study was to identify the molecular mechanisms involved in *Rv3167c* mediated inhibition of host cell death. Work done towards this goal revealed that *Rv3167c* is required for inhibition of not apoptotic but rather necrotic host cell death and it does so by suppressing the generation of mitochondrial ROS and inactivation of Akt, these results are described in Chapter 2. Serendipitously, we also uncovered a role for *Rv3167c* in regulating Mtb mediated macroautophagy as well and explored possible mechanisms involved in this phenomenon, this work is described in Chapter 3. Finally we investigated the role of *Rv3167c* in Mtb virulence in mice and found that *Rv3167c* is an anti-virulence gene required for tempering virulence of Mtb, these results are described in Chapter 4.

## CHAPTER 2. *Rv3167c* IS REQUIRED FOR NECROSIS INHIBITION

### 2.1 INTRODUCTION

Modulation of host cell death via apoptotic and necrotic mechanisms is one of the several strategies Mtb employs in order to evade the host innate immune response. Previous studies have shown that while Mtb inhibits apoptosis, the pathogen after infection and multiplication induces necrosis in order to escape from infected cells (reviewed in 49). Modulation of host cell eicosanoid generation by Mtb favoring production of LXA4 over PGE2 has been found to contribute to necrosis induction via three mechanisms – loss of mitochondrial membrane potential, inhibition of plasma membrane repair and inhibition of apoptotic envelop formation (Fig 7) (102,105,106). Other mechanisms implicated in Mtb induced necrosis include high intracellular bacillary load, activation of NLRP3 inflammasome and escape of the pathogen from the phagosome to the cytosol of the host cell (Fig 7) (21,32,42,107,108).

The Mtb gene *Rv3167c* was previously identified as an anti-apoptotic gene in our lab (unpublished data). In this study we determined that *Rv3167c* is required for the inhibition of Mtb induced caspase independent, necrotic cell death. The *Rv3167c* mutant strain ( $\Delta 3167c$ ) induced higher levels of necrosis in macrophages compared to Mtb or the complement strain. Using a combination of chemical inhibitors and bone marrow derived macrophages from different knock-out mice, we screened for host factors required for  $\Delta 3167c$  mediated cell death and were able to eliminate involvement of known regulated necrosis pathways. Necrosis induction by  $\Delta 3167c$  was however found to be dependent on reactive oxygen species (ROS) generated by mitochondria.

## 2.2 MATERIALS AND METHODS

### 2.2.1 Materials

*M.tuberculosis* H37RV (ATCC 25618) was obtained from ATCC. *Rv3167c* mutant ( $\Delta$ 3167c) and complement strains were generated in the H37Rv background by Jessica Miller and Serdar Gurses respectively. C57Bl6, *Nox2*<sup>-/-</sup>, *Casp3*<sup>-/-</sup>, Harlequin mice and matched wildtype controls and mCAT transgenic mice were purchased from Jackson Laboratories. *RIPK3*<sup>-/-</sup> mice were sourced from Genentech. *Parp1*<sup>-/-</sup> mice, *Casp1/11*<sup>-/-</sup> mice, *Ifn $\beta$* <sup>-/-</sup> mice were kind gifts from Dr.Ted Dawson, Dr.Denise Monack and Dr.Stefanie Vogel respectively. Immortalized wild type, *Nlrp3*<sup>-/-</sup> and *Trif*<sup>-/-</sup>*MyD88*<sup>-/-</sup> BMDM's were obtained from Dr.Igor Brodsky. *Il1r1*<sup>-/-</sup>, *Tnfr1*<sup>-/-</sup>, *Trif*<sup>-/-</sup> and *MyD88*<sup>-/-</sup> mice were kind gifts from Dr. Katrin Mayer-Barber. THP1 monocytes were obtained from ATCC (TIB 202). THP1shASC and THP1shASC control cells were a kind gift from Dr.Jenny Ting. zVAD-fmk, Ca074Me, Necrostatin 1 (Nec1) and Diphenyl iodonium (DPI) were purchased from Calbiochem. Chlorpormazine hydrochloride, BafilomycinA1, Pepstatin A, glutathione and N-acetyl cysteine (NAC) were sourced from Sigma. Antibodies used in this study and their sources are listed in Appendix A.

### 2.2.2 Bacterial culture

Bacterial strains were grown in 7H9 medium supplemented with 10% ADC, 0.5% glycerol and 0.05% Tween 80 at 37°C. Cultures were constantly shaken at 100rpm to inhibit bacterial clumping. Hygromycin (50 $\mu$ g/ml) and kanamycin (40 $\mu$ g/ml) were added to the mutant and complement cultures respectively. For infection, cultures with an OD<sub>600</sub> between 0.6-0.8 (corresponding to the late log phase of growth) were pelleted by centrifugation at 2000g for 7 minutes and resuspended in 0.05% PBS-Tween 80.

Following another spin at 80g for 3 minutes to pellet bacterial clumps, bacteria present in the supernatant were added to cells.

### **2.2.3 Cell culture and infection**

THP1 monocytes were maintained in RPMI 1640 supplemented with 10% heat inactivated FCS. Cells were differentiated with 20ng/ml PMA for 20-24 hours, washed with PBS followed by addition of infection media consisting of RPMI growth medium supplemented with 5% human serum (Sigma-Aldrich). Bacteria were added to cells at MOI3 for 4 hours at 37°C, following which extracellular bacteria were removed by PBS washes and chase medium consisting of growth medium and 100µg/ml gentamicin was added.

Human monocyte derived macrophages (HuMDM's) were prepared from elutriated monocyte fractions obtained from Dr. Bruno Andrade at National Institutes of Health, Bethesda, MD. Monocyte fractions were washed twice in cold RPMI and seeded in serum free RPMI for 1 hour at 37°C. Non-adherent cells were removed and adherent cells were differentiated in medium containing 5% off-the-clot AB human serum (Gemini) and 10ng/ml human MCSF (Peprotech) for 7 days. Cells were infected as indicated above in RPMI containing 5% human serum and chased in growth medium containing gentamicin. An MOI of either 5 or 10 was used for infection of HuMDM's

Bone marrow derived macrophages (BMDM's) were prepared from cells obtained from femurs and tibia of various mouse strains using DMEM supplemented with 10% heat inactivated FCS, 25% L929 supernatant and 1% Penicillin-Streptomycin (124). Growth medium was replaced with DMEM containing 10% non-heat inactivated FCS for 4hrs and cells were infected in same medium in the manner described above. BMDM's

were infected at MOI 10. Chase media contained 10% L929 supernatant in order to avoid cell death induction due to cytokine withdrawal. Immortalized BMDM's were maintained in DMEM containing 10% heat inactivated FCS and infected in media similar to that used for primary BMDM's.

Inhibitors and neutralizing antibodies when used were added to cells 1 hour prior to infection and included in chase medium unless otherwise stated. For all experiments, 0 hpi time point refers to end of infection period when cells have been exposed to bacteria for 4 hours. For all assays that required cells and bacteria to be brought out from the BSL-3 facility, 4% PFA fixation was performed overnight to ensure non-viability of bacteria.

#### **2.2.4 Determination of *invitro* bacterial growth rate**

To measure *invitro* bacterial growth, bacteria were added to 7H9 medium to obtain a starting OD<sub>600</sub> of 0.01 and OD<sub>600</sub> measurements were made at 24 hour intervals until 7 days.

#### **2.2.5 Determination of bacterial uptake and *ex vivo* bacterial growth**

For measuring bacterial uptake, at 0 hpi cells were fixed with 4% PFA and stained using TB Stain Kit ZN (BD Bioscience) as per manufacturers instructions. Briefly, slides were flooded with carbolfuchsin ZN and heated until steaming. Cells were then treated with TB Decolorizer for 2 minutes to get rid of excess stain and finally counterstained with methylene blue for 30 seconds. Cells were observed using a phase contrast microscope (Zeiss AxioObserver) and number of uninfected and infected cells enumerated.

*Ex vivo* growth of bacteria was determined by infecting THP1 macrophages at

MOI 0.5 and chasing the infection in gentamicin free medium. At indicated time points post infection, cells were lysed with 0.1% Triton X 100 in PBS and appropriate dilutions were plated on 7H11 medium in triplicate. Inoculated plates were incubated at 37°C and colonies were counted approximately 2 weeks after plating.

### **2.2.6 DNA fragmentation assays**

DNA fragmentation was visualized by staining cells with propidium iodide (PI) and Hoechst stain at 6hpi, 12hpi and 24hpi. Cells were infected on 8 well slides, stained with 1µg/ml PI for 10 minutes at room temperature and fixed with 4% PFA overnight. This was followed by staining with 10µg/ml Hoechst 33342 for 3 minutes. Cells were observed using a fluorescence microscope (Zeiss AxioObserver) and numbers of cells exhibiting nuclear fragmentation; nuclear condensation and nuclear staining with PI were enumerated.

DNA laddering pattern was determined by preparing DNA from infected cells using the Apoptotic DNA Ladder Kit (Roche) at 24hpi. As a positive control, DNA was prepared from THP1 monocytes treated with 1µM of staurosporine for 4 hours. U937 cell extract provided in the kit was also used as a positive control. 2µg of each DNA sample was run on 1.8% TBE-agarose gel and stained with ethidium bromide.

### **2.2.7 Cell death assays**

TUNEL assay was performed to detect DNA fragmentation in infected cells using the InSitu Cell Death Detection Kit (Roche). Infected cells fixed with 4% PFA overnight were washed and permeabilized at 4°C for 4 minutes in a 0.1% sodium citrate, 0.1% Triton X-100 buffer. Cells were then stained with the TUNEL stain at 37°C for 1 hour,

washed and resuspended in FACS buffer (2% FCS in PBS). Percentage of TUNEL positive cells was determined by flowcytometry (Accuri or FACSCantoII).

During cell death, fragmented nuclear DNA is eventually lost from the cell and this can be detected by hypodiploid staining (125). Infected cells were fixed overnight in 70% ethanol at -20°C, washed and stained with PI/RNase staining buffer (BD Pharmingen) for 10 minutes at room temperature. Percentage of hypodiploid cells was determined by flowcytometry (Accuri or FACSCantoII).

Increase in plasma membrane permeability was determined by performing propidium iodide (PI) staining, as the stain cannot enter cells with intact plasma membranes. Following infection, cells were harvested at specified time points and resuspended in PBS containing 5% FCS and 1µg/ml PI for 10 minutes at room temperature. Percentage of PI positive cells was determined by flowcytometry (Accuri).

Detection of adenylate kinase activity in cell culture supernatants using the ToxiLight™ Bioassay kit (Lonza) was employed to determine increase in plasma membrane permeability. 20µl of supernatants from infected cells were mixed with 100µl of adenylate kinase detection reagent and incubated at room temperature for 5 minutes. Changes in luminescence were measured using a Biotek Synergy 4 plate reader.

### **2.2.8 DIOC<sub>6</sub> staining**

DIOC<sub>6</sub> staining was utilized to determine loss of mitochondrial membrane potential. Cells were stained with 40nM of DIOC<sub>6</sub> (Molecular Probes) at 37°C for 15 minutes in complete medium. Following harvesting and PBS wash, cells were stained with 1µg/ml PI in FACS buffer for 10 minutes and analyzed by flowcytometry (Accuri).

### **2.2.9 Preparation of whole cell lysates, cytoplasmic, mitochondrial and nuclear fractions**

Whole cell lysates were prepared by lysing cells in RIPA buffer (50mM Tris HCl, 150mM NaCl, 1% Triton X100, 0.5% sodium deoxycholate, 0.1% SDS) followed by centrifugation at 12,000g for 5 minutes to remove debris.

Mitochondrial fractions were prepared as described previously (126) by lysing cells in CLAMI buffer (250mM sucrose, 70mM KCl, 200µg/ml digitonin) followed by centrifugation at 1000g for 5 minutes. The supernatant (cytosolic fraction) was separated and the pellet containing intact mitochondria were lysed in RIPA buffer to obtain the mitochondrial fraction.

Nuclear fractions were prepared using the NE-PER Nuclear and Cytoplasmic Extraction Reagents (Thermo Scientific) as per manufacturer's instructions.

All fractions were prepared at 4°C and protease inhibitor cocktail (Complete, Mini, EDTA-Free, Roche) and phosphatase inhibitor cocktail (PhosSTOP, Roche) were included in the lysis buffers.

### **2.2.10 Western Blotting**

Prior to western blotting, protein concentrations of the samples were determined using the Pierce™ BCA Protein Assay Kit (Thermo Scientific) as per manufacturers instructions. Equal amounts of samples (10-20µg) were resolved on Criterion™ TGX™ Precast Gels (Bio-Rad). Proteins were transferred onto PVDF membrane (100V, 1 hour) and membranes were blocked using 5% milk in Tris buffered saline containing 0.1% Tween 20 (TBST) for 1 hour. All primary antibody incubations were performed

overnight at 4°C while secondary antibody incubations were carried out at room temperature for one hour.

### **2.2.11 Measurement of LXA<sub>4</sub> and PGE<sub>2</sub>**

For detection of LXA<sub>4</sub> and PGE<sub>2</sub> in supernatants from THP1 cells infected in OptiMEM were collected and ELISA's were performed. Kits were obtained from Oxford Biochemicals.

### **2.2.12 Measurement of cellular and mitochondrial ROS levels**

For measurement of ROS levels in BMDM's, cells were deprived of L929 supernatant in phenol red free medium for 16 hours prior to infection to lower basal levels of ROS (127). Infection and chase were performed under these conditions as well. CM-H2DCFDA (Molecular Probes) was used for detection of cellular ROS and MitoSOX™ Red (Molecular Probes) was utilized to assess mitochondrial ROS levels. At indicated time points after infection, cells were harvested and stained with 10µM CM-H2DCFDA or 1.25µM MitoSOX™ Red for 30 minutes at 37°C in HBSS. Cells were washed in HBSS, resuspended in FACS buffer and fluorescence intensity measured by flowcytometry (Accuri). For each time point, fluorescence intensity of uninfected cells was subtracted from that of the samples and percentage increase in fluorescence intensity compared to uninfected cells was calculated.

### **2.2.12 Statistical analysis**

ANOVA with Tukey post-test was used for statistical analysis unless otherwise indicated. Data is represented as mean ± SD. p-value significance is as follows – p ≤ 0.05 - \*, p ≤ 0.01 - \*\*, p ≤ 0.0001 - \*\*\*.

## **2.3 RESULTS AND DISCUSSION**

### **2.3.1 Characterization of the *Rv3167c* mutant ( $\Delta 3167c$ )**

#### **2.3.1.1 $\Delta 3167c$ does not have *invitro* growth defects**

*Rv3167c* was previously identified in a gain of function genetic screen for anti-apoptotic genes of Mtb (Velumurugan K, unpublished). The role of *Rv3167c* in host cell death inhibition was confirmed by generating the *Rv3167c* knockout strain in the Mtb H37Rv background ( $\Delta 3167c$ ) (Miller J, Gurses S, unpublished). In order to ensure that any effects seen in host cells infected with  $\Delta 3167c$  were not due to bacterial growth defects, the growth of the mutant was compared with wild type Mtb. Both strains were inoculated into 7H9 liquid medium at a starting OD<sub>600</sub> of 0.01 and OD<sub>600</sub> measurements were made every 24 hours. No differences were observed in the *invitro* growth of Mtb and  $\Delta 3167c$  at any of the time points (Fig 12A).

Therefore, any effects exerted by  $\Delta 3167c$  on host cells cannot be attributed to *invitro* growth differences compared to Mtb.

#### **2.3.1.2 Uptake of Mtb and $\Delta 3167c$ by host cells is similar**

Increased host cell death induction by  $\Delta 3167c$  could possibly be due to increased phagocytic uptake of the bacteria compared to Mtb. Therefore, the rate of infection of host cells by Mtb and  $\Delta 3167c$  was determined. HuMDM's were infected with Mtb and  $\Delta 3167c$  at MOI 5 and at 4 hours post infection (hpi), cells were washed and fixed with 4% PFA. Ziehl-Neelsen's staining was performed and the numbers of uninfected and infected cells were enumerated. Both Mtb and  $\Delta 3167c$  infected approximately 80% of

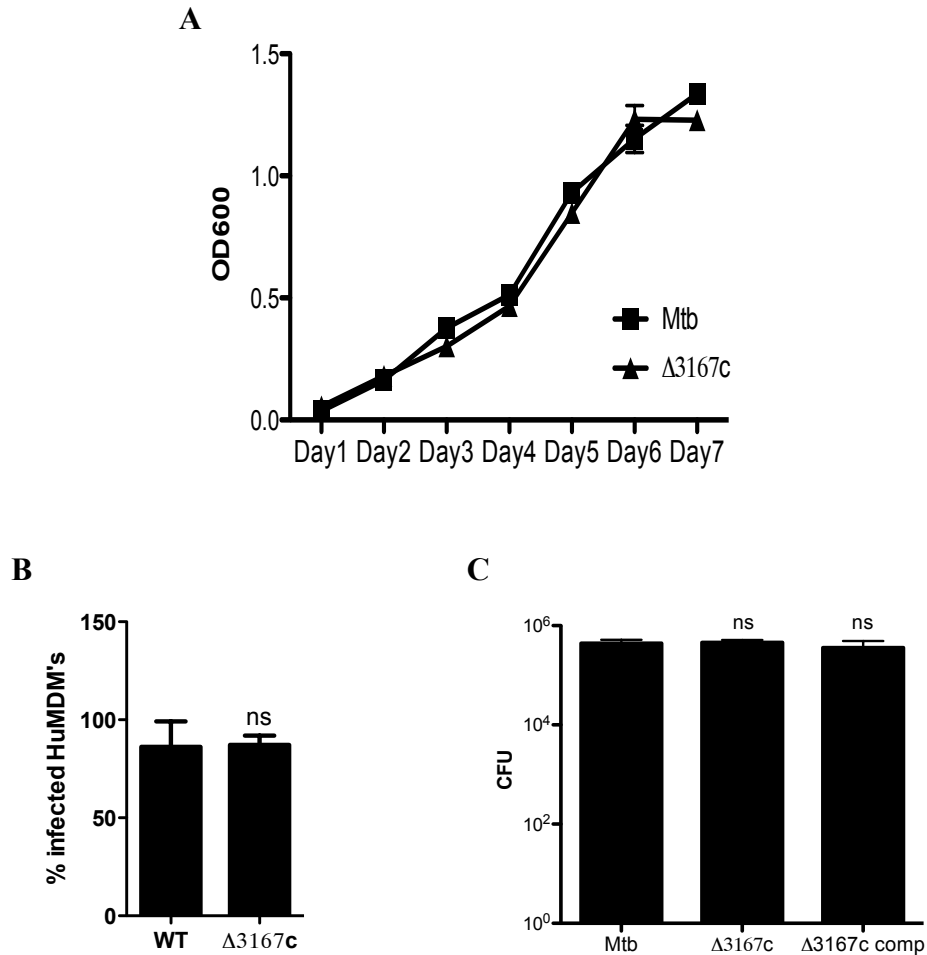


**Fig 12. Deletion of *Rv3167c* does not affect *in vitro* growth of Mtb and Mtb uptake by macrophages**

- (A) Growth rate of Mtb and  $\Delta 3167c$  in 7H9 medium was measured every 24 hours. Data is from three independent experiments (n=3).
- (B) Percentage of infected HuMDM's was determined by Ziehl-Neelsen's staining of infected macrophages. At least 400 macrophages were enumerated per condition. Data is from two independent experiments (n=2).
- (C) Uptake of indicated bacterial strains by THP1 cells was determined by estimating bacterial CFU's at 4hpi. Data is from three independent experiments (n=9).

Statistical significance was estimated relative to Mtb infected cells.

HuMDM's (Fig 12B). Uptake of the bacterial strains by THP1 macrophages was also determined. THP1 macrophages were infected at MOI 0.5 with Mtb,  $\Delta 3167c$  and complement strains. At 4hpi, cells were lysed and appropriate dilutions were plated onto 7H11 media. Colonies were enumerated approximately 2 weeks after plating and colony forming units (CFU) calculated. Similar CFU's were recovered from cells infected with Mtb,  $\Delta 3167c$  and the complement strain (Fig 12C).

These results indicate that deletion of the *Rv3167c* gene does not affect uptake of Mtb by macrophages.

### **2.3.1.3 $\Delta 3167c$ induces cell death in both cell lines and primary macrophages**

The gain of function genetic screen for Mtb anti apoptotic genes that led to the identification of *Rv3167c* was performed in THP1 macrophages. 83.40% of THP1 macrophages infected with  $\Delta 3167c$  are TUNEL positive compared to 15.75% of Mtb infected macrophages. Complementation of *Rv3167c* reduces cell death induction to levels similar to that of Mtb (Fig 13A) (Gurses S, unpublished). To ensure that the ability of  $\Delta 3167c$  strain to induce cell death was not restricted to a particular cell type, cell death induction by  $\Delta 3167c$  was determined in HuMDM's and BMDM's. HuMDM's were infected at MOI 10 and cell death levels were measured by performing hypodiploid stain at 48hpi. During cell death, DNA undergoes fragmentation and is eventually lost from the cell. The hypodiploid stain differentiates cells with normal DNA content from those with reduced DNA content.  $\Delta 3167c$  induces approximately 7 fold higher level of cell death compared to Mtb (63.42% vs 9.14%) in HuMDM's and complementation of *Rv3167c* rescues the phenotype (Fig 13B). BMDM's were infected at MOI 10 and TUNEL

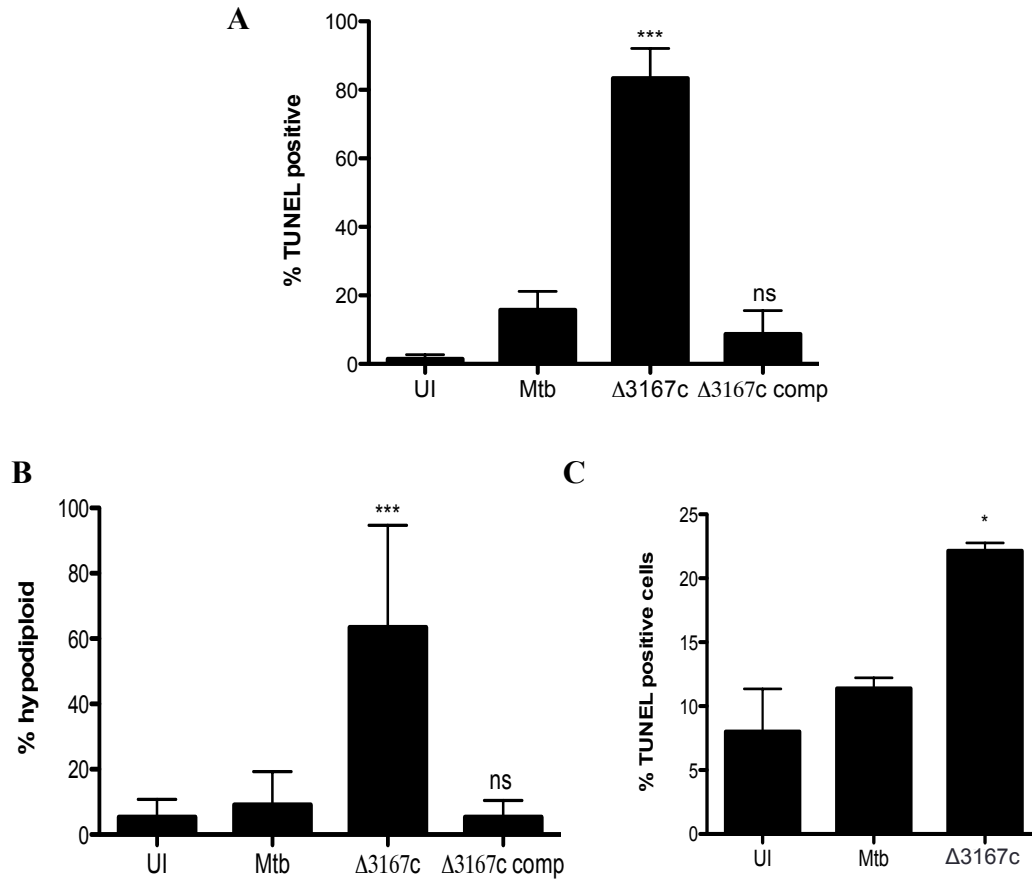


**Fig 13.  $\Delta 3167c$  induces cell death in both cell lines and primary macrophages**

- (A) Cell death induction in THP1 cells at 24hpi measured by TUNEL staining and flowcytometry. Data is from three independent experiments (n=6).
- (B) Cell death induction in HuMDM's at 48hpi measured by hypodiploid staining and flowcytometry. Data is from three independent experiments (n=6).
- (C) Cell death induction in BMDM's at 24hpi measured by TUNEL staining and flowcytometry. Data is from two independent experiments (n=4).

Statistical significance was estimated relative to Mtb infected cells.

staining was performed at 24hpi to determine cell death levels. Approximately 2-fold increase in cell death induction by  $\Delta 3167c$  was observed in comparison to Mtb (Fig 13C).

Therefore,  $\Delta 3167c$  is able to induce cell death in both cell lines as well as human and murine primary macrophages.

#### **2.3.1.4 $\Delta 3167c$ strain replicates similar to Mtb *ex vivo***

Host cell death by apoptosis has been reported to reduce mycobacterial viability in *ex vivo* macrophage infections (49,95,97). As *Rv3167c* was identified in a screen for anti apoptotic genes, intracellular viability of  $\Delta 3167c$  and the complement strain was compared to Mtb. THP1 macrophages were infected at MOI 0.5 and chased in antibiotic free medium to prevent killing of any bacteria that may be released after cell death. Cells were lysed at indicated time points and the lysates were plated on 7H11 plates. Colonies were enumerated 2 weeks later and CFU's were calculated. Similar CFU's were recovered from macrophages infected with any of the three strains at all time points (Fig 14).

These results demonstrate that the intracellular viability of  $\Delta 3167c$  is similar to Mtb even though the mutant strain induces much higher levels of cell death. This brings into question the mode of cell death induced by  $\Delta 3167c$ .

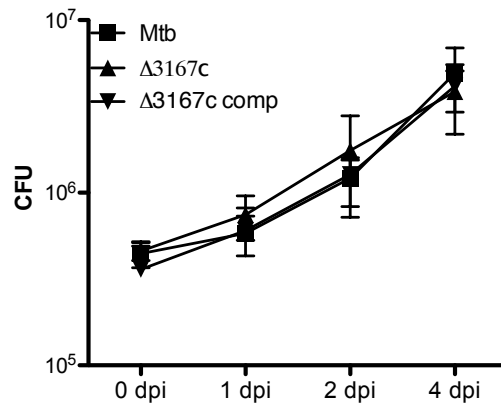


**Fig 14. Δ3167c strain replicates similar to Mtb *ex vivo***

THP1 cells infected at MOI 0.5 were lysed at the indicated time points and plated on 7H11 media. Colonies were enumerated and CFU estimated. Data is from three independent experiments (n=9).

## **2.3.2 $\Delta$ 3167c induces necrotic cell death**

### **2.3.2.1 $\Delta$ 3167c induces host cell membrane rupture**

A characteristic feature of cells undergoing apoptosis is preservation of cell membrane integrity. Contents of apoptotic cells are packaged in apoptotic vesicles and released. This is in contrast to necrotic cells that undergo membrane rupture and spill their contents into the extracellular milieu (55). To determine whether  $\Delta$ 3167c induces apoptotic or necrotic cell death, THP1 macrophages were infected with Mtb and  $\Delta$ 3167c at MOI 3. At the indicated time points cells were stained with the membrane impermeable stain PI and percentage of PI positive cells was determined by flowcytometry. A time dependent increase in the percentage of PI positive cells was observed for  $\Delta$ 3167c infected macrophages compared to Mtb infected macrophages (Fig 15A). Supernatants collected from Mtb,  $\Delta$ 3167c and complement infected cells at the indicated time points were used for the toxilight assay that measures adenylate kinase activity. Adenylate kinase is present within healthy cells and is released upon necrotic cell death due to loss of membrane integrity. Results are represented as fold change in adenylate kinase activity with respect to uninfected (UI) cells. At 24hpi and 48hpi, an approximately three fold higher level of adenylate kinase activity was detected in supernatants of  $\Delta$ 3167c-infected cells compared to those infected with either Mtb or the complement (Fig 15B). Mtb infected macrophages also undergo necrotic cell death (albeit at levels lower than  $\Delta$ 3167c infected cells) as determined by both PI staining and toxilight assay (Fig 15A, 15B). Mtb has been previously shown to induce necrosis in a dose and time dependent manner (107) and our data supports this observation.

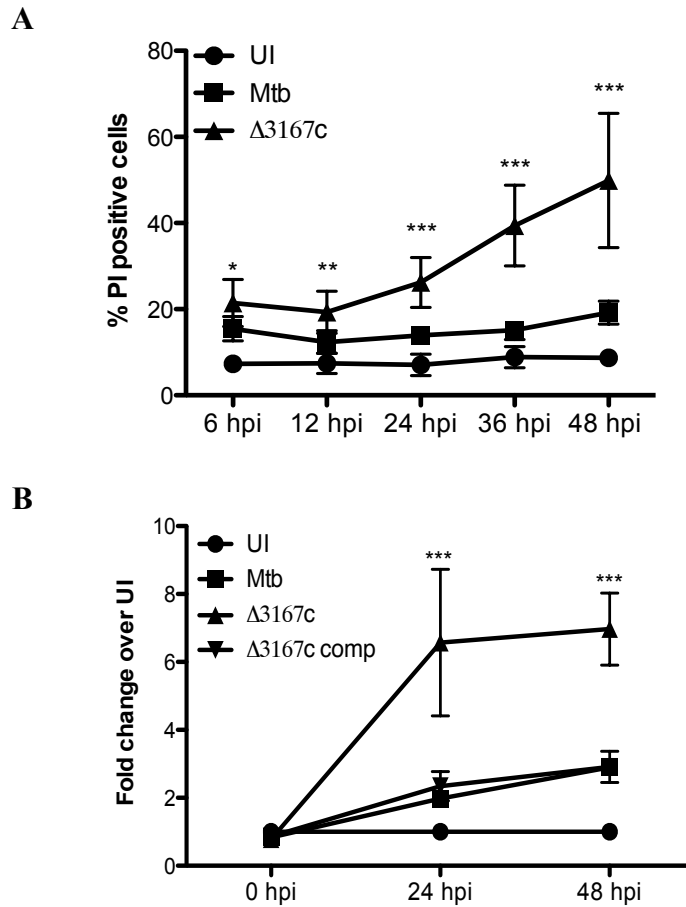


**Fig 15.  $\Delta 3167c$  infected cells lose plasma membrane integrity**

- (A) Infected THP1 cells were stained with PI at the indicated time points and percentage of PI positive cells determined by flowcytometry. Data is from three independent experiments (n=6).
- (B) Release of adenylate kinase into supernatants from uninfected and infected THP1 cells was measured by toxilight assay. Data is from three independent experiments (n=6).

Statistical significance was estimated relative to Mtb infected control.

Therefore,  $\Delta 3167c$  induces higher levels of host cell membrane damage compared to Mtb, which is indicative of necrotic cell death induction.

### **2.3.2.2 Non apoptotic DNA fragmentation is seen during $\Delta 3167c$ mediated cell death**

Although apoptotic cells do not lose membrane integrity, in the absence of phagocytic uptake these cells can proceed to secondary necrosis. Cells undergoing secondary necrosis have permeable membranes (57). Therefore using state of cell membrane permeability as the sole indicator of primary necrotic cell death is unwise. One of the earliest changes detectable in a cell undergoing apoptosis are nuclear changes – namely condensation and fragmentation (56). To determine the kinetics of nuclear changes and loss of membrane permeability, macrophages infected with  $\Delta 3167c$  were stained with PI and Hoechst at 6hpi, 12hpi and 24hpi and cells were observed using a fluorescence microscope. Percentage of cells that exhibited nuclear condensation (pyknosis) and fragmentation (karyorrhexis) alone or in combination with membrane permeability was calculated. Infected cells exhibited nuclear changes either alone or in combination with increased membrane permeability as early as 6 hpi. Percentage of  $\Delta 3167c$  infected cells exhibiting these changes was higher than those infected with either Mtb or the complement at 24hpi. Only a minor fraction of cells detected at all the time points were PI positive alone (Fig 16A).

During apoptosis, genomic DNA is fragmented between nucleosomes to generate fragments that are multiples of 180-200 base pairs in size via the activity of a caspase activated DNAase (CAD) (54). These fragments form a ladder like pattern when run on an agarose gel. As  $\Delta 3167c$  infected cells undergo nuclear fragmentation, the pattern of DNA fragmentation was analyzed. Genomic DNA of  $\Delta 3167c$  infected cells was prepared

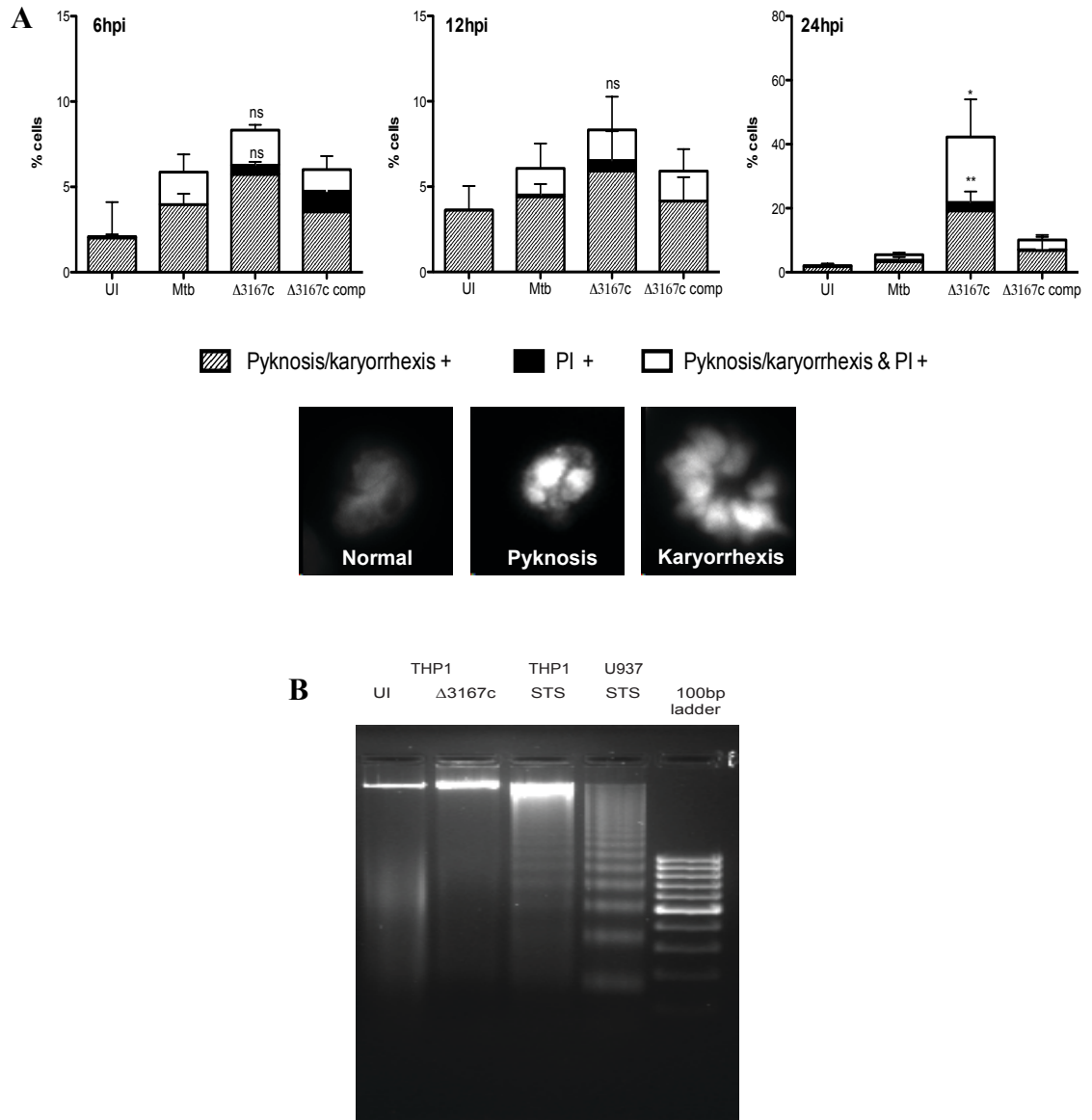


**Fig 16. Δ3167c induces non – apoptotic DNA fragmentation**

- (A) Infected THP1 cells were stained with Hoechst-PI and observed by fluorescence microscopy. At least 400 cells were counted and percentage of cells exhibiting nuclear changes and PI positivity alone or together was estimated. Data is from three independent experiments (n=3). Statistical significance was estimated relative to Mtb infected control.
- (B) Genomic DNA prepared from infected cells was run on a 1.8% agarose gel to look for DNA laddering. STS - staurosporine. Image is representative of three independent experiments.

using the Roche Apoptotic DNA Ladder Kit and resolved on a 1.8% TBE agarose gel. As a positive control, genomic DNA from THP1 monocytes treated with staurosporine (a classical apoptosis inducer) was prepared. Genomic DNA from U937 monocytes treated with staurosporine (provided with the kit) was also used as a positive control. DNA from both the positive control samples form a ladder like pattern in the agarose gel (Lane 3 and 4, Fig 16B). In contrast, no such pattern is detected in DNA prepared from  $\Delta 3167c$ -infected cells (Lane 2, Fig 16B).

These results indicate that genomic DNA of macrophages infected with  $\Delta 3167c$  undergoes fragmentation. However, the fragmentation pattern is not similar to that induced during apoptotic cell death.

### **2.3.2.3 $\Delta 3167c$ induced cell death is caspase independent**

Apoptotic stimuli lead to the caspase activation cascade comprising of the activator caspases (caspase 8 and 9) and the effector caspases (caspase 3, 6 and 7) (52). Role of caspases in  $\Delta 3167c$  induced cell death was assessed by using *Casp3*<sup>-/-</sup> BMDM's. Cells were infected at MOI 10 and percentage of TUNEL positive cells was determined by flowcytometry. Approximately 70% of both wild type and *Casp3*<sup>-/-</sup> BMDM's infected with  $\Delta 3167c$  were TUNEL positive (Fig 17A). To ensure that the lack of a phenotype in the *Casp3*<sup>-/-</sup> BMDM's was not due to redundancy of caspase 3 functions with other effector caspases, both wild type and *Casp3*<sup>-/-</sup> BMDM's were infected with  $\Delta 3167c$  in the presence of the pan-caspase inhibitor zVAD-fmk and TUNEL staining was performed at 24hpi. Inclusion of zVAD-fmk did not inhibit  $\Delta 3167c$  mediated cell death in *Casp3*<sup>-/-</sup> cells (Fig 17A). Rather, a marginal increase was seen in the percentage of TUNEL positive cells following addition of the inhibitor. zVAD-fmk activity was assessed by

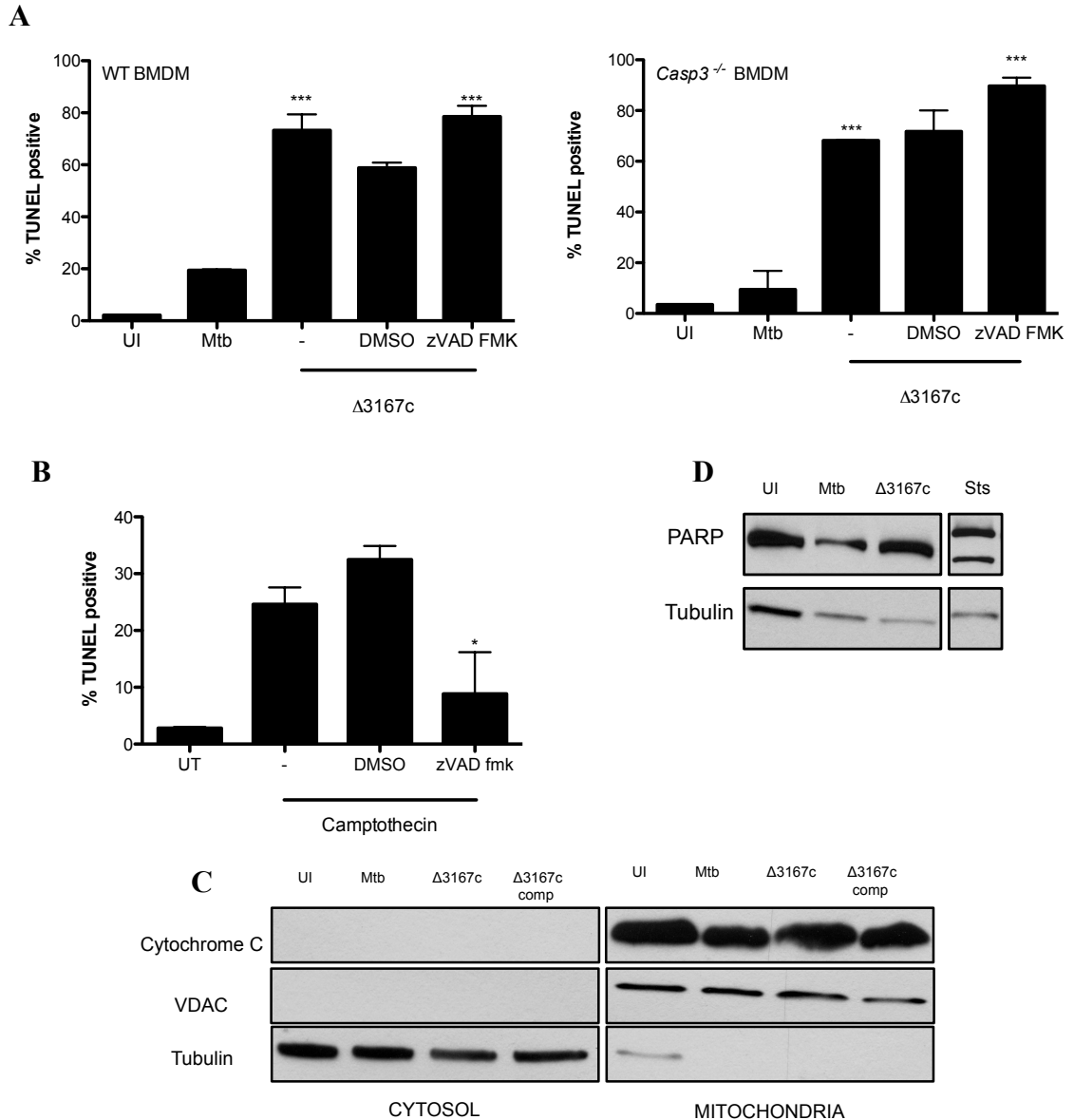


**Fig 17.  $\Delta 3167c$  induces caspase independent cell death**

- (A) Cell death induction in WT and *Casp3*<sup>-/-</sup> BMDM's was determined by TUNEL staining and flowcytometry at 24hpi. zVAD-fmk was used at a 40 $\mu$ M concentration. Data is representative of three independent experiments (n=3).
- (B) Efficacy of zVAD-fmk in camptothecin treated THP1 cells was determined by TUNEL staining and flowcytometry. Data is representative of one experiment (n=3).
- (C) Cytochrome C translocation from mitochondria to cytosol was determined by western blotting. VDAC and tubulin are loading controls for mitochondria and cytosolic fractions respectively. Data is representative of two independent experiments.
- (D) PARP1 cleavage in infected THP1 cells at 24hpi. Sts – staurosporine. Data is representative of three independent experiments.

For (A), statistical significance was estimated relative to Mtb. For (B), statistical significance was estimated relative to solvent control.

adding the inhibitor to THP1 macrophages treated with camptothecin, a widely used apoptosis inducer. Inclusion of the inhibitor reversed camptothecin mediated cell death as measured by TUNEL staining (Fig 17B).

Cytochrome C release from mitochondria is observed in avirulent mycobacteria infected macrophages undergoing caspase dependent apoptosis (104). Cytosolic cytochrome C in association with Apaf forms the apoptosome complex that leads to downstream caspase 9 processing. Translocation of mitochondrial CytC to the cytosol was examined by immunoblotting of mitochondrial and cytosolic fractions of infected THP1 macrophages at 24hpi. No CytC was detected in cytosolic fraction of either Mtb or  $\Delta 3167c$  infected macrophages (Fig 17C).

PARP1 is a nuclear enzyme utilized for repair of breaks in DNA and it's cleaved during apoptosis. PARP1 cleavage in Mtb and  $\Delta 3167c$  infected THP1 cells was determined by preparing whole cell lysates at 24hpi and immunoblotting for PARP1. As expected, PARP1 cleavage was seen in THP1 macrophages treated with staurosporine. However, no PARP1 cleavage was seen in macrophages infected with either Mtb or  $\Delta 3167c$  (Fig 17D).

These results demonstrate that cell death induction by  $\Delta 3167c$  is caspase independent.

### **2.3.3 Molecular mechanisms of $\Delta 3167c$ induced necrosis**

#### **2.3.3.1 Necrosis induction by $\Delta 3167c$ does not involve LXA<sub>4</sub> and PGE<sub>2</sub>**

The balance between the host cell lipid mediators lipoxin A<sub>4</sub> (LXA<sub>4</sub>) and prostaglandin E<sub>2</sub> (PGE<sub>2</sub>) plays a critical role in determining mode of mycobacteria mediated cell death. Virulent Mtb upregulates LXA<sub>4</sub> levels in infected cells that in turn

inhibits PGE<sub>2</sub> production and induces necrosis (102,105,106). The role of LXA<sub>4</sub> and PGE<sub>2</sub> in Δ3167c-induced necrosis was examined by determining the levels of these lipid mediators in the supernatants of infected THP1 macrophages harvested at 24hpi. LXA<sub>4</sub> levels in supernatants of Mtb, Δ3167c and complement infected cells were similar to background levels detected in the supernatant of uninfected cells (Fig 18A, 18B). Higher PGE<sub>2</sub> levels were detected in supernatants of infected macrophages compared to the uninfected control. However similar amounts of PGE<sub>2</sub> were detected in supernatants of macrophages infected with Mtb, Δ3167c and the complement strain (Fig 18C). Contribution of LXA<sub>4</sub> was also assessed by PI staining of *Alox5*<sup>-/-</sup> BMDM's (deficient in 5-lipoxygenase and thus unable to synthesize LXA<sub>4</sub>) infected at MOI 10. Necrosis induction by Δ3167c reduced marginally from 59.63% in wild type cells to 49% in *Alox5*<sup>-/-</sup> cells. Although Mtb induced higher levels of necrosis in *Alox5*<sup>-/-</sup> BMDM's, necrosis induction by Δ3167c is still significant.

Therefore, necrosis induction by Δ3167c does not depend on the eicosanoids LXA<sub>4</sub> and PGE<sub>2</sub>.

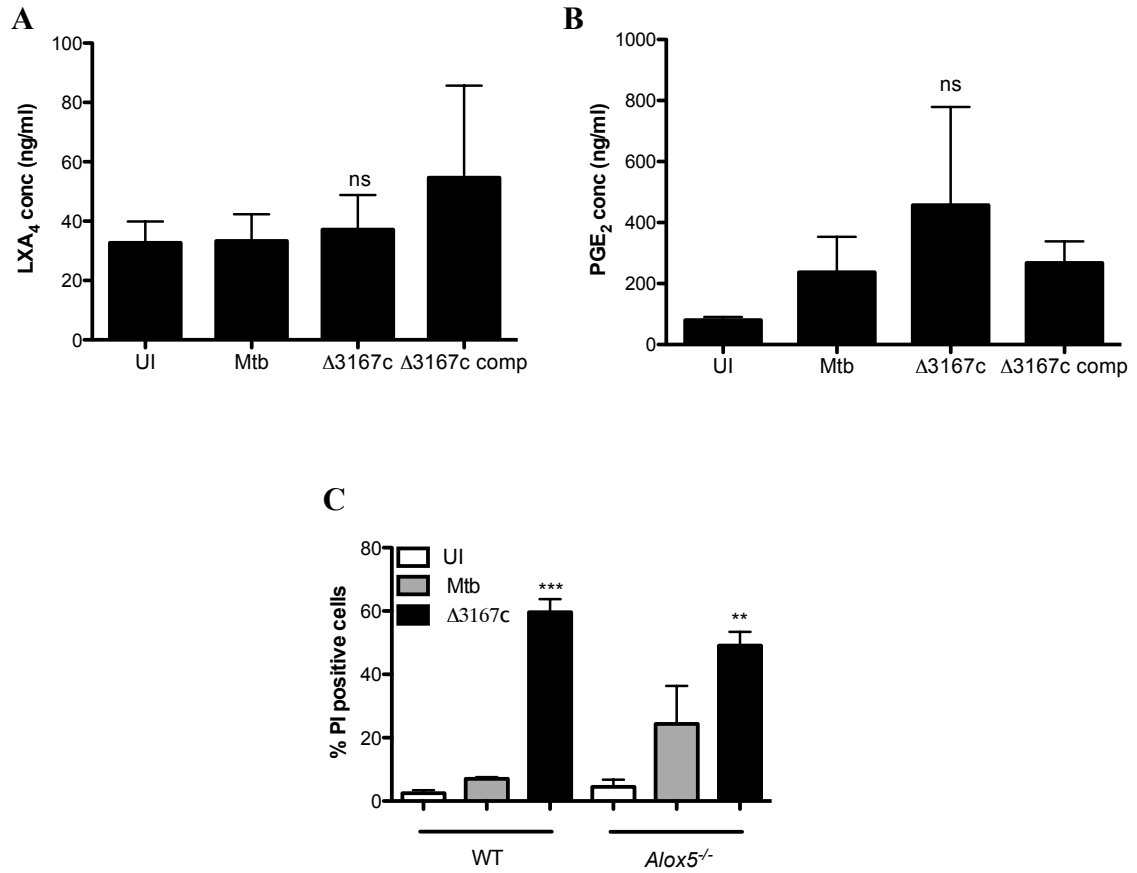


**Fig 18.  $\Delta 3167c$  induced necrosis is independent of LXA<sub>4</sub> and PGE<sub>2</sub>**

- (A) LXA<sub>4</sub> concentration in supernatants of infected cells at 24hpi was measured by ELISA. Data is representative of two independent experiments (n=6).
- (B) PGE<sub>2</sub> concentration in supernatants of infected cells at 24hpi was measured by ELISA. Data is representative of two independent experiments (n=6).
- (C) Necrosis induction in WT and *Alox5*<sup>-/-</sup> BMDM's was measured by PI staining and flowcytometry at 24hpi. Data is representative of three independent experiments (n=3).

Statistical significance is estimated relative to Mtb infected cells.

### **2.3.3.2 Cathepsins and lysosomal lipase are not involved in necrosis induction by $\Delta 3167c$**

Previous studies have implicated both cathepsins and lysosomal lipase in necrosis induction by a high intracellular load of Mtb (107,108). The cathepsin B inhibitor Ca074Me (40 $\mu$ M) and the cathepsin D inhibitor pepstatin A (PepA) (50 $\mu$ M) were used to investigate the role of these lysosomal proteases in  $\Delta 3167c$  mediated necrotic cell death. Inhibition of neither cathepsin B nor cathepsin D individually nor in combination resulted in reversal of  $\Delta 3167c$  necrotic phenotype (Fig 19A). The inhibitors by themselves did not induce any cell toxicity as determined by the MTS assay that measures metabolic activity (Fig 19B). Treatment of  $\Delta 3167c$ -infected cells with 10 $\mu$ M of Cpz (chlorpromazine), a lysosomal lipase inhibitor, was found to completely inhibit necrosis to levels similar to that observed in uninfected cells (Fig 19C). Effect of Cpz on mycobacterial uptake was tested in BMDM's pretreated with Cpz for one hour and infected with *M.smegmatis* expressing GFP for an additional two hours. Addition of Cpz reduce uptake of GFP expressing *M.smegmatis* from 60.68% to 44.15% (Fig 19D). Further, *invitro* growth of  $\Delta 3167c$  in 7H9 liquid media was inhibited by addition of Cpz as well (Fig 19E). These effects exerted by Cpz could account for the reversal in  $\Delta 3167c$  induced necrotic death.

Therefore,  $\Delta 3167c$  induced necrosis is independent of cathepsin B, cathepsin D and liposomal lipase activity.

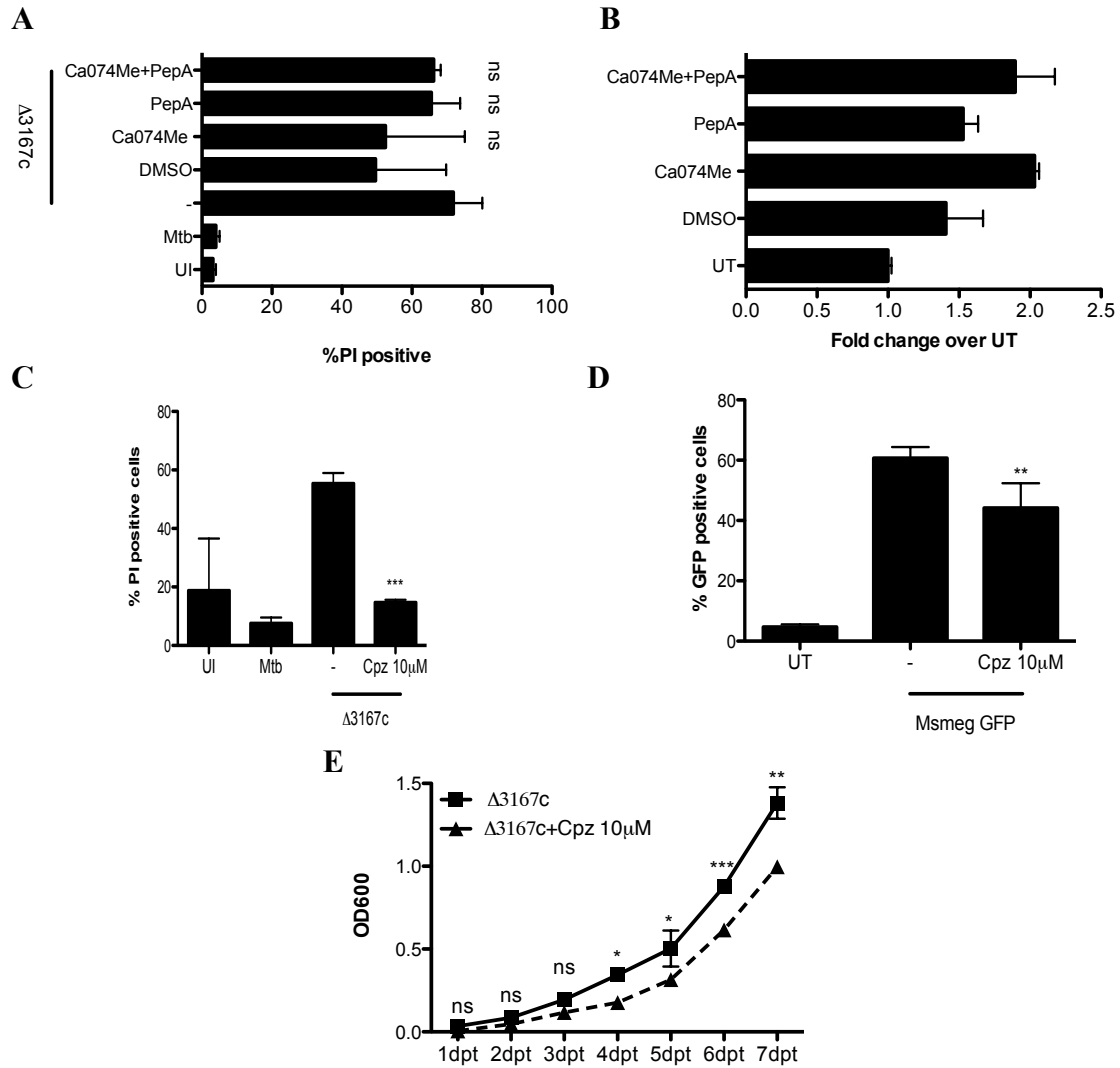


**Fig 19. Cathepsin B, cathepsin D and lysosomal lipase activity is not required for  $\Delta 3167c$  induced necrosis**

- (A) Necrosis induction by  $\Delta 3167c$  in presence and absence of Ca074Me (40 $\mu$ M) and PepA (50 $\mu$ M) in BMDM's was measured by PI staining and flowcytometry at 48hpi. Data is representative of three independent experiments (n=4).
- (B) Cytotoxicity of Ca074Me and PepA in BMDM's was measured by MTS assay at 24hpt. Data is from two independent experiments (n=6).
- (C) Necrosis induction by  $\Delta 3167c$  in presence and absence of Cpz (10 $\mu$ M) in BMDM's was measured by PI staining and flowcytometry at 4dpi. Data is representative of three independent experiments (n=3).
- (D) Effect of Cpz on mycobacterial uptake was measured in BMDM's using GFP expressing *M.smegmatis* (Msmeg GFP). Data is representative of three independent experiments (n=4).
- (E) Growth of  $\Delta 3167c$  in 7H9 medium in presence and absence of Cpz was measured by determining absorbance at OD600. Data is representative of two independent experiments (n=6).

Statistical significance was estimated relative to solvent control for (A) and  $\Delta 3167c$  and Msmeg GFP infected cells for (C) and (D) respectively.

### 2.3.3.3 $\Delta 3167c$ induced necrosis is independent of RIPK1 and RIPK3

Under conditions of caspase inhibition, RIPK1 and RIPK3 autophosphorylate and transphosphorylate each other and form a complex termed the necrosome. This leads to downstream production of ROS and cell death via necrosis (51). RIPK1 and RIPK3 have been implicated in TNF mediated necrosis induction during *M.marinum* infection (9). PI staining of infected *Ripk3*<sup>-/-</sup> BMDM's was performed to determine whether RIPK3 was required for  $\Delta 3167c$  induced necrosis. No differences were seen in levels of necrosis induction by  $\Delta 3167c$  in wild type and *Ripk3*<sup>-/-</sup> BMDM's (Fig 20A). The RIPK1 specific allosteric inhibitor necrostatin 1 (Nec1) was used to examine involvement of RIPK1 (128). Inclusion of Nec1 (100 $\mu$ M) did not inhibit necrosis induction by  $\Delta 3167c$  in THP1 cells (Fig 20B). Macrophages treated with LPS (20ng/ml) and zVAD-fmk (40 $\mu$ M) undergo RIPK1 dependent necrotic cell death (129). Activity of Nec1 was confirmed by its ability to inhibit the RIPK1 dependent necrosis induction in BMDM's treated with LPS and zVAD-fmk (Fig 20C). Nec1 did not induce cytotoxicity in uninfected cells (Fig 20D).

RIPK1 and RIPK3 mediated cell death can also be executed in a caspase dependent manner by formation of the ripoptosome complex which requires RIPK1 activity (51). To test whether  $\Delta 3167c$  induced necrosis requires both RIPK's and caspase activity, *Ripk3*<sup>-/-</sup> BMDM's were infected with Mtb and  $\Delta 3167c$  in presence of the pan caspase inhibitor zVAD fmk. A 1.74 fold increase in cell death was observed in  $\Delta 3167c$  infected cells treated with zVAD fmk compared to  $\Delta 3167c$ - infected cells treated with DMSO, excluding the contribution of both caspase activity as well as RIPK3 in  $\Delta 3167c$  mediated necrosis (Fig 120E).

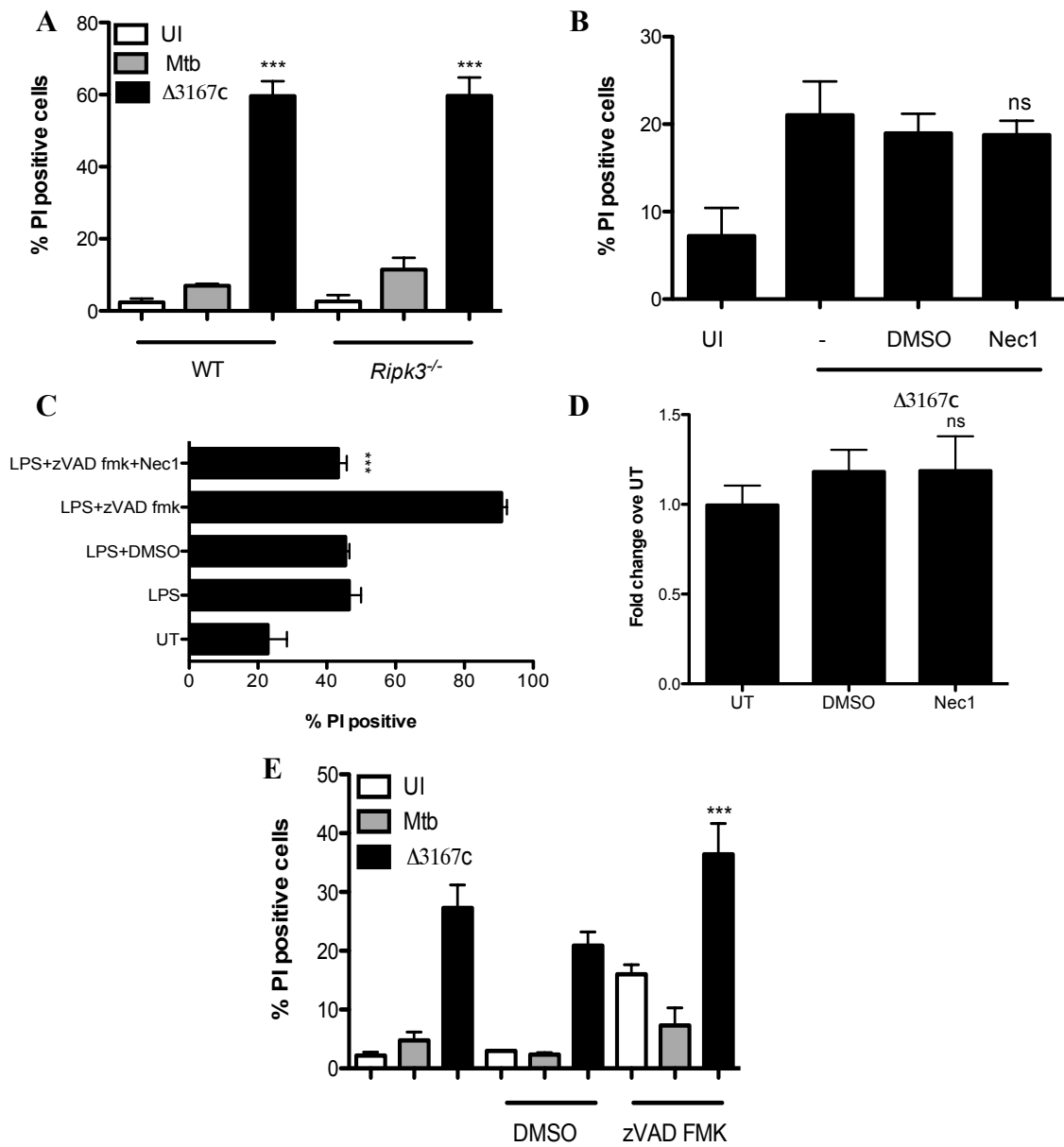


**Fig 20.  $\Delta 3167c$  induced necrosis is independent of RIPK1 and RIPK3**

- (A) Necrosis induction in infected WT and *Ripk3*<sup>-/-</sup> BMDM's was measured by PI staining and flowcytometry at 24hpi. Data is representative of three independent experiments (n=3).
- (B) Necrosis induction in infected THP1 cells was measured by PI staining and flowcytometry at 24hpi. Nec1 concentration - 100 $\mu$ M. Data is representative of two independent experiments (n=4).
- (C) Nec1 efficacy was tested in BMDM's treated with LPS (20ng/ml), zVAD fmk (40 $\mu$ M) and Nec1 (100 $\mu$ M). Data is from one experiment (n=3).
- (D) Cytotoxicity of Nec1 in THP1 cells was measured by MTS assay at 24hpt. Data is from two independent experiments (n=6).
- (E) Necrosis induction in infected *Ripk3*<sup>-/-</sup> BMDM's was measured by PI staining and flowcytometry at 24hpi. Data is representative of two independent experiments (n=3).

Statistical significance was estimated relative to Mtb infected cells for (A) and (E) and relative to solvent control for (B), (C) and (D).

These results demonstrate that necrosis induction by  $\Delta 3167c$  is independent of RIPK1 and RIPK3.

#### **2.3.3.4 $\Delta 3167c$ induced necrosis is independent of PARP and AIF**

As stated previously, the DNA repair enzyme PARP is cleaved by caspases during apoptosis. However, overactivation of PARP can also lead to necrotic cell death via depletion of cytosolic  $\text{NAD}^+$  and consequent mitochondrial dysfunction in response to DNA damaging agents (130). To evaluate role of PARP1 in  $\Delta 3167c$  induced cell death, PI staining of *Parp1*<sup>-/-</sup> BMDM's was performed. No differences in  $\Delta 3167c$  necrosis induction were observed between wild type and *Parp1*<sup>-/-</sup> BMDM's (49.38% vs 57.47%) (Fig 21A).

PARP1 mediated necrosis has also been reported to be mediated via apoptosis inducing factor (AIF) in models of glutamate excitotoxicity as well as with bacterial infections (83). Contribution of AIF to  $\Delta 3167c$  induced necrosis was examined by using BMDM's from Harlequin mice which exhibit an approximately 80% loss in AIF expression due to a retroviral insertion in *Aifm1* and from matched wild type controls.  $\Delta 3167c$  mediated necrosis in BMDM's obtained from Harlequin mice was reduced by approximately 1.5 fold compared to WT controls (Fig 21B). For AIF to mediate necrotic cell death, it needs to be translocated from the mitochondria to the nucleus where it participates in DNA condensation and fragmentation (87). Nuclear translocation of AIF in  $\Delta 3167c$ -infected cells was examined by immunoblotting for AIF in cytosolic and nuclear fractions. No differences in nuclear AIF levels of uninfected, Mtb and  $\Delta 3167c$  infected THP1 cells were detected (Fig 21C).

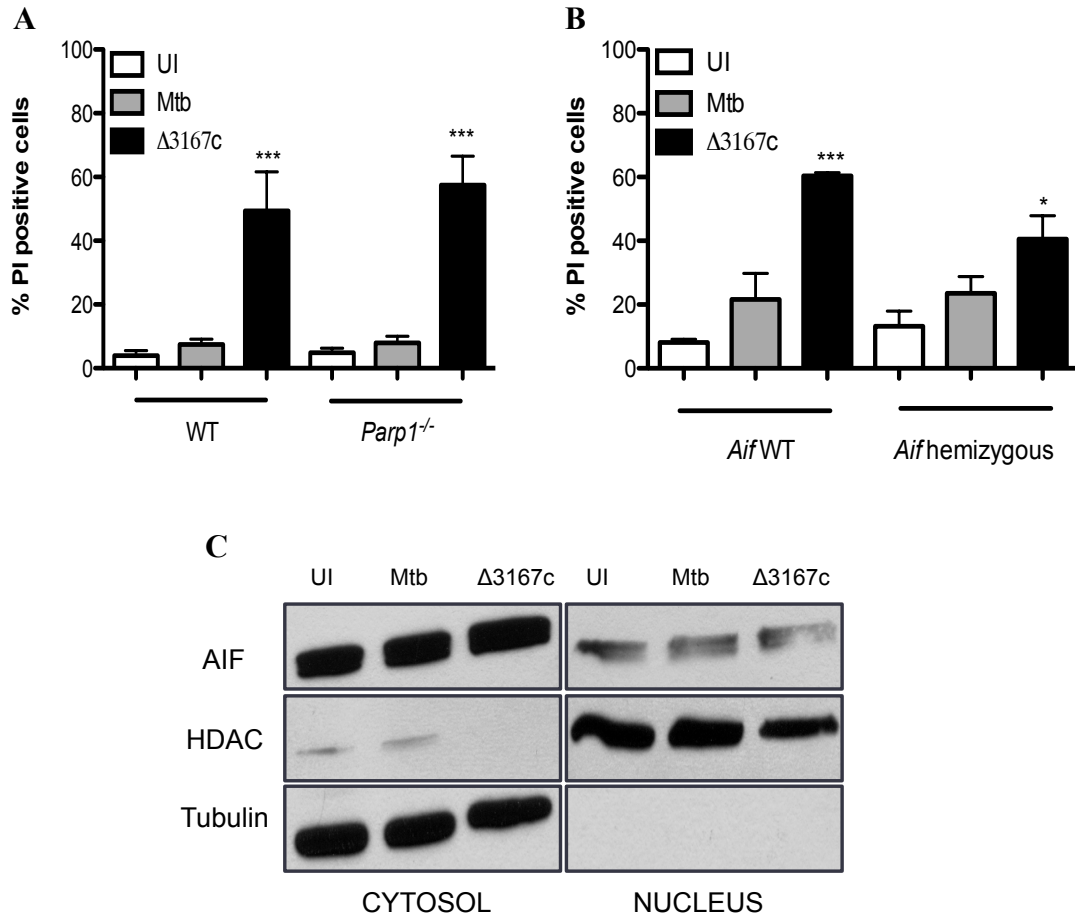


**Fig 21. Δ3167c induced necrosis is independent of PARP and AIF**

- (A) Necrosis induction in WT and *Parp1*<sup>-/-</sup> BMDM's at 72hpi was determined by PI staining and flowcytometry. Data is from two independent experiments (n=6).
- (B) Necrosis induction in *Aif* WT and *Aif* hemizygous BMDM's at 72hpi was determined by PI staining and flowcytometry. Data is representative of three independent experiments (n=3).
- (C) AIF nuclear translocation in THP1 cells at 24hpi was determined by western blotting. HDAC – Histone deacetylase, nuclear fraction loading control; Tubulin – cytosolic fraction loading control. Data is representative of two independent experiments.

For (A) and (B), statistical significance was estimated relative to Mtb infected cells for each BMDM type.

Thus involvement of AIF in  $\Delta 3167c$ -induced necrosis is suspect. Similar results for AIF translocation were obtained in BMDM's as well (data not shown).

### **2.3.3.5 Inflammasome activation and IL1R1 signaling do not contribute to $\Delta 3167c$ induced necrosis**

Inflammasome activation in response to microbial infection has been linked to induction of two different types of cell death that are differentiated based upon involvement of caspase 1 and cathepsin B (72,131). More recently non-canonical inflammasomes have been described that lead to necrotic cell death via activation of caspase 11 following Gram negative bacterial infection (70). PI staining of *Casp1/11*<sup>-/-</sup> BMDM's infected at MOI10 was performed to determine whether  $\Delta 3167c$  induced cell death was dependent on either caspase 1 or caspase 11.  $\Delta 3167c$  induced similar levels of cell death in both wild type and *Casp1/11*<sup>-/-</sup> BMDM's (44.42% vs 47.5%) (Fig 22A).

ASC and NLRP3 have been implicated in inflammasome dependent necrotic cell death. NLRP3 has been shown to be required for Mtb mediated necrosis (32). A 1.4 fold increase in  $\Delta 3167c$ -induced necrosis as measured by the toxilight assay was seen in THP1shASC macrophages compared to control macrophages (Fig 22B). Immortalized wild type and *Nlrp3*<sup>-/-</sup> cells were used to assess the role of NLRP3 in  $\Delta 3167c$ -induced necrosis. An increase in PI positive  $\Delta 3167c$  infected macrophages was seen in immortalized *Nlrp3*<sup>-/-</sup> BMDM's compared to wild type controls (Fig 22C). Surprisingly, a 1.5 fold increase in Mtb mediated necrosis was also observed in immortalized *Nlrp3*<sup>-/-</sup> BMDM's. A similar result has been previously reported by our group in dendritic cells (33).

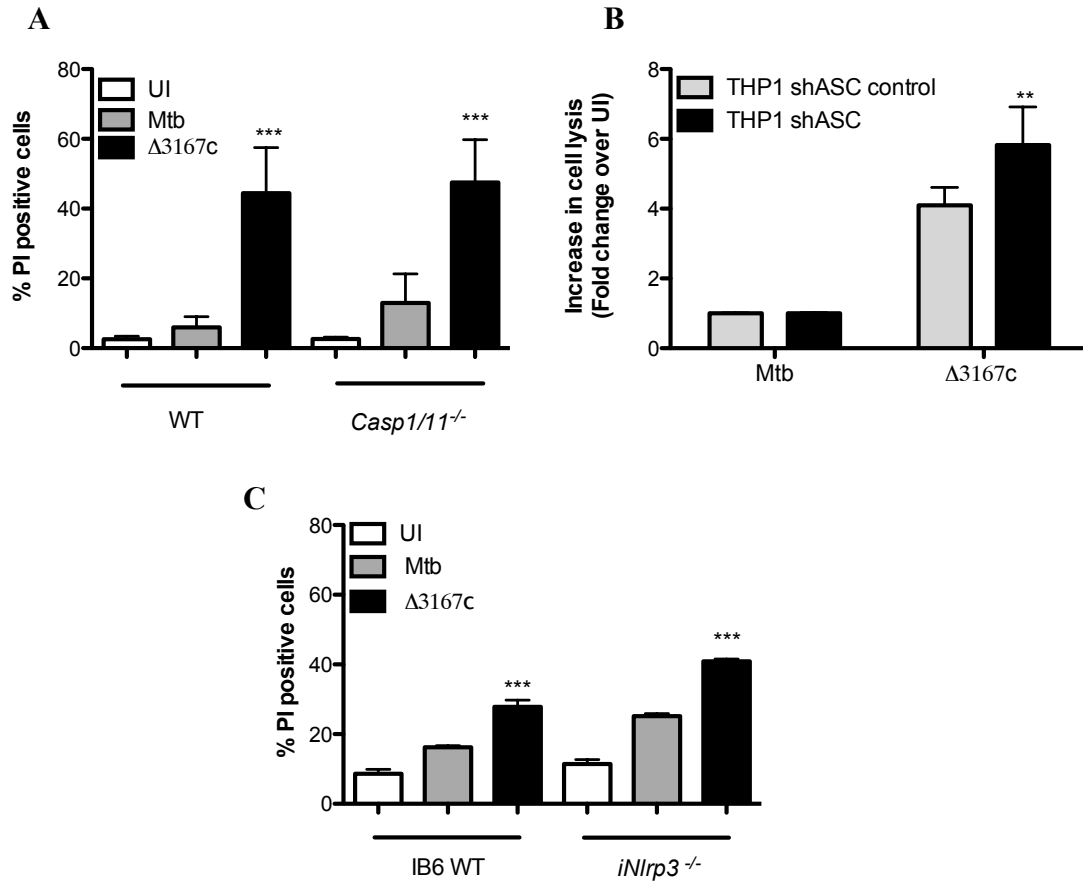


**Fig 22. Necrosis induction by  $\Delta 3167c$  is independent of inflammasomes**

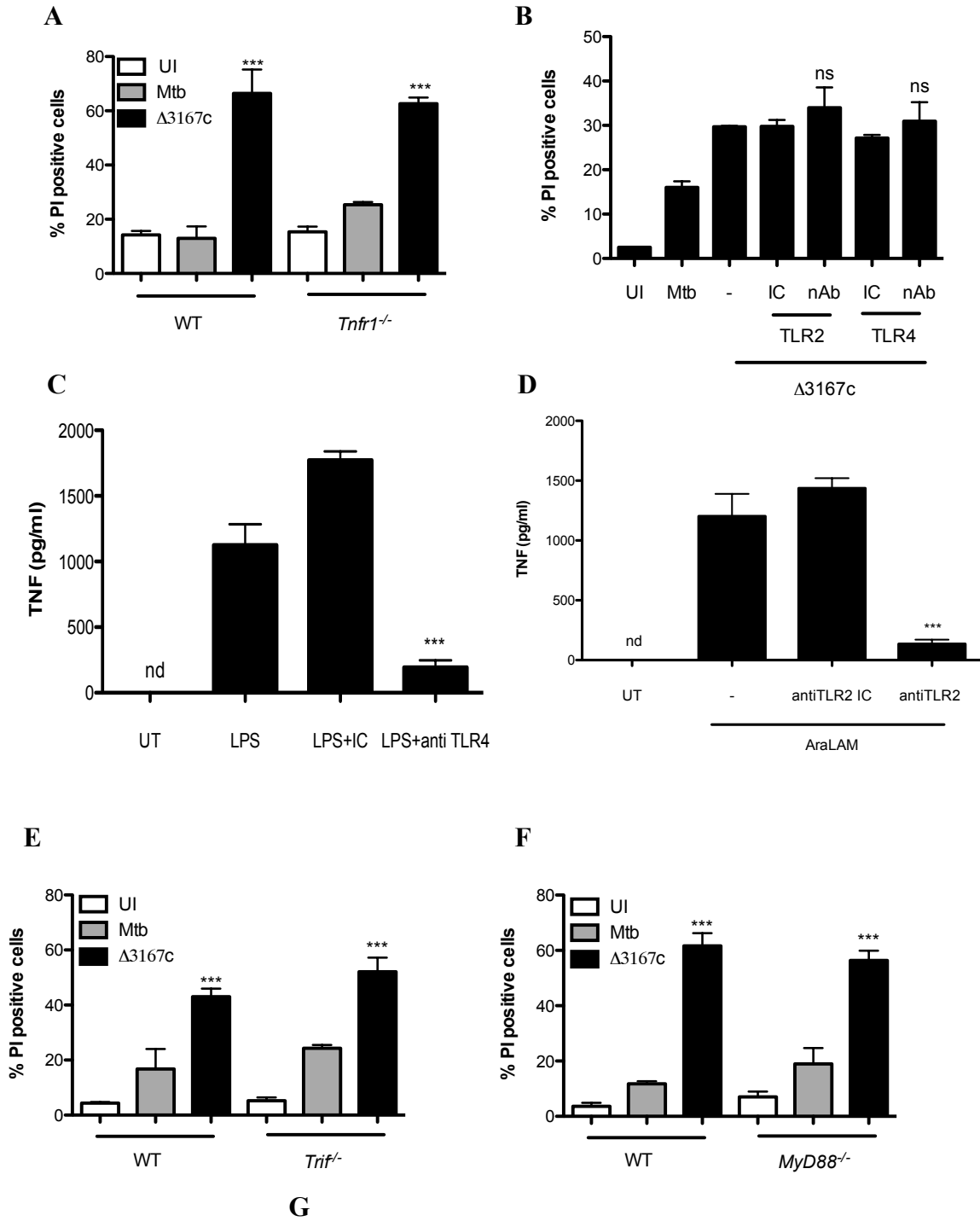
- (A) Necrosis induction in WT and *Casp1/11*<sup>-/-</sup> BMDM's was determined by PI staining and flowcytometry at 48hpi. Data is representative of five independent experiments (n=6).
- (B) Necrosis induction in THP1 shASC and control cells was determined by toxilight assay at 48hpi. Data is from three independent experiments (n=9).
- (C) Necrosis induction in immortalized WT and *Nlrp3*<sup>-/-</sup> BMDM's was determined by PI staining and flowcytometry at 24hpi. Data is representative of three independent experiments (n=3).

Therefore, necrosis induction by  $\Delta 3167c$  strain is independent of both canonical and non-canonical inflammasome components.

#### **2.3.3.6 TNF signaling, TLR signaling and type I interferon signaling does not contribute to $\Delta 3167c$ -induced necrosis**

TNF can signal via TNFR1 located on the cell surface and lead to cell death either via apoptosis or necrosis (51). TNF signaling has been implicated in apoptosis induction by Mtb mutant strains (124). *M. marinum* has been shown to induce necrotic cell death in a TNF dependent manner (9). Role of TNF in  $\Delta 3167c$  induced necrosis was determined by infection and PI staining of *Tnfr1*<sup>-/-</sup> BMDM's. No inhibition of  $\Delta 3167c$  induced necrosis was seen in *Tnfr*<sup>-/-</sup> BMDM's compared to wild type controls (Fig 23A). Work done by previous graduate student (Gurses S, data not shown) showed no differences in TNF levels in supernatants of macrophages infected with Mtb,  $\Delta 3167c$  and complement strains.

To determine the role of TLR2 and TLR4 signaling in  $\Delta 3167c$  mediated necrosis, infected THP1 macrophages were treated with neutralizing anti-TLR2 and anti-TLR4 antibodies and associated isotype controls. PI staining and flowcytometry was performed. Neutralization of neither TLR2 nor TLR4 inhibited  $\Delta 3167c$ -mediated necrosis (Fig 23B). TNF production by THP1 macrophages in response to mycobacterial arabinose capped lipoarabinomannan (AraLAM) and LPS was inhibited by the neutralizing anti TLR2 and TLR4 antibody respectively thus demonstrating efficacy of neutralizing antibodies used (Fig 23C, 23D). Contribution of the TLR signaling adaptors TRIF and MyD88 was assessed by PI staining of infected *Trif*<sup>-/-</sup> and *MyD88*<sup>-/-</sup> BMDM's.  $\Delta 3167c$  induced similar



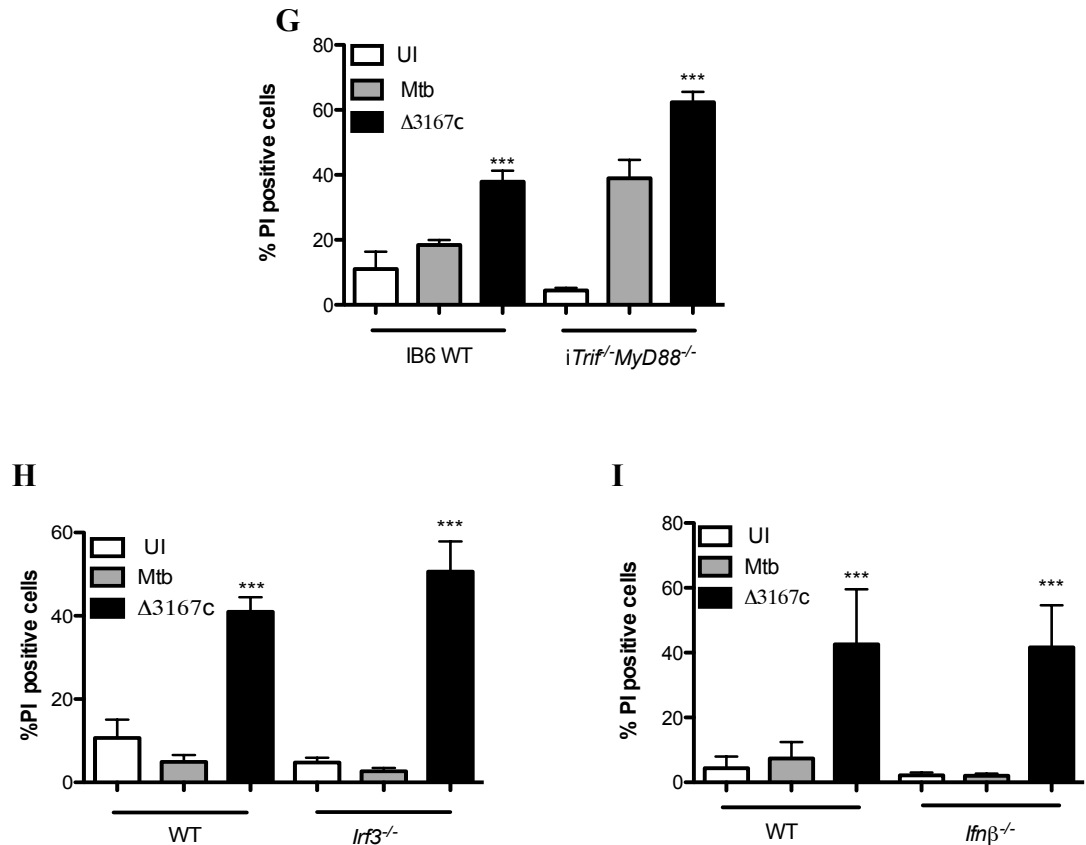


**Fig 23. Necrosis induction by  $\Delta 3167c$  is independent of TNF, TLR and type I IFN signaling**

- (A) Necrosis induction in WT and *Tnfr1<sup>-</sup>* BMDM's was determined by PI staining and flowcytometry at 72hpi. Data is representative of two independent experiments (n=3).
- (B) Necrosis induction in THP1 cells in presence of neutralizing anti TLR antibodies (nAb) and associated isotype controls (IC) was determined by PI staining and flowcytometry at 24hpi. Data is from one experiment (n=3).
- (C) Efficacy of anti TLR4 antibody was determined by measuring TNF levels in supernatants of THP1 cells treated with LPS. Data is from one experiment (n=3).
- (D) Efficacy of anti TLR2 antibody was determined by measuring TNF levels in supernatants of THP1 cells treated with AraLAM. Data is from one experiment (n=3).
- (E) Necrosis induction in WT and *Trif<sup>-</sup>* BMDM's was determined by PI staining and flowcytometry at 48hpi. Data is representative of four independent experiments (n=3).
- (F) Necrosis induction in WT and *MyD88<sup>-</sup>* BMDM's was determined by PI staining and flowcytometry at 48hpi. Data is representative of four independent experiments (n=3).
- (G) Necrosis induction in immortalized WT and *Trif<sup>-</sup> MyD88<sup>-</sup>* BMDM's was determined by PI staining and flowcytometry at 48hpi. Data is representative of four independent experiments (n=3).
- (H) Necrosis induction in immortalized WT and *Irf3<sup>-</sup>* BMDM's was determined by PI staining and flowcytometry at 48hpi. Data is representative of three independent experiments (n=3).
- (I) Necrosis induction in immortalized WT and *Ifn $\beta$ <sup>-</sup>* BMDM's was determined by PI staining and flowcytometry at 48hpi. Data is from three independent experiments (n=9).

For (A), (E), (F), (G), (H) and (I) statistical analysis was performed relative to Mtb infected cells. For (B), (C) and (D) statistical analysis was performed relative to IC control.

levels of necrosis in the wild type and knock out BMDM's (Fig 23E, 23F).

To ensure that the lack of a phenotype in the *Trif*<sup>-/-</sup> and *MyD88*<sup>-/-</sup> BMDM's is not due to redundancy between the two adaptors, immortalized *Trif*<sup>-/-</sup>/*MyD88*<sup>-/-</sup> double knockout BMDM's were infected and PI staining was performed. Necrosis induction by both Mtb and Δ3167c was elevated in immortalized *Trif*<sup>-/-</sup>/*MyD88*<sup>-/-</sup> double knockout cells compared to the wild type controls (iB6). However, Δ3167c induced 2 fold higher level of necrosis in immortalized wildtype cells and 1.6 fold higher level of necrosis in immortalized *Trif*<sup>-/-</sup>/*MyD88*<sup>-/-</sup> double knockout cells compared to Mtb (Fig 23G).

Type I (IFN) signaling has been implicated in death of macrophages infected with bacterial and viral pathogens via both inflammasome dependent and independent mechanisms (61,132). BMDM's from *Ifnβ*<sup>-/-</sup> and *Irf3*<sup>-/-</sup> mice were used to examine the role of type I IFN signaling in necrosis induction by Δ3167c. PI staining of infected BMDM's revealed no differences in necrosis induction by Δ3167c in wild type and *Irf3*<sup>-/-</sup> and *Ifnβ*<sup>-/-</sup> BMDM's (Fig 23H, 23I).

Thus TNF, TLR and type I IFN signaling do not play a role in Δ3167c induced necrotic cell death.

### **2.3.4 Δ3167c induced necrosis is dependent on mitochondrial ROS**

#### **2.3.4.1 Higher ROS levels are detected in Δ3167c infected macrophages**

ROS has been implicated in both apoptotic and necrotic cell death (127). Two dyes were used to measure ROS levels in uninfected and Mtb, Δ3167c and complement infected BMDM's. DCFDA measures cytosolic superoxide content while MitoSOX Red™ is targeted to the mitochondria and measures mitochondrial ROS levels. At indicated time points post infection, macrophages were stained with the dyes for 30

minutes and fluorescence intensity measured by flowcytometry. Representative histograms show an increase in fluorescence intensity of  $\Delta 3167c$ -infected macrophages compared to those infected with Mtb or the complement strain at 24hpi (Fig 24A). Percentage increase in fluorescence intensity of the samples was calculated compared to the uninfected control at each time point. At 0hpi, macrophages infected with any of the three strains have comparable cytosolic and mitochondrial ROS levels. However at 24hpi, increased levels of both cytosolic (2.4 fold) and mitochondrial ROS (approximately 50 fold) are detected in  $\Delta 3167c$  infected macrophages compared to Mtb infected cells (Fig 24B, 24C). Complementation of *Rv3167c* restored ROS to levels similar to that observed in Mtb infected cells. The negative values obtained indicate lower levels of ROS in the infected samples compared to uninfected cells.

Therefore, at earlier time points post infection ROS levels are similar in macrophages infected with Mtb,  $\Delta 3167c$  or the complement strain. However at longer time points post infection, higher mitochondrial and cytosolic ROS levels are detected in  $\Delta 3167c$  infected cells compared to Mtb or complement infected cells.

#### **2.3.4.2 Necrosis induction by $\Delta 3167c$ is dependent on mitochondrial ROS**

To determine the role of ROS in  $\Delta 3167c$  mediated necrosis, the flavoprotein inhibitor DPI and the ROS scavengers glutathione and NAC were added to infected THP1 macrophages. Necrosis induction was assessed by either toxilight assay or by TUNEL staining at 24hpi. Inclusion of DPI inhibited  $\Delta 3167c$  mediated necrosis by approximately three fold compared to untreated cells (Fig 25A). Inclusion of glutathione and NAC resulted in a complete inhibition of  $\Delta 3167c$  induced necrosis (Fig 25B).

There are two important sources of ROS in eukaryotic cells – NOX2 complex and

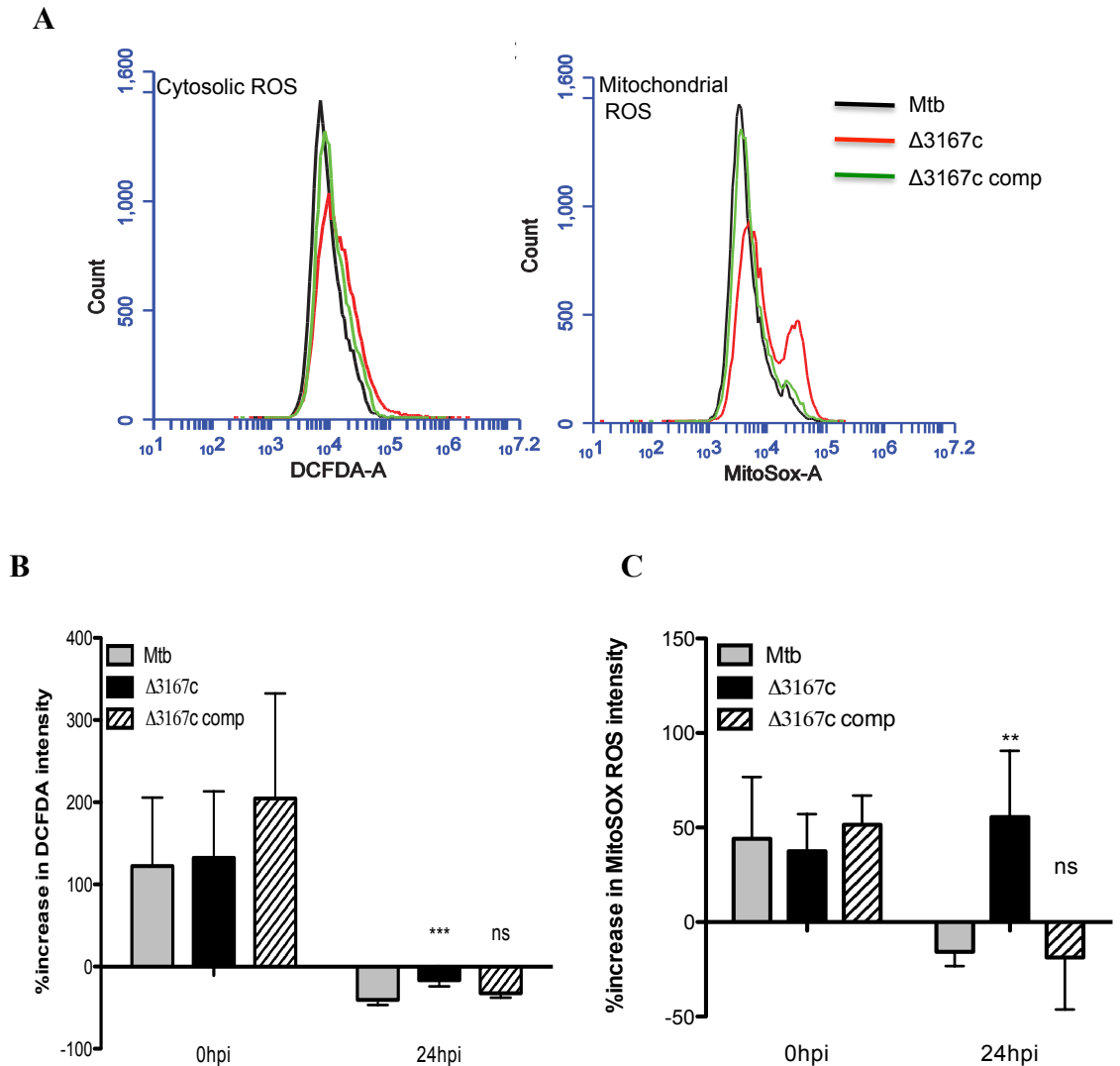


**Fig 24.  $\Delta 3167c$  induces higher levels of cytosolic and mitochondrial ROS compared to Mtb and complement strain**

- (A) Representative histogram of cytosolic and mitochondrial ROS measurement in infected BMDM's at 24hpi.
- (B) Percentage increase in DCFDA intensity measured by flowcytometry in infected BMDM's compared to uninfected cells at 0hpi and 24hpi is depicted. Data is from three independent experiments (n=6).
- (C) Percentage increase in MitoSOX Red intensity measured by flowcytometry in infected BMDM's compared to uninfected cells at 0hpi and 24hpi is depicted. Data is from three independent experiments (n=6).

mitochondria. The NOX2 complex comprises of 5 subunits and is assembled on the phagosomal membrane during phagocytosis (44). To examine role of NOX2 complex derived ROS on necrosis induction by  $\Delta 3167c$ , *Nox2*<sup>-/-</sup> BMDM's (lacking the gp91phox subunit of the NOX2 complex) were infected and necrosis levels measured by PI staining and flowcytometry.  $\Delta 3167c$  induced similar levels of necrosis in both wild type and *Nox2*<sup>-/-</sup> BMDM's (Fig 25C). Although Mtb induced higher levels of necrosis in *Nox2*<sup>-/-</sup> BMDM's, necrosis induction by  $\Delta 3167c$  is still significant compared to Mtb. Contribution of mitochondrial ROS to  $\Delta 3167c$ -induced cell death was assessed by PI staining of infected BMDM's from mCAT transgenic mice. These mice overexpress mitochondrial targeted catalase, an antioxidant (133). A reduction in necrosis induction by  $\Delta 3167c$  strain from 59.63 in WT BMDM's to 15.91% in mCAT BMDM's was observed (Fig 25D). MOMP and cytosolic translocation of CytC was not observed in Mtb and  $\Delta 3167c$  infected cells (Fig 17C). To determine whether mitochondrial membrane potential is affected, DIOC<sub>6</sub> staining was performed in infected THP1 cells at the indicated time points. Increased loss of mitochondrial membrane potential indicated by loss of DIOC<sub>6</sub> was observed in  $\Delta 3167c$  infected cells compared to those infected with Mtb starting at 12hpi. By 48hpi 79.38% of  $\Delta 3167c$ -infected cells had lost DIOC<sub>6</sub> stain compared to 16.51% of Mtb infected cells (Fig 25E).

These results indicate that mitochondrial derived ROS is required for necrosis induction by  $\Delta 3167c$  and that  $\Delta 3167c$  induces higher levels of mitochondrial damage compared to Mtb.

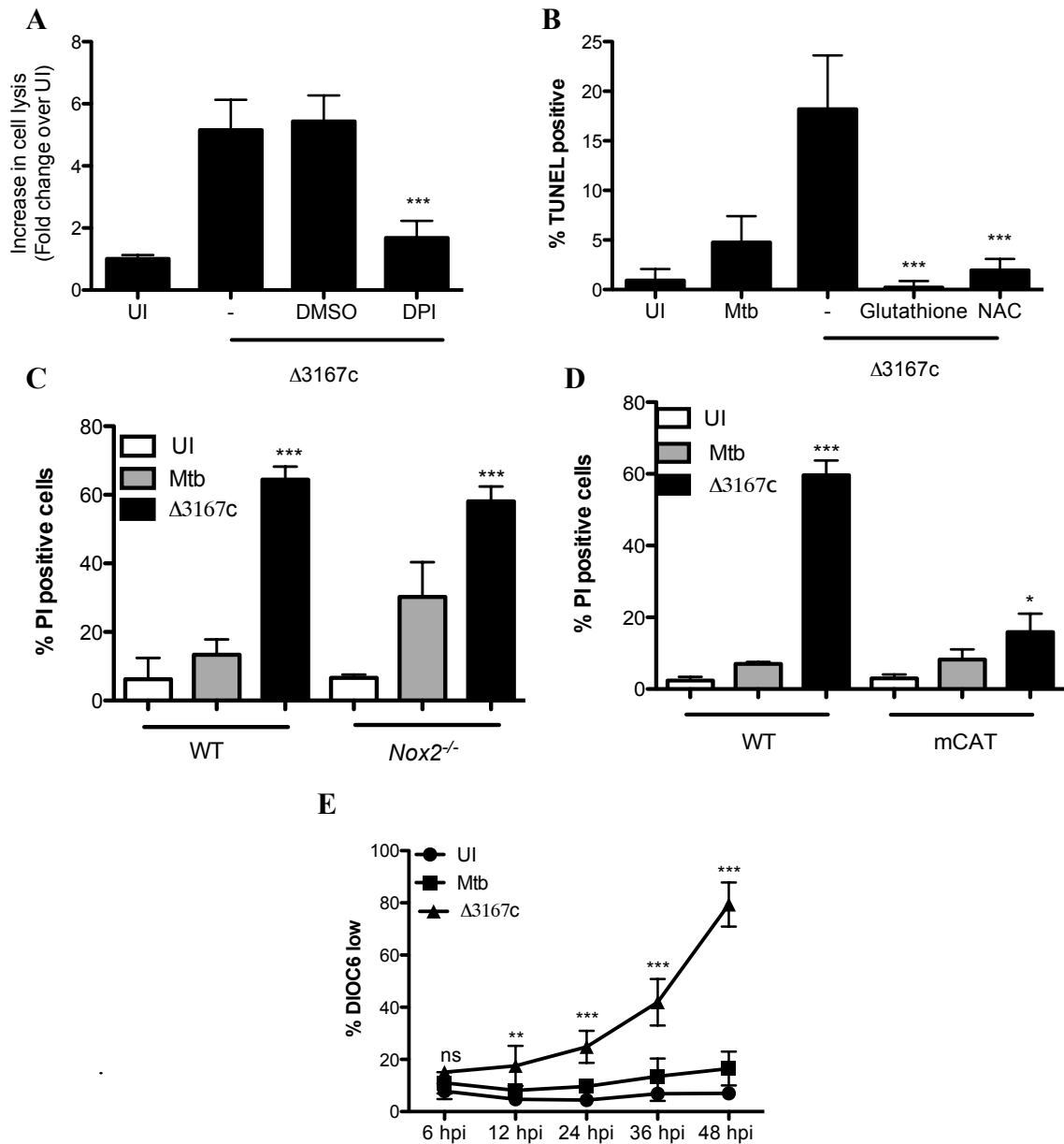


**Fig 25.  $\Delta 3167c$  induced necrosis is dependent on mitochondrial ROS**

- (A) Necrosis induction in presence of DPI was determined by toxilight assay at 24hpi. Data is from three independent experiments (n=6).
- (B) Necrosis induction in presence of glutathione and NAC was determined by TUNEL staining at 24hpi. Data is from three independent experiments (n=6).
- (C) Necrosis induction in WT and *Nox2*<sup>-/-</sup> BMDM's was determined by PI staining and flowcytometry at 48hpi. Data is from three independent experiments (n=6).
- (D) Necrosis induction in WT and mitochondrial targeted catalase overexpressing BMDM's was determined by PI staining and flowcytometry at 24hpi. Data is representative of three independent experiments (n=3).
- (E) Loss of mitochondrial membrane potential was determined by DIOC<sub>6</sub> staining in infected THP1 cells and flowcytometry. Data is from three independent experiments (n=9).

Statistical significance was estimated relative to solvent control for (A) and (B); Mtb infected cells for (C), (D) and (E).

### 2.3.5 Discussion

Following entry into a host cell, Mtb employs different mechanisms to manipulate the host immune response to its own advantage. One such mechanism is the modulation of the host cell death response. Mtb inhibits host cell death by apoptotic mechanisms in order to avoid direct bactericidal effects of apoptosis as well as bactericidal effects exerted by neighboring phagocytic cells engulfing the infected, dying cells. Further, apoptosis inhibition helps towards controlling the CD4<sup>+</sup> and CD8<sup>+</sup> T cell response (49). In contrast, Mtb induces necrosis allowing for escape from the infected cells. Necrosis induction does not exert bactericidal effects and is associated with increased susceptibility to Mtb infection (95-99,101,102). In this study, we demonstrate that the gene *Rv3167c* is required for controlling Mtb mediated necrosis.

*Rv3167c* was initially identified as an “anti-apoptotic” gene in a screen for Mtb mutants that induce cell death. Previous studies have shown that apoptosis induction in Mtb infected macrophages results in reduced recovery of bacteria compared to uninduced cells (95,97). However, we did not observe any differences in the intracellular growth of  $\Delta 3167c$  compared to Mtb in macrophages (Fig 14). As apoptosis and necrosis have different implications for Mtb pathogenesis, it is important to identify the exact mode of cell death induced by  $\Delta 3167c$ . The method used in the screen to identify pro-apoptotic mutants was TUNEL staining, a technique that labels ends of fragmented DNA and long considered to be specific for apoptotic cell identification. More recently cells undergoing necrotic cell death have been shown to stain TUNEL positive as well (60,61,134). An analysis of the morphological and biochemical features of  $\Delta 3167c$  infected dying cells revealed that the cells exhibit features of both apoptosis and necrosis. Nuclear

condensation and fragmentation, a classical apoptotic feature was observed in  $\Delta 3167c$ -infected cells (Fig 16A). The absence of DNA laddering and the loss of plasma membrane permeability however point towards a necrotic mode of cell death (Fig 15A, 15B, 16B). Secondary necrosis, which follows apoptosis and can exhibit similar features as primary necrosis was ruled out by demonstrating that  $\Delta 3167c$  mediated cell death is independent of caspases (Fig 17) (57). A mixture of apoptotic and necrotic features has been shown previously in dying cells infected with Mtb, *S.typhimurium*, *S.flexneri* and in cells undergoing AIF mediated necrosis following treatment with the DNA damage inducer MNNG (61,86,107,108,135).

Using a combination of chemical inhibitors and macrophages deficient in components involved in regulated necrosis induction, we attempted to identify the mechanism involved in  $\Delta 3167c$ -induced necrotic cell death. However none of the regulated necrosis pathways and components that we investigated were found to be required for  $\Delta 3167c$ -induced necrosis. Three mechanisms underlying necrosis induction by Mtb have been described – modulation of lipid mediators LXA<sub>4</sub> and PGE<sub>2</sub>, NLRP3 inflammasome activation and host cell membrane damage induced by high bacterial numbers in the macrophage. Mtb infection upregulates LXA<sub>4</sub> production, leading to a decrease in PGE<sub>2</sub> synthesis and consequently necrosis induction by different mechanisms targeting the mitochondria and the plasma membrane (Fig...) (102,104,106). In our experimental settings, Mtb did not induce any LXA<sub>4</sub> production and only a marginal decrease in  $\Delta 3167c$ -induced necrosis was observed in *Alox5<sup>-/-</sup>* BMDM's that are deficient in LXA<sub>4</sub> production (Fig 18). This could possibly be due to use of THP1 cells and BMDM's in our study compared to murine splenic macrophages used in the published

studies on lipid mediator regulation by Mtb. Studies performed on high MOI Mtb infection show necrosis induction occurring at an intracellular bacterial load of 20-40 bacteria and activity of lysosomal lipases was implicated in this process using the lysosomal lipase inhibitor chlorpromazine (Cpz). (21,107-109). While Cpz did inhibit necrosis induction by  $\Delta 3167c$ , we found that it also inhibited mycobacterial uptake by the macrophage and inhibited bacterial growth *in vitro* (Fig 19C, 19D, 19E). The use of Cpz as an anti-mycobacterial agent has been reported in early literature and the MIC of the compound was reported to be 1.8 $\mu$ g/ml *in vitro* and 0.23 $\mu$ g/ml *ex vivo* in HuMDM's, Cpz concentration used in our experiments was 3.55 $\mu$ g/ml (136). Thus the inhibitory effect of Cpz on  $\Delta 3167c$ -induced necrosis may just be the outcome of the anti-mycobacterial activity of the compound. As a similar bacterial burden is detected in both Mtb and  $\Delta 3167c$  infected macrophages, necrosis induction by  $\Delta 3167c$  cannot be attributed to differences in bacterial numbers.

Our inability to identify a specific mechanism responsible for  $\Delta 3167c$  mediated necrosis could point towards the existence of a novel, regulated necrosis pathway. Alternatively, co-operation and redundancy between regulated necrosis pathways may also explain this result. *S.typhimurium* triggered necrotic cell death in macrophages was found to be dependent on both RIPK1-RIPK3 and caspase 1 activation. Blocking either one of the signaling pathways led to only a marginal inhibition of necrosis while neutralizing both inhibited the phenotype completely (61). In another study, *S.typhimurium* induced macrophage cell death was found to require the activities of both caspase 1 and caspase 11 (79). *M.marinum* induced TNF dependent necrosis in zebrafish embryos with a LTA4H high genotype requires the activities of both cyclophilin D

(CypD) dependent MPTP formation and acid sphingomyelinase (ASMase) dependent ceramide generation. Inhibition of both CypD and ASMase was needed to completely inhibit necrosis induction in this study (9). Mtb mediated necrosis induction was reported to require the activity of both the cysteine cathepsin B and the aspartic cathepsin D (107). Treatment of  $\Delta 3167c$  infected cells with the cathepsin B inhibitor (Ca074-Me) and the cathepsin D inhibitor (Pepstatin A) either alone or in combination did not inhibit necrosis induction (Fig 19A). Eukaryotic cells possess eleven cysteine cathepsins and redundancy between cathepsins could explain this outcome. Inhibition of one mechanism of cell death may induce the cell to adopt another pathway to achieve the same goal. For instance, treatment of certain cell types with TNF induces RIPK1 dependent necrotic cell death and inhibition of RIPK1 using chemical inhibitors does not rescue cells from dying, the cells proceed towards death by an apoptotic mechanism instead (51). To determine if a similar mechanism was responsible for  $\Delta 3167c$ -induced necrosis observed in presence of the RIPK1 inhibitor Nec1,  $\Delta 3167c$  infected *Rip3k<sup>-/-</sup>* macrophages were treated with the pan caspase inhibitor zVAD-fmk as well. However, we did not observe any changes in  $\Delta 3167c$ -mediated necrosis under these conditions (Fig 16E). Nevertheless, this does not exclude similar crosstalk occurring between other necrotic pathways that may be activated in  $\Delta 3167c$ -infected cells.

The only factor identified in our study that leads to inhibition of  $\Delta 3167c$  mediated necrosis is mitochondrial ROS. Control of the NOX2 complex generated phagosomal ROS levels by the Mtb *nuoG* gene is required for apoptosis inhibition in infected cells (45). None of the studies on Mtb mediated necrosis have directly implicated mitochondrial ROS in this phenomenon although mitochondrial involvement has been

shown by demonstrating loss of mitochondrial membrane potential in Mtb infected cells (96,104).  $\Delta 3167c$  induced necrosis was found to be dependent on ROS generated in mitochondria but not by the phagosomal NOX2 complex and this was accompanied by mitochondrial damage as indicated by the loss of mitochondrial membrane potential (Fig 25C, 25D, 25E). The PE-PGRS33 protein of Mtb upon ectopic expression in mammalian cells was found to localize to mitochondria and induce cell death (120). Infection of macrophages with non-pathogenic *M.smegmatis* overexpressing PE-PGRS33 also resulted in necrotic cell death (137). A bioinformatics study identified 136 Mtb proteins to contain predicted mitochondrial targeting sequences out of which 19 were predicted to be secreted proteins. (138). It would be interesting to see if expression and/or secretion of these predicted mitochondrial-targeted proteins is upregulated in  $\Delta 3167c$  compared to Mtb.

In conclusion, this study identified the role of the gene *Rv3167c* in the control of Mtb induced necrosis by suppressing generation of mitochondrial ROS production.

## CHAPTER 3 *Rv3167c* IS REQUIRED FOR AUTOPHAGY INHIBITION

### 3.1 INTRODUCTION

Autophagy is an evolutionarily conserved catabolic process that involves sequestration of cytosolic contents into *de novo* generated double membrane vesicles termed as autophagosomes that eventually fuse with lysosomes. Initial studies on Mtb and autophagy focused on the effect of physiological, pharmacological and immunological autophagy inducers on mycobacteria infected cells (145,158,159,160,161,163,164,165). More recently it was found that Mtb induced autophagy in an EsxA dependent manner (150). Formation of pores on the phagosomal membrane in an EsxA dependent manner allowed mycobacterial extracellular DNA to access the cytosol. This in turn led to ubiquitination of Mtb by the ubiquitin ligase Parkin and recruitment of the selective autophagy markers p62 and NDP52 (Fig 11). Autophagy induction either by additional stimuli or by the bacteria itself results in anti-mycobacterial effects.

In this study we evaluated the role of *Rv3167c* in Mtb induced autophagy. *Rv3167c* was determined to be required for inhibition of host cell autophagy. Mitochondrial ROS, inhibition of Akt activation and upregulation of JNK activation contributed to  $\Delta 3167c$ -induced autophagy. Inhibition of Akt activation was also found to be required for  $\Delta 3167c$ -induced necrosis. Previous studies on Mtb induced autophagy have shown that Mtb co-localizes with autophagosomes, leading to lysosomal mediated bacterial destruction. Surprisingly, we did not observe Mtb or  $\Delta 3167c$  co-localization with autophagosomes indicating Mtb has the ability to inhibit selective autophagy mediated killing.

## **3.2 MATERIALS AND METHODS**

### **3.2.1 Materials**

THP1 cells and BMDM's expressing LC3 tagged with GFP (LC3GFP) were obtained from Dr. John Kehrl at National Institutes of Health, Bethesda, MD (143). SP600125 (JNK inhibitor), SB203580 (p38 MAPK inhibitor), SB202190 (p38 MAPK inhibitor), SC-79 (Akt activator) and DPI were purchased from Calbiochem. BafilomycinA1, rapamycin and 3-MA were purchased from Sigma, LC labs and Tocris BioSciences respectively. Antibodies used in this study and their sources are listed in Appendix A.

### **3.2.2 Bacterial cultures**

Bacterial cultures were maintained as described in 2.2.2.  $\Delta$ 3167c strains expressing myc tagged Eis, pore forming toxin listeriolysin O (LLO) and both myc tagged Eis and LLO were generated by Jeff Quigley.

### **3.2.3 Cell culture and infection**

THP1 LC3GFP cells were maintained in RPMI supplemented with 10% non-heat inactivated FCS and 100 $\mu$ g/ml geneticin. Cells were differentiated and infected as described in 2.2.3.

LC3GFP expressing murine monocytes were differentiated into macrophages in DMEM containing 10% heat inactivated FCS, 50ng/ml murine MCSF (Peprotech) and 1% Pencillin-Streptomycin. Macrophages were infected in DMEM, 10% non-heat inactivated FCS and 50ng/ml MCSF for 4 hours at 37°C and chased in growth medium containing 100 $\mu$ g/ml gentamicin. Inhibitors and neutralizing antibodies when used were

added to cells 1 hour prior to infection and included in chase medium. 3-MA was added only during chase.

### **3.2.4 Electron microscopy analysis**

Infected THP1 cells were treated with 2.5% glutaraldehyde in 0.1M sodium cacodylate buffer (pH7.4) for 30 minutes at room temperature and 30 minutes at 4°C followed by fixation with 2% PFA. TEM samples were generated by Serdar Gurses.

### **3.2.5 Autophagy assays**

LC3GFP expressing cells were processed for autophagy analysis by flowcytometry as described previously (184). At indicated time points, infected cells were harvested and washed with PBS prior to permeabilization with 0.05% saponin for 5 minutes. Cells were washed once with PBS and resuspended in FACS buffer. Permeabilization resulted in loss of cytosolic LC3I while LC3II bound to autophagosome membranes was retained, which was measured by flowcytometry (Accuri).

For immunofluorescence analysis, bacteria were stained with AF647-NHS ester (Molecular Probes) as per manufacturers instructions. Briefly, bacteria were pelleted and stained in 0.1M sodium bicarbonate solution containing 0.4mg/ml AF647-NHS ester for 30 minutes at 37°C. Bacteria were washed, resuspended in 0.05% PBS-Tween80 and used for infecting BMDM LC3GFP on slides. At specified time points, cells were fixed with 4% paraformaldehyde overnight, stained with Hoechst 33342 and observed by confocal microscopy (Zeiss LSM 710) for presence of LC3 punctae.

### **3.2.6 Preparation of bacterial cell lysates and culture filtrates**

Late log phase bacterial cultures ( $OD_{600}$  0.6-0.8) were passaged into Sauton's medium containing 0.05% Tween80 to  $OD_{600}$  0.05 and grown to late log phase. A second

passage into Sauton's medium containing 0.005% Tween 80 to OD<sub>600</sub> 0.05 was performed and bacteria were grown to late log phase once again. At this point, bacterial pellets and culture supernatants were collected. Bacterial pellets were resuspended in 20mM Tris HCl, pH 7.6 and lysates were prepared by bead beating. Culture filtrates were concentrated to a final volume of 300µl using Amicon Ultra 15 Centrifugal Filter Unit (Millipore). Protease inhibitor cocktail for bacterial cells (Sigma) was added to both cell lysates and culture filtrates at a final concentration of 0.43mg/ml.

### **3.2.7 Western Blotting**

Whole cell lysates were prepared as described in section 2.2.9. Western blotting of host cell lysates and bacterial lysates and culture filtrates was performed as described in 2.2.10. For bacterial lysates and culture filtrates, primary antibody incubation was carried out at room temperature for one hour.

### **3.2.8 MTS assay**

Toxicity of inhibitors on macrophages was assessed by performing the CellTiter 96® AQueous One Solution Cell Proliferation Assay (MTS) from Promega as per manufacturers instructions. Briefly, 20µl of the MTS reagent was added to cells in a total volume of 100µl and incubated at 37°C for 1-3 hours. Cellular metabolic activity correlated with color development monitored by measuring absorbance at 490nm.

### **3.2.9 Statistical analysis**

ANOVA with Tukey post-test was used for statistical analysis unless otherwise indicated. Data is represented as mean ± SD. p-value significance is as follows – p ≤ 0.05 - \*, p ≤ 0.01 - \*\*, p ≤ 0.0001 - \*\*\*.

### **3.3 RESULTS AND DISCUSSION**

#### **3.3.1 $\Delta$ 3167c induces autophagy**

##### **3.3.1.1 $\Delta$ 3167c induces autophagy in both cell lines and primary macrophages**

In order to further describe the characteristics of cell death induced by  $\Delta$ 3167c, infected THP1 macrophages were processed for TEM (Gurses S, unpublished). Ultrastructural analysis of the infected macrophages by electron microscopy revealed the presence of onion like structures characteristic of autophagic vacuoles (Fig 26C') (148). To determine whether  $\Delta$ 3167c induced autophagy, BMDM LC3GFP cells were infected with Mtb and  $\Delta$ 3167c stained with AF647-NHS ester at MOI3. At 8hpi, cells were fixed with 4% PFA overnight, followed by staining of nuclei with Hoechst 33342. Cells were observed by confocal microscopy for LC3 aggregates and percentage of autophagic cells enumerated. A higher percentage of  $\Delta$ 3167c-infected macrophages were autophagic compared to macrophages infected with Mtb (Fig 26A, 26B). Mtb has been previously shown to induce autophagy and bacteria have been demonstrated to be present within autophagic vacuoles (150). However, in our experiments less than 1% of Mtb and  $\Delta$ 3167c were observed to colocalize with LC3 aggregates by confocal microscopy. Examination of TEM images confirmed results obtained by confocal microscopy. As expected a higher number of autophagosomes were found in  $\Delta$ 3167c-infected cells when compared to Mtb infected controls. Interestingly about 3-4% of both Mtb and  $\Delta$ 3167c bacteria found to colocalize with autophagosomal structures (Fig 26D). The lower estimates of autophagosome-bacteria co-localization obtained by confocal microscopy may be attributed to use of surface stained bacteria in these experiments, bacteria left unlabeled by the AF647-NHS ester co-localizing with LC3 would not be detected.

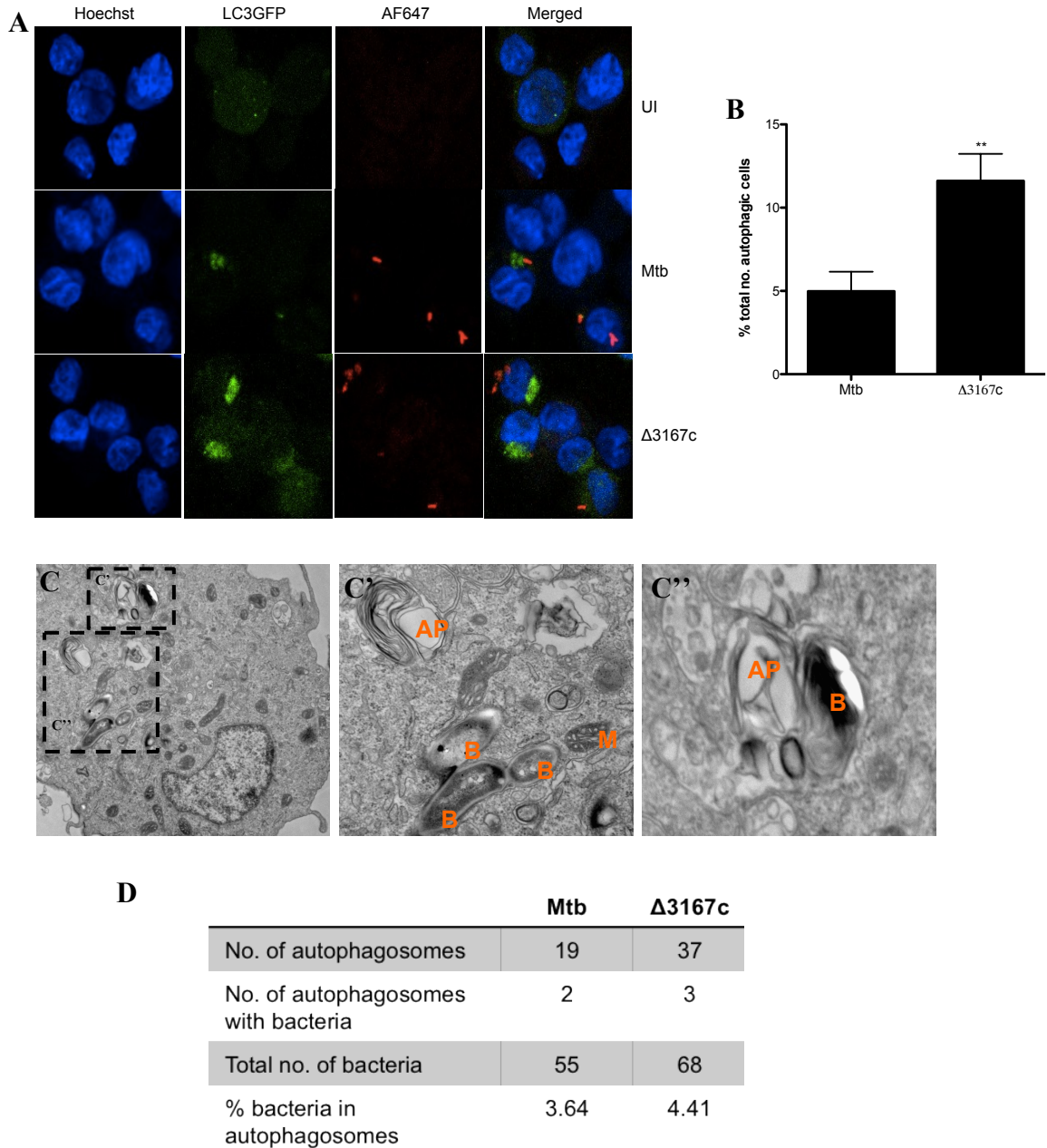


**Fig 26. Δ3167c induces autophagy**

- (A) Autophagy induction by AF647 NHS ester stained bacteria in THP1 LC3GFP cells at 8hpi examined by confocal microscopy.
- (B) Quantitative analysis of cells (A). Data is from 3 independent experiments and at least 450 cells were counted per condition per experiment. Statistical analysis was performed using unpaired Student's t test.
- (C) Representative TEM image of infected THP1 cells at 24hpi. (C') and (C'') are magnified images of regions marked in (C). AP- autophagosome; B- bacteria; M- mitochondria.
- (D) Table shows data obtained from TEM images. Data is from one experiment.

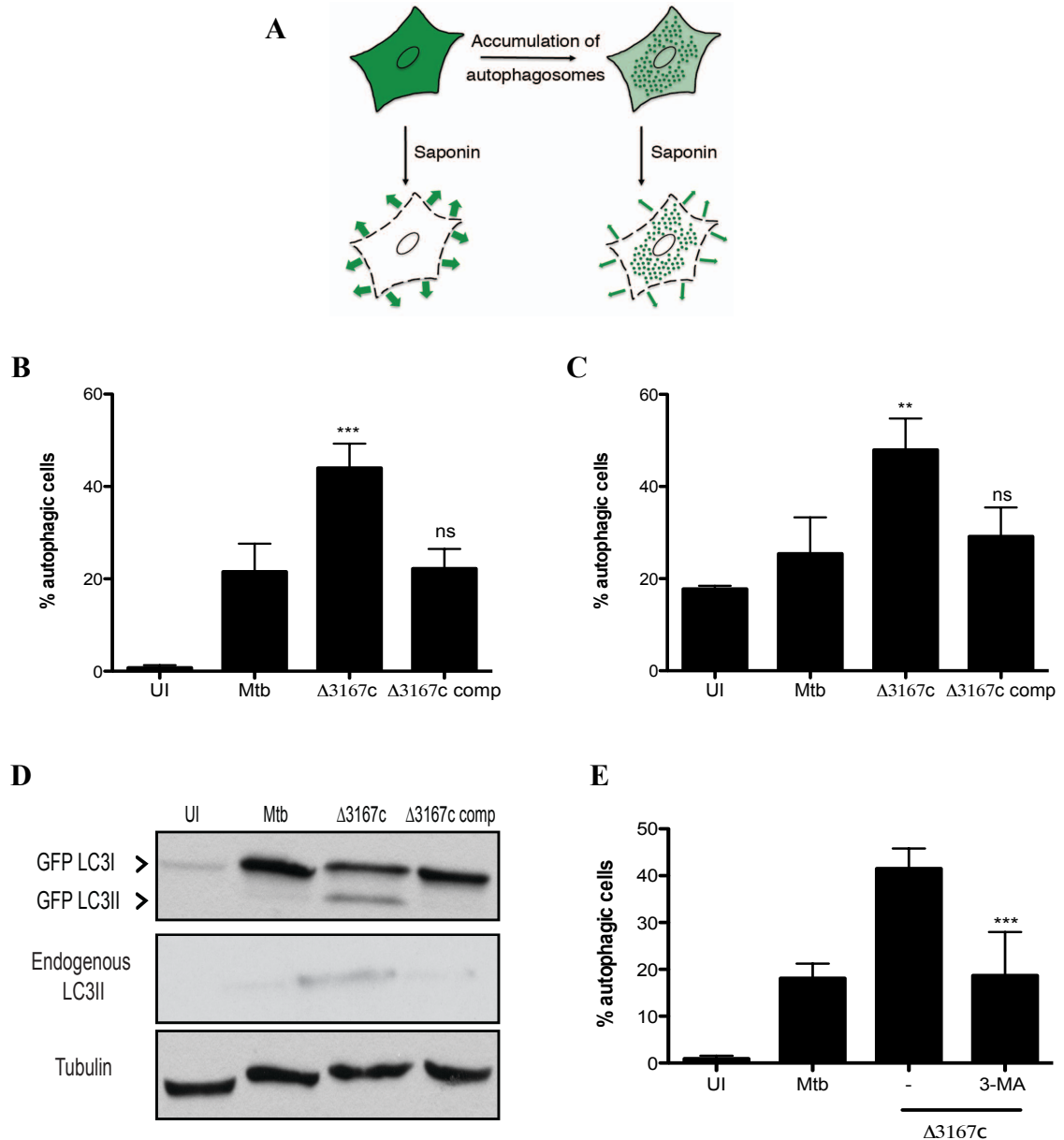


**Fig 27. Δ3167c induces autophagy**

- (A) Principle of autophagy detection by flowcytometry. Image is adapted from (184).
- (B) Autophagy induction in THP1 LC3GFP cells measured at 16hpi by flowcytometry. Data is from three independent experiments (n=6).
- (C) Autophagy induction in BMDM LC3GFP cells measured at 72hpi by flowcytometry. Data is from two independent experiments (n=4).
- (D) Conversion of GFP tagged and endogenous LC3I to LC3II detected by western blotting in whole cell lysates. Data is representative of three independent experiments.
- (E) Inhibition of Δ3167c-induced autophagy in presence of 3-MA (5mM) measured by flowcytometry. Data is representative of three independent experiments (n=4).

Asterisks indicate statistically significant differences compared to Mtb except for (E) where they indicate statistically significant differences compared to 3-MA untreated condition.

Conversion of LC3I to LC3II was also monitored by flowcytometry in infected THP1 LC3GFP and BMDM LC3GFP macrophages at 16hpi. The assay involves permeabilization of cells leading to loss of cytosolic LC3I and detection of LC3II bound to the autophagosomal membrane (Fig 27A) (184).. A two-fold increase in autophagy induction by  $\Delta 3167c$  was observed compared to either Mtb or the complement in both cell types (Fig 27B, 27C). Conversion of LC3I GFP to LC3II GFP was detected by immunoblotting as well in whole cell lysates prepared from infected THP1 LC3GFP macrophages at 16hpi. Higher levels of both endogenous LC3II and LC3II tagged with GFP were detected by this approach in  $\Delta 3167c$  infected cells compared to Mtb or complement infected cells (Fig 27D). Autophagy induction by  $\Delta 3167c$  was confirmed using 3-MA, a widely used autophagy inhibitor (177). Inclusion of the inhibitor during chase of infected THP1 LC3GFP macrophages reduced autophagy induction by  $\Delta 3167c$  to levels similar to that induced by Mtb (Fig 27E).

These data demonstrate that  $\Delta 3167c$  induces higher levels of autophagy compared to both Mtb and the complement strain. Neither Mtb nor  $\Delta 3167c$  were found to co-localize with the autophagosome marker LC3 indicating that *Rv3167c* is required for controlling macroautophagy induction by Mtb.

### **3.3.1.2 Autophagy induction by $\Delta 3167c$ culminates in degradation**

Increased levels of LC3II can be attributed to either an increase in autophagosome formation or to a decrease in LC3II degradation due to inhibition of autophagosome maturation (147). To distinguish between these two possibilities  $\Delta 3167c$  infected cells were treated with the vacuolar proton ATPase inhibitor bafilomycin A1 (BafA1). By inhibiting phagosomal acidification, BafA1 inhibits degradation of lysosomal contents

and thus in the case of *denovo* autophagosome generation results in increased LC3II accumulation. If LC3II accumulation occurs due to a defect in autophagosome maturation, then BafA1 addition will not result in increased LC3II collection. Higher levels of LC3II were detected in  $\Delta 3167c$  infected and BafA1 treated macrophages compared to untreated controls (60% in BafA1 treated vs 40% in untreated control cells) (Fig 28A).

Another way of analyzing autophagosome maturation is following the delivery of the LC3GFP fusion protein to the lysosomal compartment where it is degraded to yield free GFP (185). Whole cell lysates prepared from infected THP1 LC3GFP macrophages at 16hpi were utilized for the detection of GFP by immunoblotting. GFP was detected only in  $\Delta 3167c$ -infected macrophages and is indicative of higher levels of autophagy induction and degradation induced by  $\Delta 3167c$  (Fig 28B).

In conclusion, the increased levels of LC3II observed in  $\Delta 3167c$ -infected cells are due to a stimulation of *de novo* formation of autophagosomes and not due to an inhibition of autophagosome maturation.

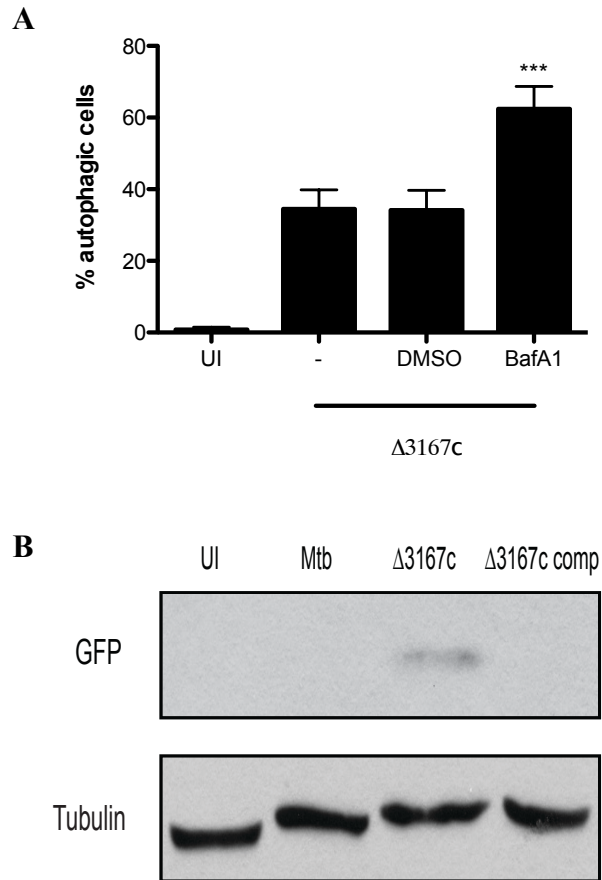


**Fig 28.  $\Delta 3167c$  does not mediate inhibition of autophagosome maturation**

- (A) Autophagy induction by  $\Delta 3167c$  in presence of BafA1 (250nM) at 16hpi measured via flowcytometry. Data is from 3 experiments (n=6). Asterisks indicate statistical significance compared to DMSO treated control.
- (B) Free GFP generated during lysosomal degradation of LC3GFP detected by western blotting in whole cell lysates. Data is representative of three independent experiments.

### 3.3.1.3 $\Delta 3167c$ induced autophagy is independent of *eis*

The enhanced intracellular survival gene (*eis*) of Mtb encodes for a secreted protein that can be detected in the cytoplasm of infected macrophages (186,187). The Mtb *eis* gene has been shown to be required for autophagy inhibition (175). Transcriptome analysis demonstrated reduced *eis* expression in  $\Delta 3167c$ -compared to Mtb after macrophage infection (work done by Jeff Quigley, data not shown). To determine whether  $\Delta 3167c$  induced autophagy is linked to Eis, THP1 LC3GFP macrophages were infected with  $\Delta 3167c$  and  $\Delta 3167c$  transformed with either empty plasmid (pSY1) or plasmid encoding for *eis* (pSY1::*eis*). Autophagy induction was analyzed by flowcytometry at 16hpi. No inhibition of autophagy induction was observed in cells infected with  $\Delta 3167c$  overexpressing Eis compared to those infected with the parent  $\Delta 3167c$  strain (Fig 29A).

The lack of autophagy inhibition in cells infected with  $\Delta 3167c$  overexpressing Eis could be attributed to the inability of Eis to access the host cell cytosol. Therefore an alternative strategy was needed to examine the contribution of Eis to  $\Delta 3167c$ -mediated autophagy in a manner dissociated from its cytosolic translocation. To do so,  $\Delta 3167c$  overexpressing Eis and the auto activated form of the pore forming toxin listerolysin O (LLO) was generated. Formation of pores on the phagosomal membrane by LLO should allow for cytosolic access of Eis within the infected macrophage. Autophagy induction was measured in infected THP1 LC3GFP macrophages by flowcytometry at 16hpi. No differences in autophagy induction were observed in cells infected with  $\Delta 3167c$  or the mutant strain overexpressing LLO and Eis (Fig 29B). To check whether expression and secretion of Eis is affected in  $\Delta 3167c$ , cell lysates and culture filtrates prepared from Mtb

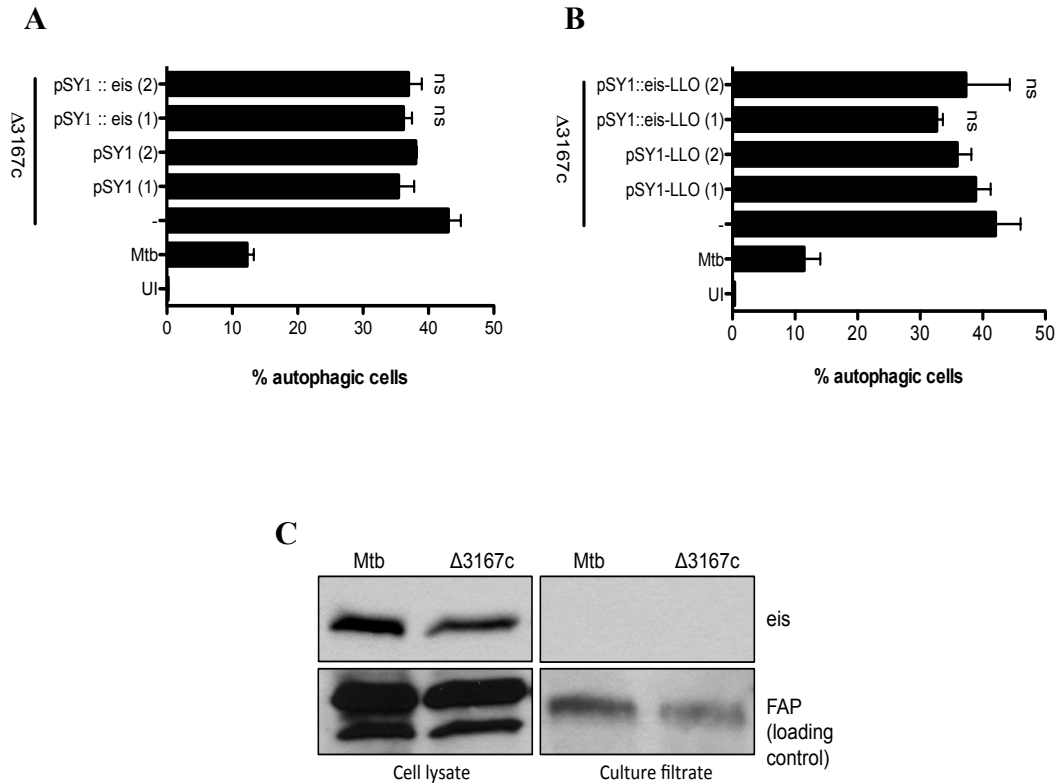


**Fig 29.  $\Delta 3167c$  mediated autophagy is independent of Eis**

- (A) Autophagy induction by  $\Delta 3167c$  expressing Eis at 16hpi measured by flowcytometry. Data is from one experiment (n=3). Statistical significance was estimated relative to  $\Delta 3167c$  containing pSY1.
- (B) Autophagy induction by  $\Delta 3167c$  expressing either LLO alone or both Eis and LLO at 16hpi measured by flowcytometry. Data is from one experiment (n=3). Statistical significance was estimated relative to  $\Delta 3167c$  containing pSY1-LLO.
- (C) Expression and secretion of Eis by Mtb and  $\Delta 3167c$ . Data is from one experiment.

and  $\Delta 3167c$  were immunoblotted for Eis. Contrary to previous reports, we did not detect Eis secretion by Mtb.  $\Delta 3167c$  did not secrete Eis either and no differences were observed in Eis expression in the cell lysates of the two strains. (Fig 29C).

These data indicate that Eis is not involved in autophagy induction by  $\Delta 3167c$ .

### **3.3.2 Molecular mechanisms of $\Delta 3167c$ induced autophagy**

#### **3.3.2.1 JNK activation is required for autophagy induction by $\Delta 3167c$**

The MAPK's JNK and p38 have been implicated in autophagy induction by Mtb mutants, as well as in response to cytokines and other autophagy inducers (160,163,177). To investigate the role of MAPK's in  $\Delta 3167c$  induced autophagy, their activation in infected THP1 LC3GFP macrophages was assessed by immunoblotting for phosphorylated forms in whole cell lysates prepared 16hpi. An approximately 10-fold increase in phosphorylated JNK was detected in  $\Delta 3167c$ -infected cells at 18hpi compared to those infected with either Mtb or the complement (Fig 30A). About 2-fold higher levels of phosphorylated p38 MAPK were detected at 0hpi in  $\Delta 3167c$ -infected cells compared to those infected with Mtb and complement, which returned to Mtb levels by 18hpi (Fig 30A). A similar result was obtained from whole cell lysates prepared from infected HuMDM's at 24hpi (Fig 30B).

JNK and p38 MAPK inhibitors (SP600125 and SB230580 respectively) were utilized to assess the contribution of these MAPK's in autophagy induction by  $\Delta 3167c$ . Inhibitors were added to THP1 LC3GFP macrophages prior to infection and were maintained throughout the infection and the chase. Autophagy induction was analyzed by flowcytometry at 16hpi. Inclusion of the JNK inhibitor SP600125 led to a dose dependent decrease in autophagy induction by  $\Delta 3167c$  while no changes were seen in macrophages

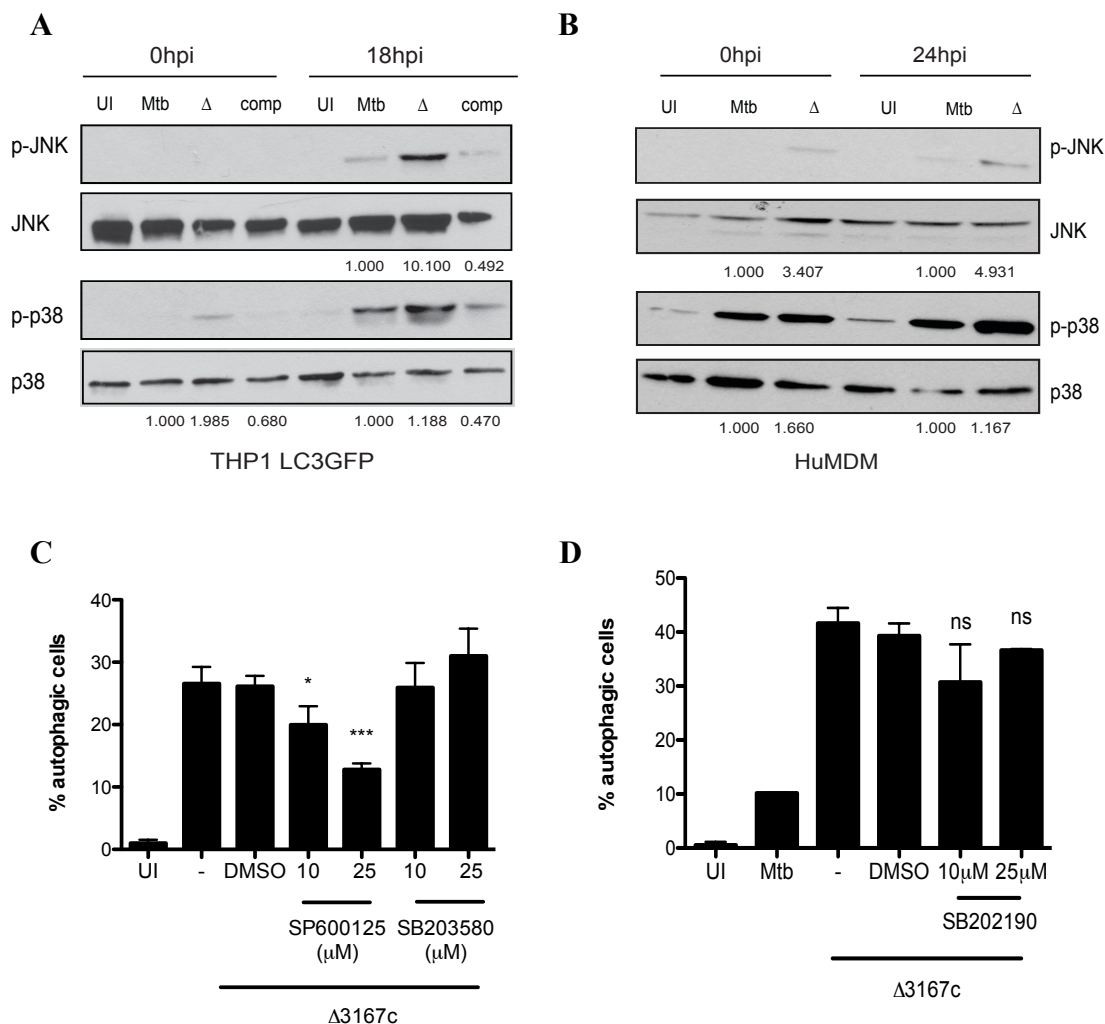


**Fig 30. Autophagy induction by  $\Delta 3167c$  is dependent on JNK but not p38 MAPK activation**

- (A) JNK and p38 MAPK phosphorylation in THP1 LC3GFP WCL's at 18hpi detected by western blotting. Numbers below indicate fold change in band intensity compared to Mtb sample after normalization to loading control. Data is representative of three independent experiments.
- (B) JNK and p38 MAPK phosphorylation in HuMDM WCL's at 24hpi detected by western blotting. Numbers below indicate fold change in band intensity compared to Mtb sample after normalization to loading control. Data is representative of three independent experiments.
- (C) Autophagy induction by  $\Delta 3167c$  in presence of JNK (SP600125) and p38 MAPK (SB203580) inhibitors detected by flowcytometry. Data is representative of three independent experiments (n=6).
- (D) Autophagy induction by  $\Delta 3167c$  in presence of p38 MAPK inhibitor (SB202190) detected by flowcytometry. Data is representative of two independent experiments (n=4).

For (C) and (D), statistical significance was estimated relative to DMSO solvent control.

treated with the p38 MAPK inhibitor SB203580 (Fig 30C). Only a partial inhibition of  $\Delta$ 3167c-induced autophagy was seen with the highest concentration (25 $\mu$ M) of SP600125, this could be due to an incomplete inhibition of JNK activation. p38 MAPK inhibition with another inhibitor - SB202190 did not affect  $\Delta$ 3167c induced autophagy as well (Fig 30D).

Therefore, while  $\Delta$ 3167c induces activation of both JNK and p38 MAPK, only JNK activation is involved in autophagy induction.

### **3.3.2.2 $\Delta$ 3167c induced autophagy does not involve Beclin1 upregulation and Bcl2 phosphorylation**

During autophagy, Beclin1 is required for autophagosome membrane nucleation along with Atg14L and class III PI3K (139). Beclin1 transcription has been shown to be upregulated in Vitamin D<sub>3</sub> treated, Mtb infected macrophages undergoing autophagy (160). Increased levels of Beclin1 have also been implicated in autophagy induction by the hepatitis C virus (188). To determine whether  $\Delta$ 3167c induced autophagy involves an increase in Beclin1 levels, whole cell lysates were prepared from infected THP1 LC3GFP macrophages at 16hpi and Beclin1 protein levels detected by immunoblotting. Macrophages infected with Mtb,  $\Delta$ 3167c and complement had similar levels of Beclin1 (Fig 31A).

The amount of Beclin1 present in the host cell is not the only factor that governs the role of Beclin1 in autophagy induction. Beclin1 has a BH3 domain through which it binds to Bcl2 and is rendered unavailable for autophagy induction. Phosphorylation of Bcl2 disrupts this interaction allowing Beclin1 to participate in autophagy induction (146). To determine the role of Beclin1 regulation by phosphorylation of Bcl2 in  $\Delta$ 3167c

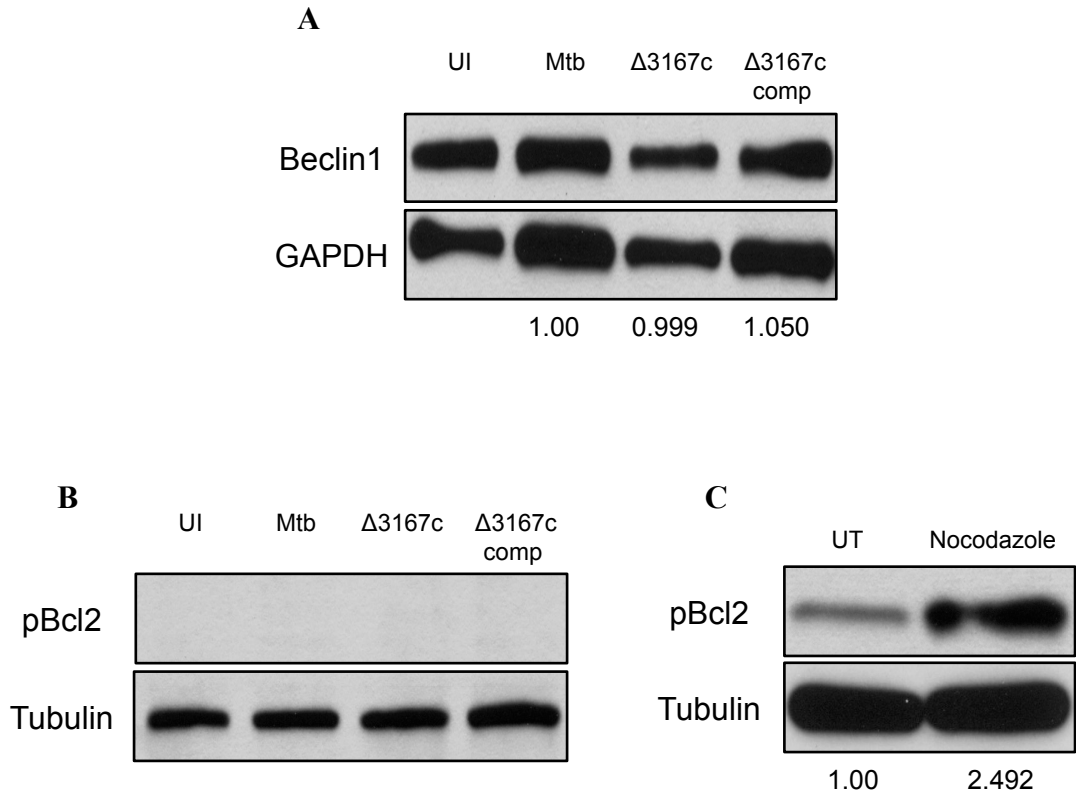


**Fig 31. Autophagy induction by  $\Delta 3167c$  is independent of Beclin1 levels and Bcl2 phosphorylation**

- (A) Beclin1 levels in THP1 WCL's at 16hpi detected by western blotting. Numbers below indicate fold change in band intensity compared to Mtb sample after normalization to loading control. Data is representative of three independent experiments.
- (B) Bcl2 phosphorylation in THP1 WCL's at 16hpi detected by western blotting. Data is representative of three independent experiments.
- (C) Induction of Bcl2 phosphorylation by nocodazole treatment in THP1 monocytes. Numbers below indicate fold change in band intensity compared to untreated (UT) sample. Data is from one experiment.

induced autophagy, whole cell lysates of infected THP1 LC3GFP macrophages prepared at 16hpi were immunoblotted for phosphorylated Bcl2 (pBcl2). A complete absence of phosphorylated Bcl2 (pBcl2) was observed in both infected macrophages as well as uninfected controls (Fig 31B). To ensure that the antibody used could detect pBcl2, a positive control was established using THP1 monocytes treated with nocodazole. Treatment with nocodazole, a microtubule depolymerizing agent has been previously reported to increase Bcl2 phosphorylation (189). Following nocodazole treatment, increased levels of pBcl2 were detected compared to untreated control cell (Fig 31C), thus validating the antibody used. While no pBcl2 was detected in uninfected THP1 macrophages (obtained by PMA treatment of monocytes), pBcl2 was present in uninfected THP1 monocytes.

Thus, induction of autophagy by  $\Delta 3167c$  does not require an increase in Beclin1 levels and phosphorylation of Bcl2.

### **3.3.2.3 Inhibition of Akt activation is required for $\Delta 3167c$ -induced autophagy**

The serine threonine kinase Akt influences several host cell processes such as cell proliferation, migration and cell death. Akt is also involved in inhibition of autophagy via mTOR activation and via phosphorylation of Beclin1 (190). The role of Akt in  $\Delta 3167c$ -induced autophagy was examined by first determining whether Akt activation is inhibited in infected macrophages. Whole cell lysates were prepared from uninfected and infected THP1 LC3GFP macrophages at 16hpi and immunoblotted for total Akt and phosphorylated Akt. Akt phosphorylation was found to be severely inhibited in  $\Delta 3167c$  infected cells (Fig 32A). To confirm the role of Akt in autophagy induction by  $\Delta 3167c$ , THP1 LC3GFP macrophages were infected in presence and absence of sc-79 and

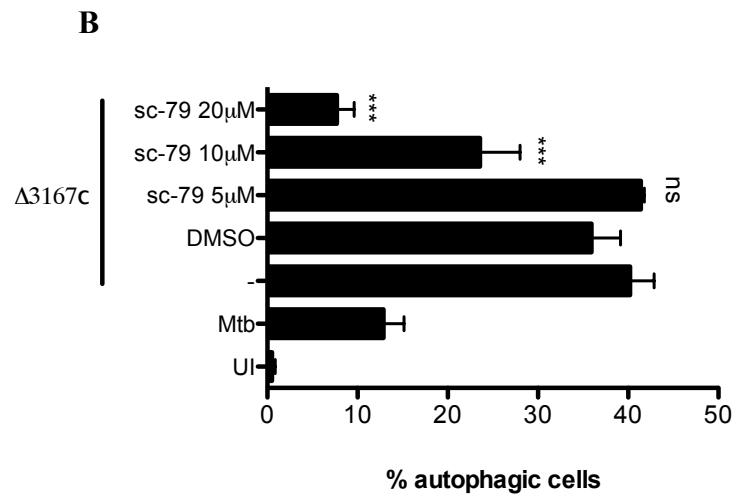
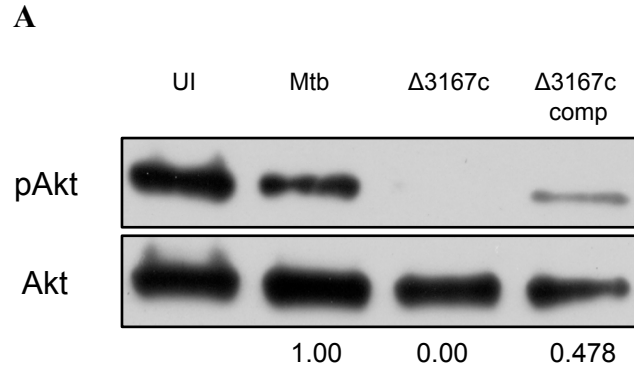


**Fig 32. Autophagy induction by  $\Delta 3167c$  is dependent on inhibition of Akt activation**

(A) Akt phosphorylation in THP1 cells detected at 16hpi by western blotting. Numbers below indicate fold change in band intensity compared to Mtb sample after normalization to loading control. Data is representative of three independent experiments.

(B) Autophagy induction by  $\Delta 3167c$  in presence of Akt activator sc-79 detected by flowcytometry at 16hpi. Data is from 4 experiments (n=8). Statistical significance was estimated compared to DMSO treated solvent control.

autophagy induction examined by flowcytometry. sc-79 is a small molecule activator which binds to Akt, leading to a conformational change allowing for Akt phosphorylation and activation in the cytosol (191). A dose dependent decrease in  $\Delta 3167c$ -mediated autophagy was observed in macrophages treated with sc-79 (Fig 32B).

These data indicate that autophagy induction by  $\Delta 3167c$  requires inhibition of Akt phosphorylation and activation.

### **3.3.3 Crosstalk between $\Delta 3167c$ induced necrosis and autophagy**

#### **3.3.3.1 $\Delta 3167c$ mediated necrosis is independent of JNK and p38 MAPK but requires inhibition of Akt activation while $\Delta 3167c$ -induced autophagy is dependent on ROS.**

Following infection with  $\Delta 3167c$ , increased phosphorylation of JNK and p38 MAPK were observed and autophagy induction was found to be dependent on JNK activation (Fig 30A, 30B, 30C). To examine whether JNK and/or p38 MAPK were required for necrosis induction by  $\Delta 3167c$ , THP1 macrophages were infected in presence and absence of the inhibitors SP600125 and SB203580 and PI staining was performed at 24hpi. Inclusion of neither the JNK nor the p38 MAPK inhibitor reversed the pro-necrotic phenotype of the mutant strain, rather an increase in necrosis induction was observed in both cases (Fig 33A, 33B). To ensure that the inhibitors are not toxic to the cells, metabolic activity of SP600125 and SB203580 treated THP1 macrophages was tested using the MTS assay. At 24-hour post treatment, SB203580 had no toxic effects on cells (Fig 33C). Cells treated with SP600125 at 25 $\mu$ M displayed a 1.4 fold decrease in metabolic activity (Fig 33C). This may account for the modest increase in necrosis induction observed in  $\Delta 3167c$ -infected cells in presence of the inhibitor.

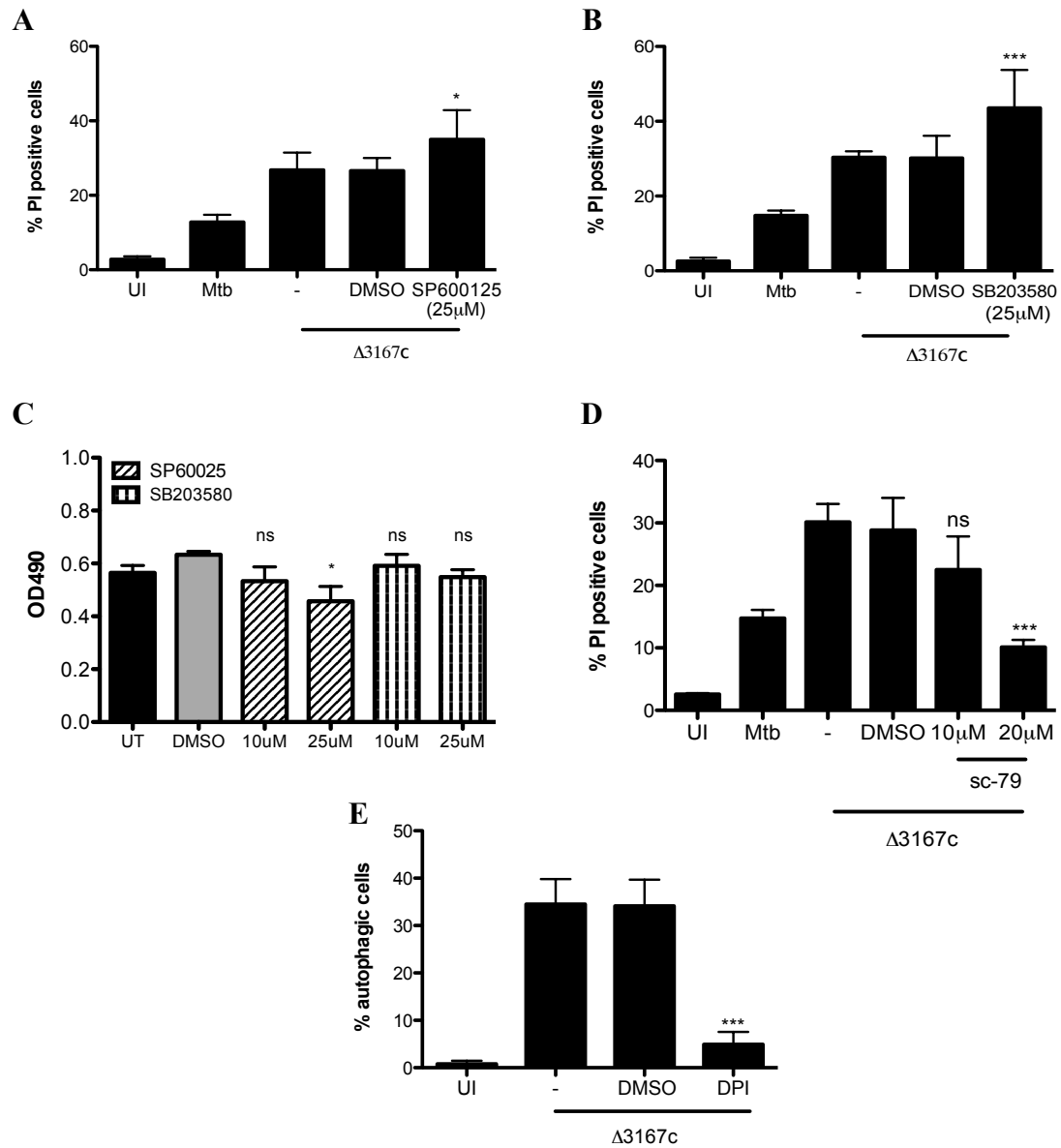


**Fig 33. Necrosis induction by  $\Delta 3167c$  is dependent on Akt while autophagy induction requires ROS**

- (A) Necrosis induction by  $\Delta 3167c$  in presence of JNK inhibitor (SP600125) in THP1 macrophages measured by flowcytometry at 24hpi. Data is from 3 independent experiments (n=6).
- (B) Necrosis induction by  $\Delta 3167c$  in presence of p38 MAPK inhibitor (SB203580) in THP1 macrophages measured by flowcytometry at 24hpi. Data is from 3 independent experiments (n=6).
- (C) MTS assay to determine JNK and p38 MAPK inhibitor toxicity in THP1 cells at 24hpi. Data is from one experiment (n=3).
- (D) Necrosis induction by  $\Delta 3167c$  in presence of Akt activator sc-79 in THP1 macrophages measured by flowcytometry at 24hpi. Data is from 3 independent experiments (n=6).
- (E) Autophagy induction by  $\Delta 3167c$  in presence of ROS inhibitor DPI in THP1 LC3GFP macrophages measured by flowcytometry at 24hpi. Data is from 3 independent experiments (n=6).

Statistical significance was estimated relative to the DMSO treated solvent control.

Inhibition of Akt activation by was found to be required for  $\Delta 3167c$  mediated autophagy (Fig 32B). The role of Akt in  $\Delta 3167c$ -induced necrosis was assessed by infecting THP1 macrophages in presence of the Akt activator sc-79 and performing PI stain at 24hpi. Necrosis induction by the mutant in the presence of sc-79 was inhibited to levels induced by Mtb (Fig 33D).

ROS has been previously implicated in Mtb mediated autophagy induction (177). Mitochondrial ROS was demonstrated to be required for necrosis induction by  $\Delta 3167c$  (Fig 25D). To determine whether ROS is required for autophagy induction by  $\Delta 3167c$ , THP1 LC3GFP macrophages were infected in presence of the flavoprotein inhibitor DPI and autophagy induction assessed by flowcytometry at 16hpi. Inclusion of DPI led to a complete inhibition of autophagy induction by  $\Delta 3167c$ , thus demonstrating the requirement of ROS for this process (Fig 33E).

In conclusion, mitochondrial ROS generation and inhibition of Akt activation underly both necrosis and autophagy induction by  $\Delta 3167c$  while JNK activation is required for  $\Delta 3167c$ -mediated autophagy induction alone.

### **3.3.3.2 Inhibition of $\Delta 3167c$ -induced autophagy does not inhibit necrosis**

Autophagy via breakdown of cellular contents helps cells survive during starvation. However, excessive autophagy induction can also lead to cell death (192). To examine whether  $\Delta 3167c$  induced necrosis is dependent on autophagy induction, infected THP1 macrophages were treated with the autophagy inhibitor 3-MA during the chase period and at 24hpi necrosis induction was measured by PI staining. Inclusion of 3-MA resulted in increased necrosis of  $\Delta 3167c$  infected macrophages (Fig 34A). However, increased necrosis observed in 3-MA treated cells could be due to toxic effects of 3-MA

itself as uninfected cells treated with 3-MA undergo necrosis as measured by the toxilight assay (Fig 34B). As an alternative approach, autophagy deficient BMDM's from  $Atg5^{flox/flox}$  LysM-Cre<sup>+</sup> mice were infected and at the indicated timepoints, supernatants used for toxilight assay. No differences were seen in necrosis induction by  $\Delta 3167c$  in autophagy deficient  $Atg5^{flox/flox}$  LysM-Cre<sup>+</sup> BMDM's and associated  $Atg5^{flox/flox}$  LysM-Cre<sup>-</sup> control macrophages (Fig 34C).

These data indicate that autophagy induction by  $\Delta 3167c$  does not lead to necrosis.

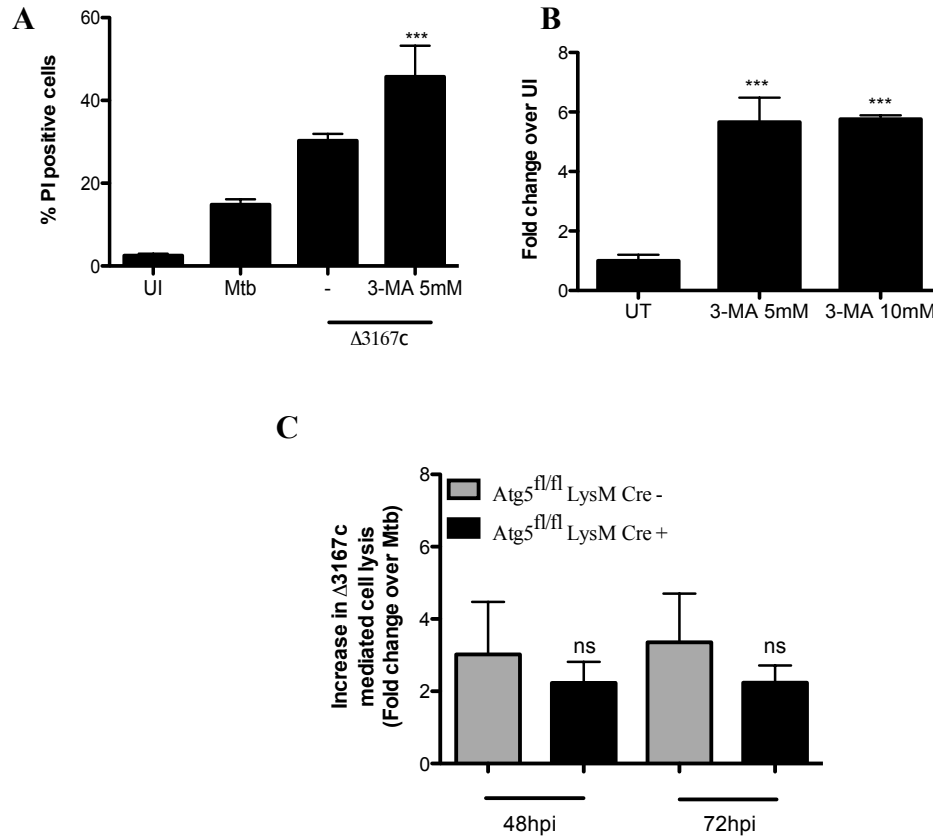


**Fig 34.  $\Delta 3167c$  induced autophagy does not result in necrosis**

- (A) Effects of autophagy inhibitor 3-MA on necrosis induction by  $\Delta 3167c$  measured by PI staining. Data is representative of two independent experiments (n=4). Statistical significance was estimated relative to  $\Delta 3167c$ -infected cells.
- (B) Toxicity of 3-MA in uninfected THP1 macrophages measured by toxilight assay. Data is representative of one independent experiment (n=3). Statistical significance was estimated relative to untreated (UT) cells.
- (C) Necrosis induction in autophagy competent (Atg5<sup>fl/fl</sup> LysM-Cre<sup>-</sup>) and autophagy deficient (Atg5<sup>fl/fl</sup> LysM-Cre<sup>+</sup>) BMDM's measured using Toxilight assay. Data is from 3 independent experiments (n=6). Statistical significance was calculated compared to autophagy competent control for each time point.

### 3.3.4 Discussion

While several studies detail the effects of autophagy induction by physiological, pharmacological and immunological stimuli on the outcome of Mtb infection, the ability of Mtb to manipulate autophagy by itself has only been more recently described. (145,150,168). At present only the *eis* gene of Mtb has been identified as an anti-autophagic gene (177). This study reveals that the gene *Rv3167c* is required for the inhibition of Mtb induced autophagy in an Akt, JNK and ROS dependent manner.

Infection with  $\Delta 3167c$  results in inhibition of Akt activation and restoration of Akt activation resulted in inhibition of  $\Delta 3167c$  induced autophagy (Fig 32A, 32B). Inhibition of Akt activation has been implicated both in macroautophagy induction in response to nutritional stresses as well as in selective autophagy induction in response to pathogens such as *T.gondii* and *S.typhimurium* (141,193,194). Akt inhibition results in downstream inhibition of mTOR activation and autophagy induction (141). Alternatively, activated Akt has also been implicated in mTOR independent modulation of autophagy via phosphorylation of Beclin1, rendering Beclin1 unavailable to participate in formation of the autophagy nucleation complex (190). Conflicting reports exist regarding the role of mTOR in Mtb mediated autophagy modulation. Zullo *et al* demonstrated mTOR to be activated in Mtb infected macrophages undergoing autophagy indicating Mtb mediated autophagy induction to be mTOR independent (167). On the other hand, Wang *et al* implicated Mtb mediated transcriptional downregulation of Rheb, an mTOR activator, in induction of autophagy, indicating Mtb mediated autophagy to be mTOR dependent (180).  $\Delta 3167c$  mediated autophagy could therefore be mTOR dependent or independent and Akt could potentially modulate either mechanism. Increased activation of the MAPK

JNK was found to be associated with  $\Delta 3167c$  induced autophagy as well (Fig 30A, 30B, 30C). JNK mediated autophagy has been shown to depend on phosphorylation of Bcl2 resulting in its dissociation from Beclin1 in HeLa cells in response to starvation and in mouse embryonic fibroblasts (MEF's) in response to viral infection (195,196). No Bcl2 phosphorylation was detected in  $\Delta 3167c$  infected macrophages (Fig 31B). The lack of a role for Bcl2 phosphorylation in  $\Delta 3167c$ -induced autophagy could be due to the use of macrophages in this study. Our study does not completely rule out the role of Beclin1 and Bcl2 in  $\Delta 3167c$  mediated autophagy as Beclin1-Bcl2 dissociation can be achieved via other mechanisms as well (Fig 10B) (146). Increased ROS levels in  $\Delta 3167c$  cells could contribute to autophagy induction by potentiating JNK activation. ROS has been reported to inactivate JNK phosphatases thereby leading to prolonged JNK activation (197). A feedback loop between ROS generation and JNK activation could therefore exist in  $\Delta 3167c$ -infected cells thereby leading to robust autophagy induction. Alternatively, the positive effect of ROS on  $\Delta 3167c$ -mediated autophagy could be attributed to effects of ROS on autophagic machinery. ROS has also been demonstrated to contribute to starvation-induced autophagy via regulation of Atg4, a cysteine protease that is required for the delipidation of LC3. In an oxidative environment, Atg4 is inactivated thereby leading to enhanced autophagosome formation (198), (199).

The enhanced intracellular survival (*eis*) gene is currently the only known Mtb gene that contributes to regulation of autophagy induction by Mtb. The phenotype of *eis* mutant infected cells is very similar to cells infected with  $\Delta 3167c$ . Both mutants induce increased levels of autophagy and caspase independent cell death compared to Mtb in a ROS dependent manner (177). Comparative transcriptome analysis revealed decreased

expression of *eis* in  $\Delta 3167c$  compared to Mtb (data not shown) making *eis* an attractive gene target possibly regulated by *Rv3167c*. We found  $\Delta 3167c$ -induced autophagy to be independent of *eis* (Fig 29), indicating that Mtb possesses other genes that can regulate autophagy. Caspase independent cell death induced by the *eis* mutant was found to be dependent on autophagy induction (177). However, in our experimental settings,  $\Delta 3167c$ -mediated necrosis does not depend on autophagy (Fig 34C). Mechanistically, ROS generation and Akt inactivation underly both autophagy and necrosis induction by  $\Delta 3167c$ , but JNK contributes only to  $\Delta 3167c$ -mediated autophagy (Fig 25A, 25D, 32B, 33A, 33E). This indicates the presence of divergent signaling modules downstream of ROS and Akt regulating autophagy and necrosis in  $\Delta 3167c$ -infected cells.

Recent studies on Mtb induced autophagy in the absence of other external stimuli have shown that Mtb co-localizes with autophagosomes, leading to lysosomal mediated destruction of the bacteria (150,151,168). However in our studies using two different approaches (confocal microscopy and TEM), we found that neither Mtb nor  $\Delta 3167c$  co-localized with autophagosomes. This could explain why similar numbers of Mtb and  $\Delta 3167c$  were recovered from infected THP1 macrophages at 24hpi (Fig 14) even though  $\Delta 3167c$  induces higher levels of autophagy that culminates in lysosomal degradation. A similar phenomenon was described in the case of the measles virus where viral infection lead to an increased accumulation of autophagosomes but viral proteins did not colocalize with these structures (200,201). Studies detailing selective autophagy of Mtb were performed on murine macrophages and dendritic cells and used a different strain of Mtb (Mtb Erdman compared to Mtb H37Rv used in this study) and this could account for the disparity observed. It is interesting to note that increased autophagy induction by the *eis*

mutant did not result in decreased bacterial recovery compared to Mtb in *ex vivo* macrophage infections as well (177). Treatment of *M.marinum* infected zebrafish embryos with Ar-12, an inhibitor of Akt activation resulted in increased autophagosome formation but not increased bacterial targeting to the autophagosomes compared to untreated, infected embryos (181). This suggests a role for Akt in modulation of selective autophagy targeting in mycobacterial infections. The host ubiquitin ligase Parkin has been implicated in both mitophagy as well as xenophagy of Mtb (151,202). We did not observe mitochondria in autophagosomes by electron microscopy in THP1 macrophages infected with either Mtb or  $\Delta 3167c$ . It is possible that in human macrophages, Mtb inhibits parkin expression and thus avoids co-localizing with autophagosomes. Induction of macroautophagy could be advantageous for Mtb via modulation of cytokine responses. Autophagy has been shown to negatively regulate AIM2 and NLRP3 inflammasome activation and IL1 $\beta$  production in macrophages (143). TNF production by Mtb sonicate treated human peripheral blood monocyctic cells (PBMC's) was reduced following addition of the autophagy inhibitor 3-MA (203). Additionally, autophagy may also control inflammatory responses by eliminating endogenous DAMP's that could be released from infected necrotic cells.

In conclusion, data from this study indicates Mtb induces macroautophagy in human macrophages and identifies *Rv3167c* as an anti-autophagic gene.

## CHAPTER 4 *Rv3167c* MANIPULATES Mtb VIRULENCE

### 4.1 INTRODUCTION

Pathogens possess a wide variety of genes that contribute to virulence - deletion/disruption of these virulence genes leads to attenuation. However, there are numerous reports in literature of “anti-virulence genes” whose deletion or disruption enhances the ability of the pathogen to cause disease and results in hypervirulence as measured by lower infectious dose, reduced clearance and decreased host survival time. Hypervirulence in Mtb has been reported in clinical strains as well as in defined gene mutants.

In this study we evaluated the contribution of *Rv3167c* to Mtb virulence using C57Bl6 mice infected via aerosol route. Deletion of *Rv3167c* results in an increase in Mtb virulence as demonstrated by the higher bacterial burden in the lungs and extra-pulmonary organs and the lower median survival time observed in  $\Delta 3167c$  infected mice compared to Mtb infected control animals. Higher cellular infiltration and increased levels of inflammatory cytokines and chemokines were also observed in lungs of  $\Delta 3167c$ -infected mice compared to the controls.

## **4.2 MATERIALS AND METHODS**

All animals were handled in accordance with guidelines approved by the Institutional Animal Care and Use Committee at the University of Maryland (IACUC).

### **4.2.1 Materials**

Female C57Bl6 mice were purchased from Jackson Laboratories.

### **4.2.2 Aerosol infection of mice**

Mice were infected with approximately 100 CFU of H37Rv,  $\Delta$ 3167c and complement strains via the aerosol route using a Glass-Col<sup>®</sup> Full Body Inhalation Exposure System. 25 mice were infected with each strain. Late log phase bacterial cultures were pelleted and resuspended in PBS. 5ml of bacterial culture containing  $50 \times 10^6$  bacteria were introduced into the nebulizer gently using a syringe and the aerosol chamber was run using the following protocol –

Nebulizing time: 1800 seconds

Cloud decay time: 1800 seconds

Decontamination time: 900 seconds

A new, clean, sterile nebulizer was used for infection with the different bacterial strains.

### **4.2.3 Determination of organ bacterial loads**

At the indicated time points, 3 infected mice were sacrificed by sedation with Isoflurane followed by cervical dislocation. Lungs were perfused with PBS through the right ventricle. The superior lobe was fixed in 10% buffered formalin for histopathology work. Remaining lobes were harvested, cut up in small pieces, resuspended in 3ml PBS and were broken down further in the Stomacher<sup>®</sup> 80 Biomaster for 10 minutes. The

homogenate was filtered to eliminate large tissue fragments and spun at 2000g for 15 minutes. The supernatant was refiltered and used for determination of lung cytokine levels. The pellet containing bacteria was resuspended in 500µl of 7H9 medium, appropriate dilutions were prepared and at least two dilutions were plated onto 7H11 plates in duplicate. Colonies were counted approximately 2 weeks after incubation at 37°C.

The uppermost left lobe of the liver and a section of spleen were fixed in 10% buffered formalin for histopathology work. Remainder of both liver and spleen were processed as described above for determination of bacterial loads.

#### **4.2.4 Measurement of lung homogenate cytokine levels**

Lung homogenate supernatants were obtained as described in section 4.2.3. Cytokine levels were determined using magnetic bead based multiplex assays (R&D Systems) on the Luminex MAGPIX<sup>®</sup> platform.

#### **4.2.5 Histopathology work**

AML Labs, Baltimore, MD, performed paraffin embedding, sectioning and hematoxylin-eosin (HE) staining of lung tissue sections. Lungs harvested from mice at 56dpi were sectioned at 2 levels with a distance of 100 microns between them. A total of 6 sections (3 from each level; 5 micron thickness) were stained with hematoxylin and eosin. This pattern of organ sectioning was followed to ensure that different regions in the lung could be analyzed. Total lung area and areas of inflammation in hematoxylin and eosin stained lung section images was determined using ImageJ. Total lung area and inflamed portions were outlined using the ROI tool and area of these regions was

measured. Percentage of inflamed area was calculated using the formula (Area of inflammation/Total lung area) x 100.

#### **4.2.6 Animal survival study**

7 infected mice per group were observed daily and weights of the animals were monitored and recorded on a weekly basis. Mice were sacrificed at humane time points as defined in the animal study protocol R-12-55 approved by IACUC. Some of the mice developed ulcerative dermatitis characterized by the formation of ulcerative lesions non responsive to broad-spectrum antibiotic treatment. Ulcerative dermatitis is an idiopathic condition that occurs spontaneously amongst C57Bl6 mice (224). Mice suffering from dermatitis were excluded from the survival study thus leaving a total of 3 subjects in the complement strain infected group.

#### **4.2.7 Statistical analysis**

For measurement of bacterial loads in organs and lung cytokine levels statistical analyses was performed on triplicate measurements obtained per animal with 3 animals tested per group per time point. ANOVA with Tukey post-test was used for estimation of statistical significance unless otherwise noted in the figure legends. Data is represented as mean  $\pm$  SD. For comparison of survival curves the Log-Rank (Mantel-Cox) test was performed. p-value significance is as follows –  $p \leq 0.05$  - \*,  $p \leq 0.01$  - \*\*,  $p \leq 0.0001$  - \*\*\*.

## 4.3 RESULTS AND DISCUSSION

### 4.3.1 Higher bacterial burden is recovered from organs of $\Delta 3167c$ infected mice

The ability to induce necrosis has been linked to virulence of Mtb. Infection with the virulent H37Rv strain results in cell death via necrosis compared to the avirulent H37Ra strain that causes apoptosis (104). The hypervirulent clinical strain 1471 of the Beijing family was found to induce higher levels of macrophage necrosis compared to the virulent H37Rv strain (211). As  $\Delta 3167c$  induces more necrosis compared to Mtb *ex vivo* we hypothesized that this mutant would exhibit hypervirulence *in vivo*. To assess the virulence of  $\Delta 3167c$ , C57Bl6 mice were infected with approximately 100 CFU of Mtb,  $\Delta 3167c$  and complement strains via the aerosol route. Animals were sacrificed at the indicated time points and homogenates of lung, spleen and liver were plated on 7H11 medium for estimation of CFU's. The lung bacterial burden at 1dpi was found to be similar in mice infected with the three strains indicating comparable initial inoculum of infection (Fig 35A). Starting at 14dpi, increased bacterial burden was recovered from the lungs of  $\Delta 3167c$ -infected mice compared to Mtb infected animals. At 28 dpi, growth of Mtb plateaued out, consistent with onset of the adaptive immune response. However, increased bacterial burdens were recovered from lungs of  $\Delta 3167c$ -infected mice compared to Mtb infected animals at both 28dpi (approximately 1 log) and 56dpi (about 2 logs) (Fig 35A). Lung bacterial burden in mice infected with the complement strain was comparable to animals infected with Mtb at all time points (Fig 35A).

$\Delta 3167c$  was not deficient in dissemination as indicated by the similar CFU's recovered from spleen and liver of Mtb and mutant infected animals at 14dpi (Fig 35B, 35C). Similar to the lung, higher bacterial burdens were recovered from the spleen

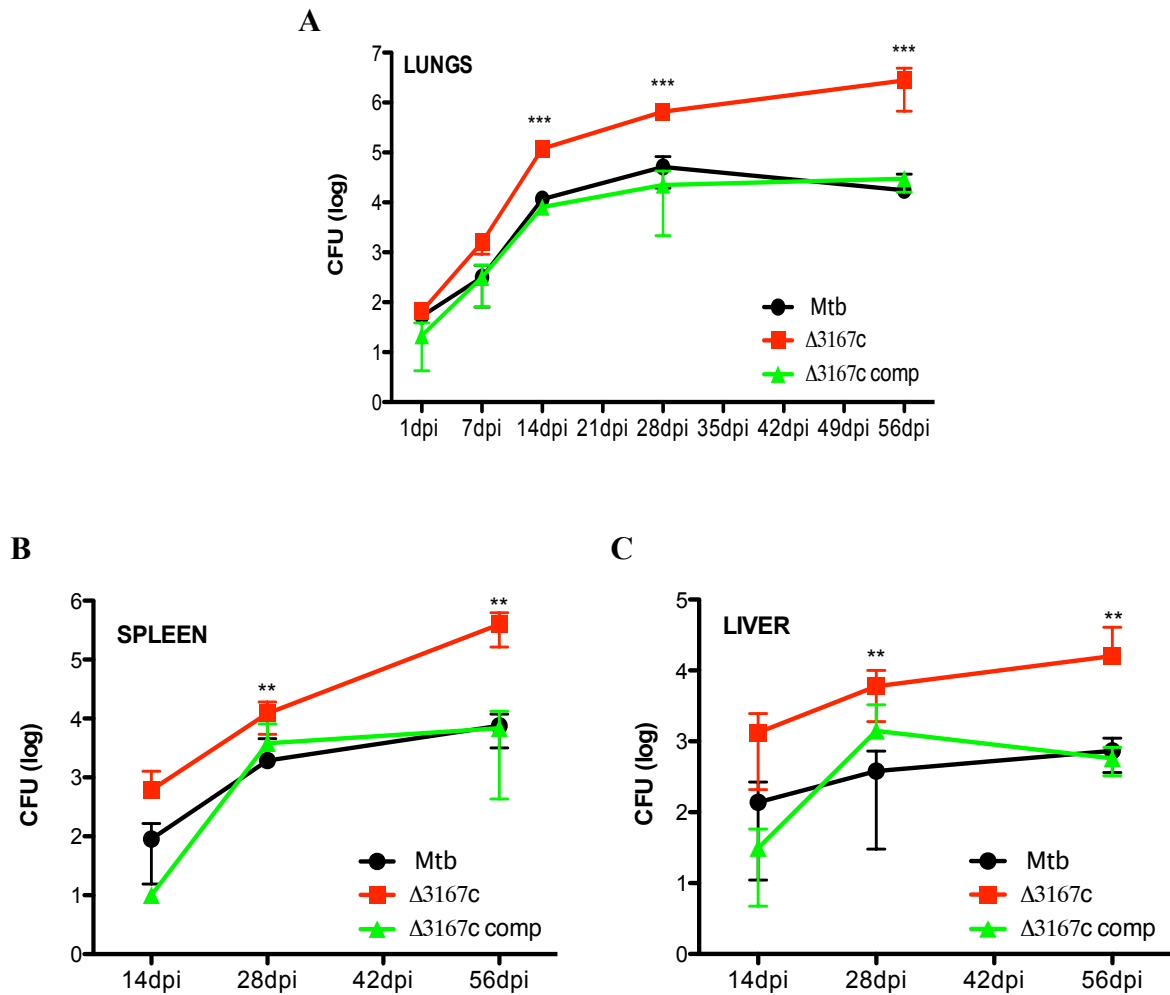


**Fig 35. Bacillary load in organs of C57Bl6 mice**

C57Bl6 mice were infected with Mtb,  $\Delta 3167c$  and  $\Delta 3167c$  complement via the aerosol route with a starting inoculum of approximately 100 CFU. Bacterial burdens were determined at the indicated time points in (A) lungs (B) spleen and (C) liver by plating out homogenates on 7H11 media and counting colonies obtained. Three mice were sacrificed at each time point per bacterial strain. Data is from one experiment. Asterisks indicate statistically significant differences compared to Mtb.

and liver of  $\Delta 3167c$  infected mice compared to Mtb infected mice at 28dpi and 56dpi (Fig 35B, 35C).

#### **4.3.2 Increased cellular infiltration is observed in the lungs of $\Delta 3167c$ infected mice**

Lungs of  $\Delta 3167c$ -infected mice had more lesions on their surface compared to organs from either Mtb or complement infected mice at 56dpi (Fig 36A). Sections were prepared from lungs harvested from infected mice at 56dpi and stained with hematoxylin and eosin and imaged by light microscopy at 40X magnification. At 7dpi, lungs of mice infected with any of the three bacterial strains appeared similar with no observable cellular infiltration (Fig 36B). At 56dpi, lungs from  $\Delta 3167c$  infected mice presented with higher levels of cellular infiltration and loss of alveolar air space compared to Mtb or complement infected mice (Fig 36B). Total lung area and area of inflamed regions (areas of intense hematoxylin and eosin staining) were measured using ImageJ and percentage of inflamed area calculated for lungs harvested at 56dpi. Massive inflammation was observed in lungs of  $\Delta 3167c$ -infected mice with approximately 40% of the total lung area involved (Fig 36C). This is in contrast to lungs of Mtb infected mice where about 15% of the lungs exhibited increased cellular infiltration (Fig...). Lungs from complement infected mice were comparable to organs obtained from Mtb infected animals – clear alveolar spaces were seen and only about 10% of the lung area was calculated to be inflamed (Fig 36C).

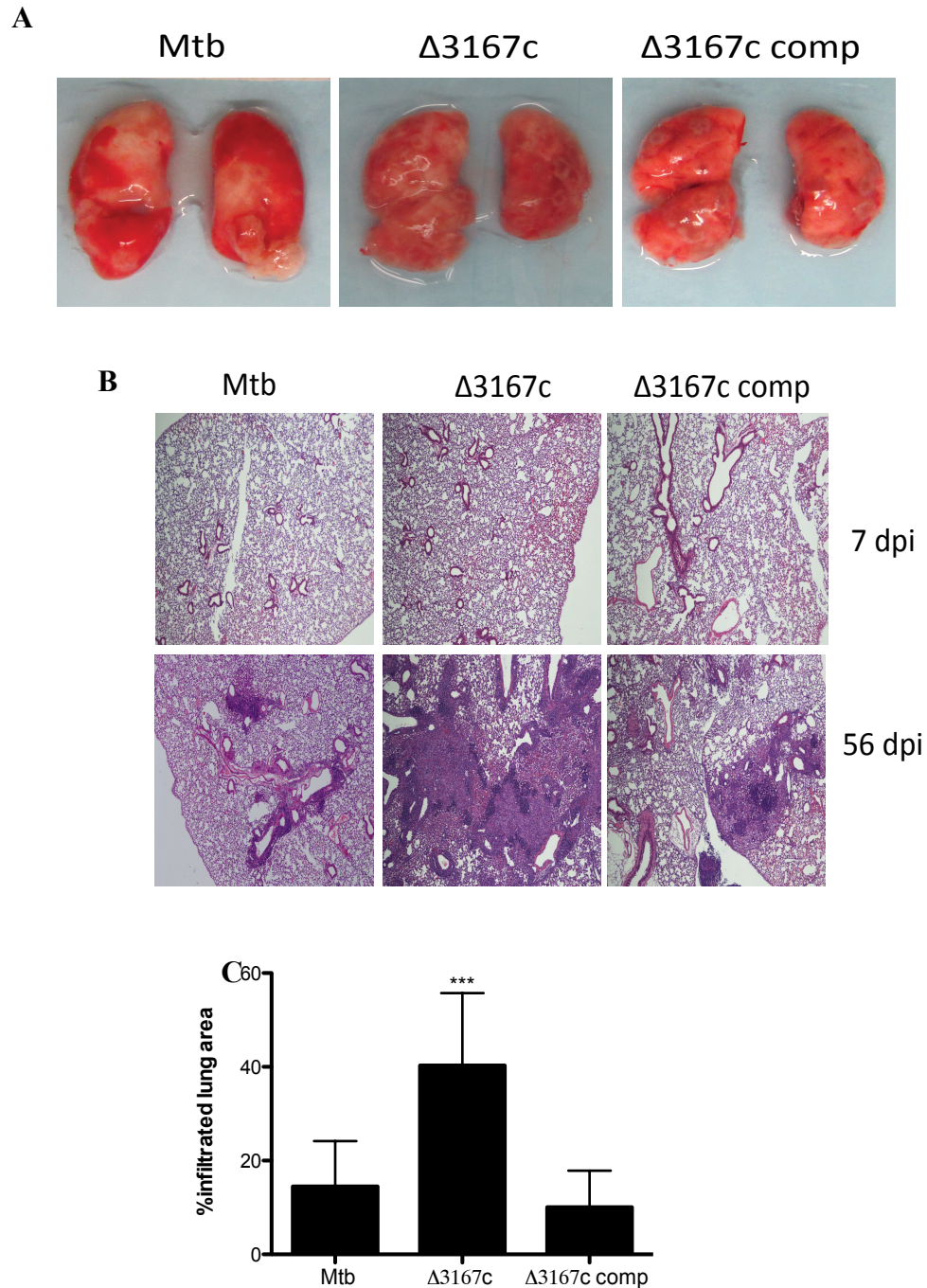


**Fig 36. Appearance and histopathology of lungs harvested from infected mice**

- (A) Superior lobe of lungs from infected mice were harvested at 56dpi and photographed prior to fixation in 10% formalin for histopathology analysis. Representative image from one out of three mice per bacterial strain.
- (B) Images of hematoxylin and eosin stained sections of lung harvested at 7dpi and 56dpi. Representative images from one out of three mice per bacterial strain.
- (C) Percentage of lung area exhibiting cellular infiltration. Combined data obtained from three mice per bacterial strain. Asterisks indicate statistically significant differences compared to Mtb.

### **4.3.3 Increased levels of inflammatory cytokines and chemokines are detected in lung homogenates of $\Delta 3167c$ infected mice.**

Cytokines and chemokines are known to play a critical role in determining the outcome of infection with Mtb (31). Homogenates prepared from lungs of infected mice at 14dpi and 56dpi were used in a Luminex assay to determine levels of various cytokines and chemokines. None of the cytokines and chemokines assayed for were detected in 14dpi samples. At 56dpi, amounts of IL12p70 and IFN $\gamma$  detected in samples from  $\Delta 3167c$  infected mice were very close to lowest limit of detection thus making interpretation of this data questionable (data not shown). Increased levels of the pro-inflammatory cytokines TNF (4.8 fold) and IL1 $\alpha$  (4 fold) were detected in lung homogenates of  $\Delta 3167c$ -infected mice compared to those obtained from Mtb infected animals (Fig 37A). IL6 and IL1 $\beta$  were detected in  $\Delta 3167c$ -infected but not Mtb infected mouse lung homogenates (Fig 37A). While the anti-inflammatory cytokine IL10 was detected only in samples from  $\Delta 3167c$ -infected mice, infection with the complement strain resulted in a similar level of IL10 production (Fig 37A). Elevated amounts of the chemokines CCL5 (11.9 fold), and MMP9 (2.95 fold) were also detected in lung homogenates from  $\Delta 3167c$ -infected mice compared to Mtb infected mice (Fig 37B). The chemokine CCL3 was detected only in samples from  $\Delta 3167c$ -infected and complement infected animals, with a three-fold reduction seen in the latter (Fig 37B).

Thus the lung milieu of  $\Delta 3167c$  infected mice has higher levels of proinflammatory cytokines and chemokines compared to Mtb and complement infected mice.

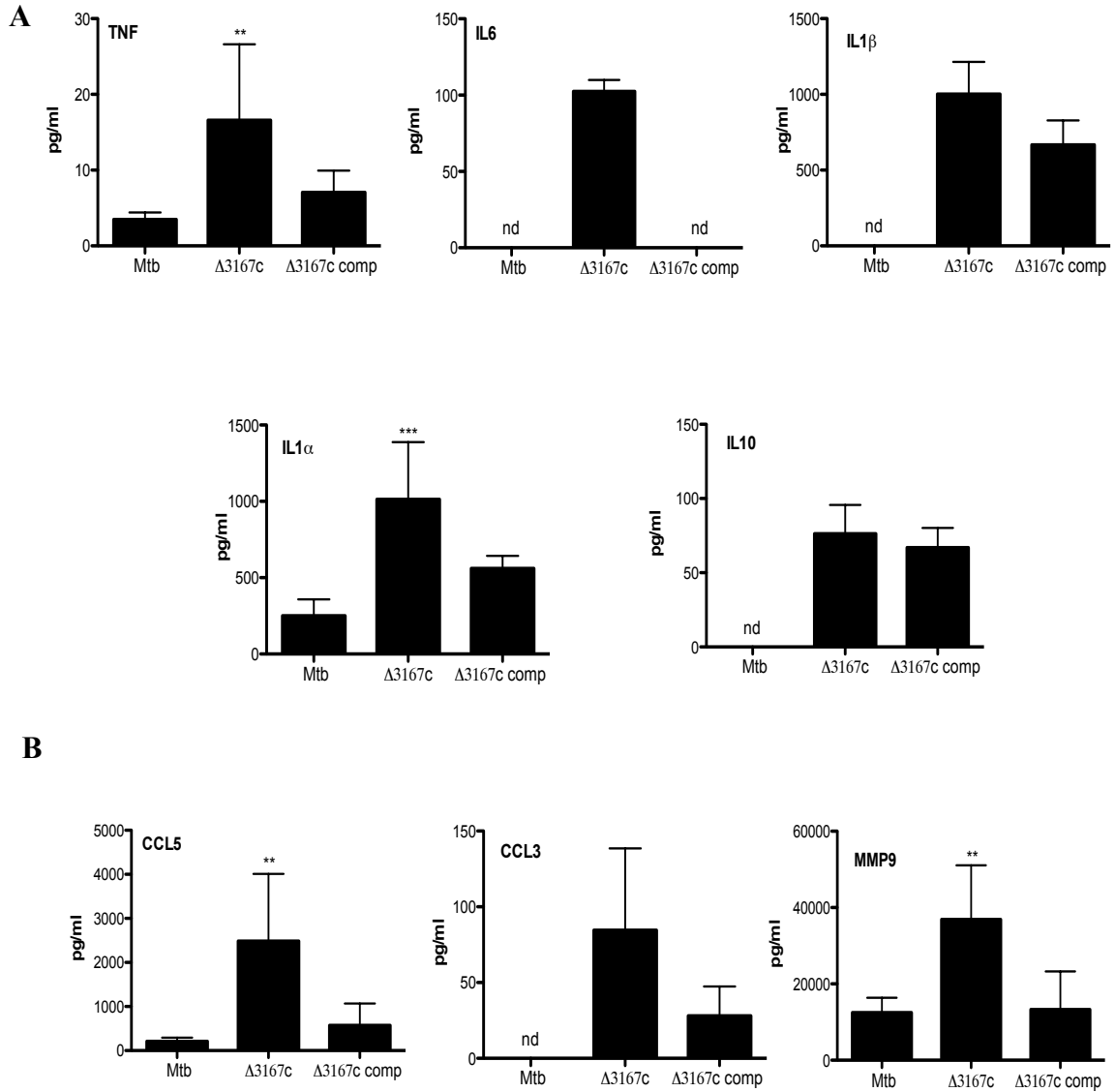


**Fig 37. Lung homogenate cytokine analysis**

Supernatants of homogenates prepared from lung tissue harvested at 56dpi were analyzed for (A) cytokines and (B) chemokines using a multiplex assay. Combined data obtained from three mice per bacterial strain. Asterisks indicate statistically significant differences compared to Mtb. (nd – not detected)

#### **4.3.4 $\Delta 3167c$ infected mice have lowered survival compared to those infected with Mtb**

To determine the contribution of *Rv3167c* to the virulence of Mtb, a survival study of mice infected with Mtb,  $\Delta 3167c$  and the complement strain via the aerosol route was performed. Mouse weights were tracked and mice were sacrificed at humane end points as defined by the IACUC approved study protocol. Mortality in  $\Delta 3167c$ -infected mice was observed starting at 33 weeks post infection, the median survival time for this group of mice was 41 weeks post infection. In contrast, while one animal in the Mtb and complement strain infected group succumbed to infection at 39 and 52 weeks post infection respectively, remaining mice in these groups survived until the end of the experiment (Fig 38). This data along with data on organ bacterial burden indicates that  $\Delta 3167c$  has increased virulence compared to Mtb.

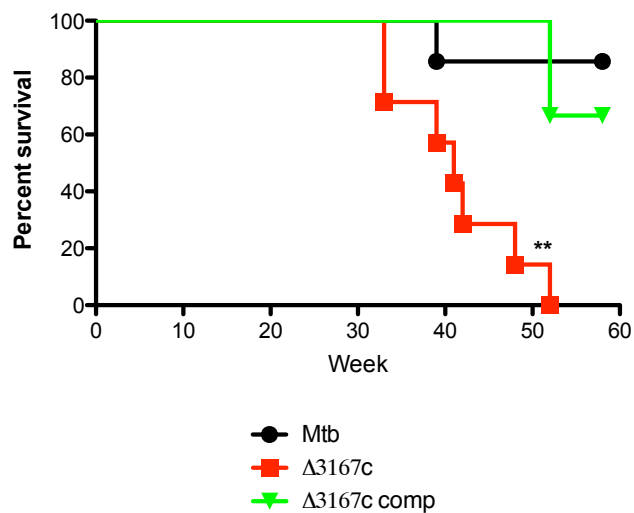


**Fig 38.  $\Delta 3167c$  infected mice have lower survival compared to Mtb**

C57Bl6 mice were infected with Mtb,  $\Delta 3167c$  and  $\Delta 3167c$  complement via the aerosol route with a starting inoculum of approximately 100 CFU and their survival monitored. Data is from one experiment. Log rank test was used for determining statistical significance. Asterisks indicate statistically significant differences compared to Mtb.

#### 4.3.5 Discussion

Mtb virulence has been linked previously to its ability to cause necrosis. Infection with the virulent H37Rv strain results in cell death via necrosis compared to the avirulent H37Ra strain that causes apoptosis (104). Hypervirulence of Beijing 1471 strain is associated with its ability to induce P2X7R dependent macrophage necrosis. (211). We found that the necrosis inducing  $\Delta 3167c$  was hypervirulent in immunocompetent C57Bl6 mice infected via the aerosol route. Mice infected with  $\Delta 3167c$  strain had a higher bacterial burden in the lungs, liver and spleen and a lower median survival time compared to Mtb infected mice. Both Mtb and  $\Delta 3167c$  replicate similarly *in vitro* as well as in *ex vivo* macrophage infections indicating that the increased bacterial burdens observed in lungs of  $\Delta 3167c$ -infected mice cannot be attributed to enhanced replication of the mutant (Fig 14). The increased pulmonary bacterial burden observed in  $\Delta 3167c$ -infected mice could be a function of necrosis elicited by the mutant. In LTA4H-high zebrafish, high levels of TNF initially control the bacterial load. However, the high levels of TNF also lead to macrophage necrosis, which in turn supports *M. marinum* extracellular growth resulting in increased bacterial burden in infected animals (9). We detected higher levels of TNF in the lungs of  $\Delta 3167c$ -infected mice compared to Mtb infected control animals. However,  $\Delta 3167c$  induced necrosis was found to be independent of TNF signaling *ex vivo* (Fig 23A). This does not exclude the possibility of necrosis induction by the mutant (by a currently uncharacterized pathway) leading to similar effects on bacterial load as observed by Roca *et al.* Infection of mice deficient in putative host factors required for necrosis induction by  $\Delta 3167c$  could help establish the link between necrosis induction and increased organ bacterial loads.

A calibrated host immune response is needed for the establishment of successful Mtb infection wherein the bacterial numbers are controlled but pathogen persistence occurs in the host alveolar space. An uncontrolled immune response could potentially lead to host tissue damage (31). Analysis of the lung cytokine profile revealed that  $\Delta 3167c$  infected mice had higher levels of the pro-inflammatory cytokines and chemokines at 56dpi compared to Mtb infected mice (Fig 37A, 37B). IL1 $\alpha$  has been implicated in neutrophilic inflammation in lungs of mice infected with *L.pneumophila* (82). Increased susceptibility of *miR223*<sup>-/-</sup> mice to Mtb has been associated with increased neutrophil recruitment by CCL3 (225). Elevated levels of CCL3 are also seen in susceptible *Ifn $\gamma$* <sup>-/-</sup> and *Nos2*<sup>-/-</sup> mice (226). Increased production of CCL3 was also observed in macrophages infected by  $\Delta 3167c$  compared to those infected with Mtb *ex vivo* (work done by Serdar Gurses, unpublished). Mtb infected *mmp9*<sup>-/-</sup> mice were found to recruit fewer macrophages to the lung and had a reduced lung bacterial burden compared to infected wild type controls (227). In zebrafish infections, *M.marinum* infected macrophages were found to upregulate MMP9 expression in neighboring epithelial cells and this was required for the recruitment of uninfected macrophages as well as an increase in bacterial burden (11). Lungs of  $\Delta 3167c$ -infected mice show higher levels of cellular infiltration (approximately 2.6 fold) compared to lungs from Mtb infected controls. It would be interesting to determine nature of inflammation (monocytic vs neutrophilic) in lungs of  $\Delta 3167c$ -infected mice.

The increased cytokine and chemokine level could be reflective of the increased bacterial burden observed with  $\Delta 3167c$  at 56dpi. Alternatively, changes in the cell wall composition of  $\Delta 3167c$  could also account for the aberrant inflammatory response. RNA

seq analysis of intracellular bacteria revealed members of the *mceI* operon (*Rv0166* - *Rv0169*) to be repressed in  $\Delta 3167c$  compared to Mtb (work done by Jeff Quigley, unpublished). An *mceI* operon mutant strain accumulated higher amounts of free mycolic acid in the cell wall and was found to be hypervirulent in C57Bl6 mice (212,214). Macrophages infected with the *mceI* operon mutant *ex vivo* however produced lower amounts of TNF and IL6 compared to Mtb infected controls. A different cytokine induction profile for the *mceI* operon mutant could be observed in the more complex *in vivo* environment. The hypervirulent *pknH* mutant is postulated to induce a hyperinflammatory response based on the low cell wall lipoarabinomannan:lipomannan ratio (217). A comparative analysis of the cell wall lipid content of Mtb and  $\Delta 3167c$  strain will provide more insight into possible bacterial components underlying hypervirulence of the mutant.

In conclusion, data obtained from this animal study indicates that *Rv3167c* is an anti-virulence gene that tempers Mtb virulence.

## CHAPTER 5 GENERAL DISCUSSION AND SIGNIFICANCE

Modulation of host cell death via apoptotic and necrotic mechanisms is one of the several strategies Mtb employs in order to evade the host innate immune response. Previous studies have shown that while Mtb inhibits apoptosis, the pathogen after infection and multiplication induces necrosis in order to escape from infected cells reviewed in (49). The Mtb gene *Rv3167c* was previously identified as an anti-apoptotic gene in our lab (unpublished data). In this study, using a combination of morphological and biochemical methods, we determined that *Rv3167c* is required for the inhibition of Mtb induced caspase independent, necrotic cell death (Chapter 2). Serendipitously, we also uncovered a role for *Rv3167c* in limiting host cell autophagy induction by Mtb (Chapter 3).

Host cell lipid mediator modulation, high bacterial numbers, and activation of NLRP3 inflammasome are factors that have been shown to contribute to Mtb mediated necrosis (Fig 7). However the involvement of these factors and other regulated necrosis pathways was ruled out in  $\Delta 3167c$ -mediated necrosis (Fig 18-23). The classical paradigm of Mtb infection is that the bacteria always reside within modified phagosomal compartments, however more recent studies have shown that Mtb can escape into the host cell cytosol and that this event is followed by necrotic death of the host cell ((41),(116),(43),(42)). Cytosolic translocation is linked to the virulence of mycobacteria as only pathogenic mycobacterial species (Mtb, *M.leprae*, *M.bovis*, *M.marinum*) escape to the cytosol while the non-pathogenic *M.smegmatis* and the BCG vaccine strain were found to remain within phagosomes of infected cells (43). Other pathogens known to reside in modified vacuoles such as *S.typhimurium* and *L.pneumophila* also can escape

into the cytosol and eventually from the host cell either by non-lytic or lytic mechanisms (228). While for these pathogens escape to the cytosol is observed within a few hours after infection, cytosolic translocation is a very late event in Mtb infection (229). Kinetic studies on human macrophages infected with a low dose of Mtb revealed that the bacteria escaped to the cytosol approximately 4-5dpi and necrosis induction occurred within 24 hours of cytosolic escape (42). Preliminary data obtained from a TEM analysis of Mtb and  $\Delta 3167c$  infected macrophages shows a higher percentage of  $\Delta 3167c$  to be present in the cytosol compared to Mtb as early as 24hpi. This indicates that *Rv3167c* is required for the temporal control of bacterial egress from the phagosome to the cytosol and ensuing necrotic host cell death.

Current literature describes a role for the ESX1 secretion system in Mtb escape to the cytosol as Mtb mutants deficient in the RD1 region that encodes for ESX1 and the vaccine strain BCG in which the RD1 region is deleted fail to escape to the cytosol (41-43,110,111). Cytosolic translocation of *M.marinum* also occurs in an ESX1 dependent manner, however bacterial escape is accomplished much earlier (approximately 24hpi) compared to Mtb (42,114). The ESX1 secretion system is required for the secretion of the pore forming EsxA protein. In addition to being a secreted effector itself, EsxA is also required for the secretion of other bacterial proteins via ESX1. *Rv3167c* could temporally control either the expression or the secretion of EsxA and/or other ESX1 substrates and manipulate Mtb cytosolic translocation. Another potential candidate would be the recently identified outer membrane channel protein CpnT, the C-terminal domain of this protein has been shown to be secreted and to be involved in host cell necrosis induction (122). Deleting the ESX1 region or CpnT encoding gene in  $\Delta 3167c$  and examining

bacterial presence in the cytosol would help evaluate the contribution of these genes to the early cytosolic escape of  $\Delta 3167c$ .

We found  $\Delta 3167c$ -induced necrosis to be dependent on ROS generated in the mitochondria but not the NOX2 complex (Fig 24, 25). During escape of  $\Delta 3167c$  from the phagosome, the phagosomal membrane and the ROS generating NOX2 complex assembled on the membrane would be damaged, this would explain why NOX2 generated ROS is dispensable for  $\Delta 3167c$  mediated necrosis. Presence of bacteria in the cytosol would allow for bacterial substrates previously restricted in the phagosomal compartment to access the mitochondria and result in subsequent mitochondrial damage and ROS generation. The PE-PGRS33 protein has been shown to localize to mitochondria and cause necrotic cell death (137). A bioinformatics study identified five PE-PGRS proteins to possess mitochondrial localization sequences (138). The ESX5 secretion system is needed for the secretion of PE- PPE proteins in Mtb and *M.marinum* and has been shown to be required for Mtb and *M.marinum* mediated necrosis induction but not escape from the phagosome (116). The engagement of separate mechanisms for cytosolic escape and ensuing host cell lysis has also been shown for the pathogen *L.pneumophila*, mutants defective for host cell necrosis induction were not found to be deficient in cytosolic translocation (230). While we have evidence indicating that *Rv3167c* is involved in temporal regulation of Mtb phagosomal escape, it would be interesting to determine whether the gene also contributes to necrosis induction independent of its role in cytosolic translocation. Analysis of the expression and secretion of the predicted mitochondrial-targeting Mtb proteins and other ESX5 substrates in  $\Delta 3167c$  compared to Mtb would help answer this question.

Damage to vacuolar membranes and presence of bacteria in the cytosol can trigger selective autophagy. Higher levels of autophagy were observed in cells infected with  $\Delta 3167c$  compared to Mtb infected controls (Fig 26, 27), this could be attributed to the early cytosolic translocation of the mutant. The increased inhibition of Akt activation observed in  $\Delta 3167c$ -infected cells could contribute to autophagy induction via mTOR inhibition (Fig 32B). One would expect cytosolic Mtb to be targeted by selective autophagy machinery. However, in our experimental set up, we did not observe co-localization of either Mtb or  $\Delta 3167c$  with autophagosomes indicating that the bacteria possess mechanisms to avoid being sequestered into autophagosomes. A similar phenomenon is seen with other bacteria known to escape to the cytosol. For example, *S.typhimurium* has been reported to escape from the salmonella containing vacuole in epithelial cells and induce an amino acid stress response leading to autophagy. However, autophagy induction was only a transient phenomenon as *S.typhimurium* eventually increased amino acid uptake by the infected cells (231,232). Cytosolic *M.marinum* has also been reported to avoid recruitment of autophagic machinery by shedding their ubiquitinated cell walls (233). Autophagy is known to negatively regulate IL1 $\beta$  production by targeting inflammasomes for degradation (143). Mtb is known to activate the NLRP3 inflammasome in an ESX1 dependent manner (32,33), this could follow detection of cytosolic Mtb. Autophagy induction in response to Mtb could potentially control inflammasome mediated cytokine production. *V.parahemolyticus* infection induced activation of the NLRC4 inflammasome in macrophages, however the bacterial protein VopQ inhibits consequent IL1 $\beta$  production by inducing autophagy (234). Increased pro-inflammatory cytokine production observed in response to macrophage

infection by the cell death and autophagy inducing *Mtb eis* mutant is also negatively regulated by autophagy (177). Macroautophagy could also target DAMP's that are released by the infected, necrotic cells for destruction and thus inhibit pro-inflammatory cytokine generation. Comparing caspase 1 activation, secretion of IL1 $\beta$  and IL18 and release of DAMP's such as HMGB1 in  $\Delta$ 3167c infected wild type and autophagy deficient macrophages would help determine whether autophagy observed in these cells contributes to regulation of proinflammatory cytokine responses. Thus the combination of necrosis and macroautophagy induction in *Mtb* infected macrophages could contribute to escape and dissemination of the pathogen accompanied by a controlled inflammatory response (Fig 39).

*Rv3167c* is annotated as a TetR-like transcriptional regulator and ongoing analysis in our lab indicates that it behaves as a TetR-like repressor (work done by Jeff Quigley, unpublished data). In  $\Delta$ 3167c, repression of *Rv3167c* regulated genes would be eliminated resulting in their expression at all times and potentially these genes could be responsible for the earlier escape of the bacteria into the host cell cytosol and ensuing necrosis. In *Mtb*, one would expect *Rv3167c*-mediated gene repression to be inhibited at later stages of infection when the bacteria escape. This can be verified by analyzing the expression kinetics of *Rv3167c* in *Mtb* following macrophage infection as *Rv3167c* regulates its own expression. Identification of *Rv3167c* regulated genes specifically involved in *Mtb* cytosolic translocation and necrosis induction presents an interesting area of future research. Comparing of the transcriptomes of intracellular *Mtb* and  $\Delta$ 3167c using RNAseq technology would provide a set of genes that are differentially regulated between the two bacterial strains. Deletion of these genes in  $\Delta$ 3167c would help confirm

their contribution to Mtb cytosolic translocation and necrosis induction. An alternative approach would be to generate a transposon mutant library in  $\Delta 3167c$  background and then screening the mutants for their inability to induce or induce reduced necrosis compared to the parent  $\Delta 3167c$  strain.

The identification of *Rv3167c* in the regulation of Mtb mediated necrosis provides more insight into a relatively unexplored area of Mtb pathogenesis. While studies have implicated *EsxA*, *ESX5* locus and the *phoPR* two component regulatory system in induction of host cell necrosis, currently there are no Mtb genes known to negatively regulate host cell necrosis (32,42,108,109,116). The ability of Mtb to escape from the phagosome and induce necrosis has been known for sometime now, the delayed kinetics of this phenomenon made it difficult to study the contributing bacterial factors and host mechanisms involved. As escape and necrosis induction by  $\Delta 3167c$  occur within 24hpi, infections with  $\Delta 3167c$  can be used as a tool to further investigate bacterial escape and necrosis induction. Targeting Mtb mediated necrosis with drugs to inhibit bacterial dissemination could be a supplement to current TB treatment regimens,  $\Delta 3167c$  could be used to screen drug libraries for potential candidates.

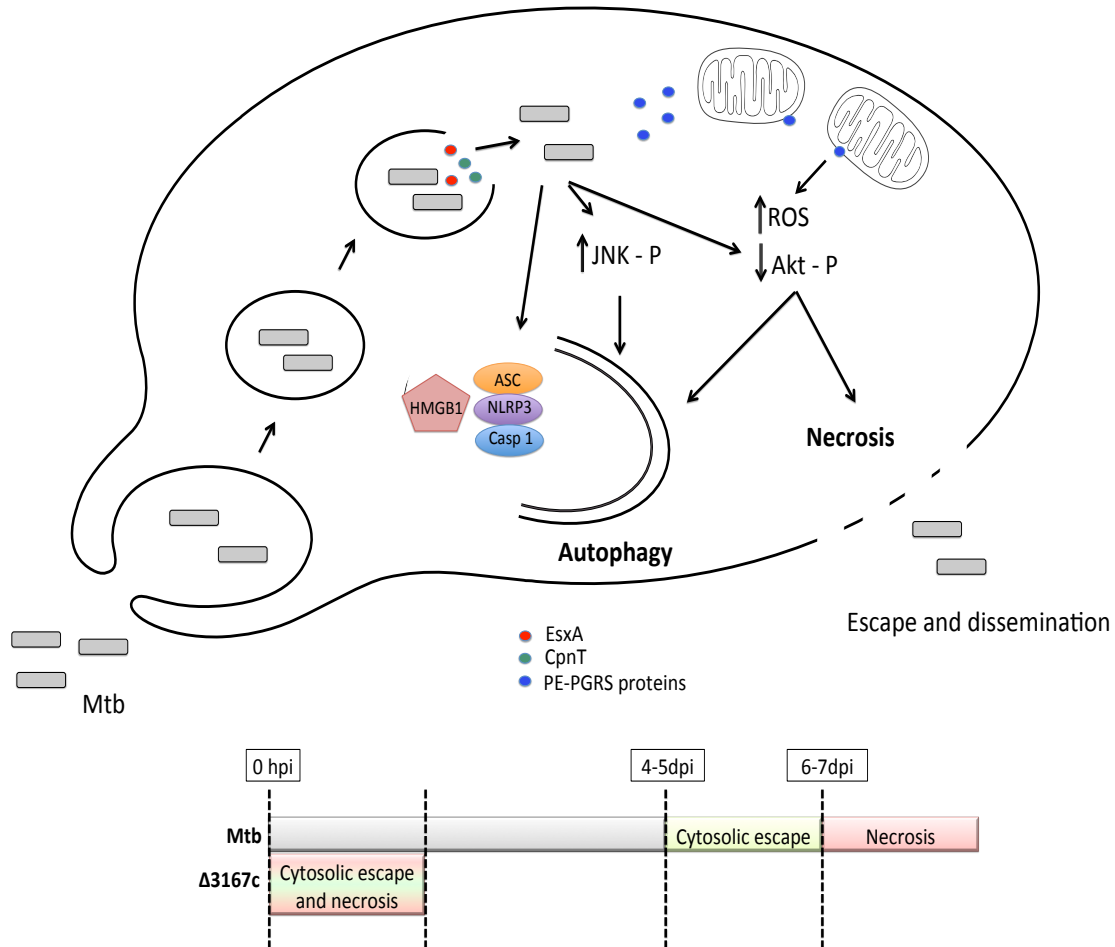


**Fig 39. Model for *Rv3167c* dependent Mtb mediated necrosis and autophagy**

Following phagocytosis, Mtb arrests phagolysosomal fusion and resides in an early endosome like compartment. Eventually (4-5 dpi), Mtb escapes from this compartment into the cytosol. *Rv3167c* exerts temporal control over Mtb escape,  $\Delta 3167c$  translocates to the cytosol within 24hpi. Potential candidates that could be regulated by *Rv3167c* and contribute to cytosolic translocation include the pore forming proteins EsxA and CpnT. Escape to the cytosol allows Mtb proteins previously sequestered within the phagosome to access the host cell cytosol. Some Mtb PE-PGRS proteins possess mitochondrial localization signals, these could localize to and damage mitochondria and lead to increased mitochondrial ROS production. Cytosolic escape of  $\Delta 3167c$  is accompanied by decreased activation of Akt and increased activation of JNK. Mitochondrial ROS and Akt inhibition contribute to both necrosis and autophagy induction, while JNK activation contribute to autophagy alone. Autophagy did not lead to bacterial killing, it may be possible that the increase in autophagy induction leads to a reduction in proinflammatory cytokine secretion and DAMP release from the dying cells.

**APPENDIX A: List of antibodies used in this study**

| <b>ANTIBODY</b>                      | <b>SOURCE</b>                         | <b>DILUTION</b>     |
|--------------------------------------|---------------------------------------|---------------------|
| Goat anti AIF                        | Santa Cruz sc-9416                    | 1:200               |
| Rabbit anti Akt                      | Cell Signaling #4691                  | 1:1000              |
| Rabbit anti Beclin 1                 | Cell Signaling #3495                  | 1:1000              |
| Rabbit anti Cytochrome C             | Epitomics #3895-1                     | 1:10,000            |
| Rabbit anti Eis                      | Dr.Eun Kyeong Jo                      | 1:1250              |
| Rabbit anti FAP                      | BEI resources NR-13817                | 1:8000              |
| Rabbit anti GAPDH                    | Cell Signaling #5174                  | 1:1000              |
| Mouse anti GFP                       | Cell Signaling #2955                  | 1:1000              |
| Mouse anti HDAC1                     | Cell Signaling#5356                   | 1:1000              |
| Rabbit anti JNK                      | Cell Signaling #9258                  | 1:1000              |
| Rabbit anti LC3                      | Epitomics #2057-1                     | 1:2000              |
| Rabbit anti p38 MAPK                 | Cell Signaling #9212                  | 1:1000              |
| Rabbit anti PARP                     | Cell Signaling #9532                  | 1:1000              |
| Rabbit anti Phospho p38MAPK          | Cell Signaling #4511                  | 1:1000              |
| Rabbit anti Phospho Akt<br>(Ser 473) | Cell Signaling #4060                  | 1:1000              |
| Rabbit anti Phospho Bcl2<br>(Ser 70) | Cell Signaling #2827                  | 1:1000              |
| Rabbit anti Phospho JNK              | Cell Signaling #4668                  | 1:1000              |
| Mouse anti Tubulin                   | Cell Signaling #3873                  | 1:1000              |
| Rabbit anti VDAC                     | Cell Signaling #4661                  | 1:1000              |
| Goat anti mouse HRP                  | Jackson ImmunoResearch<br>115-035-116 | 1:20,000 – 1:50,000 |
| Goat anti rabbit HRP                 | Jackson ImmunoResearch<br>115-035-144 | 1:20,000 – 1:50,000 |
| Donkey anti goat HRP                 | Jackson ImmunoResearch<br>705-035-003 | 1:20,000            |

## BIBLIOGRAPHY

1. Galagan JE. Genomic insights into tuberculosis. *Nat Rev Genet.* Nature Publishing Group; 2014 Mar. 25;15(5):307–320.
2. Hershkovitz I, Donoghue HD, Minnikin DE, Besra GS, Lee OY, Gernaey AM, et al. Detection and molecular characterization of 9000-year-old *Mycobacterium tuberculosis* from a Neolithic settlement in the Eastern Mediterranean. *PLoS ONE.* Public Library of Science; 2008;3(10):e3426.
3. Daniel TM. The history of tuberculosis. *Respiratory Medicine.* 2006 Nov.;100(11):1862–1870.
4. WHO. Global Tuberculosis Report 2014. WHO. World Health Organization.
5. Ottenhoff THM, Kaufmann SHE. Vaccines against Tuberculosis: Where Are We and Where Do We Need to Go? *PLoS Pathog.* Public Library of Science; 2012 May 10;8(5):e1002607.
6. Rastogi N, Legrand E, Sola C. The mycobacteria: an introduction to nomenclature and pathogenesis. *Revue Scientifique Et Technique-Office International Des Epizooties.* OIE office international des epizooties; 2001;20(1):21–54.
7. Stamm LM, Morisaki JH, Gao L-Y, Jeng RL, McDonald KL, Roth R, et al. *Mycobacterium marinum* escapes from phagosomes and is propelled by actin-based motility. *J. Exp. Med.* 2003 Nov. 3;198(9):1361–1368.
8. Cambier CJ, Takaki KK, Larson RP, Hernandez RE, Tobin DM, Urdahl KB, et al. *Mycobacteria* manipulate macrophage recruitment through coordinated use of membrane lipids. *Nature.* 2014 Jan. 9;505(7482):218–222.
9. Roca FJ, Ramakrishnan L. TNF dually mediates resistance and susceptibility to mycobacteria via mitochondrial reactive oxygen species. *Cell.* Elsevier; 2013;153(3):521–534.
10. Tobin DM, Vary JC Jr, Ray JP, Walsh GS, Dunstan SJ, Bang ND, et al. The *lta4h* Locus Modulates Susceptibility to Mycobacterial Infection in Zebrafish and Humans. *Cell.* Elsevier; 2010;140(5):717–730.
11. Volkman HE, Pozos TC, Zheng J, Davis JM, Rawls JF, Ramakrishnan L. Tuberculous Granuloma Induction via Interaction of a Bacterial Secreted Protein with Host Epithelium. *Science.* 2010 Jan. 21;327(5964):466–469.
12. Bohsali A, Abdalla H, Velmurugan K, Briken V. The non-pathogenic mycobacteria *M. smegmatis* and *M. fortuitum* induce rapid host cell apoptosis via a caspase-3 and TNF dependent pathway. *BMC Microbiol.* 2010;10:237.
13. Brennan PJ. Structure, function, and biogenesis of the cell wall of *Mycobacterium*

- tuberculosis. *Tuberculosis (Edinb)*. 2003;83(1-3):91–97.
14. Hett EC, Rubin EJ. Bacterial Growth and Cell Division: a Mycobacterial Perspective. *Microbiology and Molecular Biology Reviews*. 2008 Mar. 5;72(1):126–156.
  15. Zumla A, Nahid P, Cole ST. Advances in the development of new tuberculosis drugs and treatment regimens. *Nature Reviews Drug Discovery*. Nature Publishing Group; 2013 May 1;12(5):388–404.
  16. Sacchettini JC, Rubin EJ, Freundlich JS. Drugs versus bugs: in pursuit of the persistent predator *Mycobacterium tuberculosis*. *Nat. Rev. Microbiol*. 2008 Jan.;6(1):41–52.
  17. Dietrich J, Doherty TM. Interaction of *Mycobacterium tuberculosis* with the host: consequences for vaccine development. *APMIS*. 2009 May;117(5-6):440–457.
  18. Udhwadia ZF, Amale RA, Ajbani KK, Rodrigues C. Totally drug-resistant tuberculosis in India. *Clin. Infect. Dis*. 2012 Feb. 15;54(4):579–581.
  19. Simona LUCA TM. History of BCG Vaccine. *Mædica*. Amaltea Medical, Editura Magister; 2013 Mar. 1;8(1):53.
  20. Russell DG. Who puts the tubercle in tuberculosis? *Nat. Rev. Microbiol*. 2007 Jan.;5(1):39–47.
  21. Repasy T, Lee J, Marino S, Martinez N, Kirschner DE, Hendricks G, et al. Intracellular Bacillary Burden Reflects a Burst Size for *Mycobacterium tuberculosis* In Vivo. *PLoS Pathog*. 2013 Feb.;9(2):e1003190.
  22. Dorhoi A, Reece ST, Kaufmann SHE. For better or for worse: the immune response against *Mycobacterium tuberculosis* balances pathology and protection. *Immunological Reviews*. 2011 Feb. 23;240(1):235–251.
  23. Philips JA, Ernst JD. Tuberculosis Pathogenesis and Immunity. *Annu. Rev. Pathol. Mech. Dis*. Annual Reviews; 2012 Feb. 28;7(1):353–384.
  24. Yang CS, Shin DM, Kim KH, Lee ZW, Lee CH, Park SG, et al. NADPH Oxidase 2 Interaction with TLR2 Is Required for Efficient Innate Immune Responses to Mycobacteria via Cathelicidin Expression. *The Journal of Immunology*. 2009 Mar. 15;182(6):3696–3705.
  25. Sasindran SJ, Torrelles JB. *Mycobacterium Tuberculosis* Infection and Inflammation: what is Beneficial for the Host and for the Bacterium? *Frontiers in Microbiology*. 2011;2:2.
  26. Dorhoi A, Desel C, Yermeev V, Pradl L, Brinkmann V, Mollenkopf HJ, et al. The adaptor molecule CARD9 is essential for tuberculosis control. *Journal of*

- Experimental Medicine. 2010 Apr. 12;207(4):777–792.
27. Briken V, Ahlbrand SE, Shah S. Mycobacterium tuberculosis and the host cell inflammasome: a complex relationship. *Front Cell Infect Microbiol.* 2013;3:62.
  28. Flynn JL, Goldstein MM, Chan J, Triebold KJ, Pfeffer K, Lowenstein CJ, et al. Tumor necrosis factor-alpha is required in the protective immune response against Mycobacterium tuberculosis in mice. *Immunity.* 1995 Jun.;2(6):561–572.
  29. Ramakrishnan L. Revisiting the role of the granuloma in tuberculosis. *Nat Rev Immunol.* Nature Publishing Group; 2012 Apr. 20;12(5):352–366.
  30. Balcewicz-Sablinska MK, Keane J, Kornfeld H, Remold HG. Pathogenic Mycobacterium tuberculosis Evades Apoptosis of Host Macrophages by Release of TNF-R2, Resulting in Inactivation of TNF- $\alpha$ . *J. Immunol.* 1998 Jan. 1;161(5):2636–2641.
  31. Cooper AM, Mayer-Barber KD, Sher A. Role of innate cytokines in mycobacterial infection. *Mucosal Immunol.* 2011 May;4(3):252–260.
  32. Wong K-W, Jacobs WR Jr. Critical role for NLRP3 in necrotic death triggered by Mycobacterium tuberculosis. *Cell Microbiol.* 2011 Jul. 11;13(9):1371–1384.
  33. Abdalla H, Srinivasan L, Shah S, Mayer-Barber KD, Sher A, Sutterwala FS, et al. Mycobacterium tuberculosis Infection of Dendritic Cells Leads to Partially Caspase-1/11-Independent IL-1 $\beta$  and IL-18 Secretion but Not to Pyroptosis. *PLoS ONE.* 2012;7(7):e40722.
  34. Mayer-Barber KD, Barber DL, Shenderov K, White SD, Wilson MS, Cheever A, et al. Cutting edge: caspase-1 independent IL-1 $\beta$  production is critical for host resistance to Mycobacterium tuberculosis and does not require TLR signaling in vivo. *J. Immunol. Am Assoc Immunol;* 2010;184(7):3326–3330.
  35. Jayaraman P, Sada-Ovalle I, Nishimura T, Anderson AC, Kuchroo VK, Remold HG, et al. IL-1 $\beta$  promotes antimicrobial immunity in macrophages by regulating TNFR signaling and caspase-3 activation. *The Journal of Immunology.* 2013 Apr. 15;190(8):4196–4204.
  36. Mogue T, Goodrich ME, Ryan L, LaCourse R, North RJ. The relative importance of T cell subsets in immunity and immunopathology of airborne Mycobacterium tuberculosis infection in mice. *J. Exp. Med.* 2001 Feb. 5;193(3):271–280.
  37. Deretic V. Autophagy: an emerging immunological paradigm. *J. Immunol.* 2012 Jul. 1;189(1):15–20.
  38. Marina A Forrellad, Laura I Klepp, Andrea Gioffre, Julia Sabio y Garcia, Hector R Morbidoni, et al. Virulence factors of the Mycobacterium tuberculosis complex. *Virulence.* Landes Bioscience; 2013 Jan. 1;4(1):3.

39. Jayachandran R, Sundaramurthy V, Combaluzier B, Mueller P, Korf H, Huygen K, et al. Survival of mycobacteria in macrophages is mediated by coronin 1-dependent activation of calcineurin. *Cell*. 2007 Jul. 13;130(1):37–50.
40. Welin A, Lerm M. Inside or outside the phagosome? The controversy of the intracellular localization of *Mycobacterium tuberculosis*. *Tuberculosis (Edinb)*. Elsevier; 2012;92(2):113–120.
41. van der Wel N, Hava D, Houben D, Fluitsma D, van Zon M, Pierson J, et al. *M. tuberculosis* and *M. leprae* Translocate from the Phagolysosome to the Cytosol in Myeloid Cells. *Cell*. Elsevier; 2007;129(7):1287–1298.
42. Simeone R, Bobard A, Lippmann J, Bitter W, Majlessi L, Brosch R, et al. Phagosomal Rupture by *Mycobacterium tuberculosis* Results in Toxicity and Host Cell Death. *PLoS Pathog*. 2012 Feb.;8(2):e1002507.
43. Houben D, Demangel C, van Ingen J, Perez J, Baldeón L, Abdallah AM, et al. ESX-1-mediated translocation to the cytosol controls virulence of mycobacteria. *Cell Microbiol*. 2012 Aug.;14(8):1287–1298.
44. Lambeth JD. NOX enzymes and the biology of reactive oxygen. *Nat Rev Immunol*. Nature Publishing Group; 2004 Mar.;4(3):181–189.
45. Miller JL, Velmurugan K, Cowan MJ, Briken V. The Type I NADH Dehydrogenase of *Mycobacterium tuberculosis* Counters Phagosomal NOX2 Activity to Inhibit TNF- $\alpha$ -Mediated Host Cell Apoptosis. Deretic V, editor. *PLoS Pathog*. 2010 Apr. 22;6(4):e1000864.
46. Yang C-S, Shin D-M, Lee H-M, Son JW, Lee SJ, Akira S, et al. ASK1-p38 MAPK-p47phox activation is essential for inflammatory responses during tuberculosis via TLR2-ROS signalling. *Cell Microbiol*. 2008 Mar.;10(3):741–754.
47. Shah S, Bohsali A, Ahlbrand SE, Srinivasan L, Rathinam VAK, Vogel SN, et al. Cutting edge: *Mycobacterium tuberculosis* but not nonvirulent mycobacteria inhibits IFN- $\beta$  and AIM2 inflammasome-dependent IL-1 $\beta$  production via its ESX-1 secretion system. *J. Immunol*. 2013 Oct. 1;191(7):3514–3518.
48. Novikov A, Cardone M, Thompson R, Shenderov K, Kirschman KD, Mayer-Barber KD, et al. *Mycobacterium tuberculosis* triggers host type I IFN signaling to regulate IL-1 $\beta$  production in human macrophages. *The Journal of Immunology*. 2011 Sep. 1;187(5):2540–2547.
49. Srinivasan L, Ahlbrand S, Briken V. Interaction of *Mycobacterium tuberculosis* with Host Cell Death Pathways. *Cold Spring Harbor Perspectives in Medicine*. 2014 Aug. 1;4(8):a022459–a022459.
50. Vandenabeele P, Galluzzi L, Vanden Berghe T, Kroemer G. Molecular mechanisms of necroptosis: an ordered cellular explosion. *Nat. Rev. Mol. Cell Biol*. Nature

Publishing Group; 2010 Sep. 8;11(10):700–714.

51. Vanden Berghe T, Linkermann A, Jouan-Lanhouet S, Walczak H, Vandenabeele P. Regulated necrosis: the expanding network of non-apoptotic cell death pathways. *Nat. Rev. Mol. Cell Biol.* 2014 Feb.;15(2):135–147.
52. Galluzzi L, Vitale I, Abrams JM, Alnemri ES, Baehrecke EH, Blagosklonny MV, et al. Molecular definitions of cell death subroutines: recommendations of the Nomenclature Committee on Cell Death 2012. *Cell Death & Differentiation.* 2012 Jan.;19(1):107–120.
53. Vanlangenakker N, Vanden Berghe T, Vandenabeele P. Many stimuli pull the necrotic trigger, an overview. *Cell Death & Differentiation.* 2012 Jan.;19(1):75–86.
54. Nagata S, Enari M, Sakahira H, Yokoyama H, Okawa K, Iwamatsu A. A caspase-activated DNase that degrades DNA during apoptosis, and its inhibitor ICAD. *Nature.* Nature Publishing Group; 1998 Jan. 1;391(6662):43–50.
55. Lamkanfi M, Dixit VM. Manipulation of host cell death pathways during microbial infections. *Cell Host & Microbe.* 2010 Jul. 22;8(1):44–54.
56. Krysko DV, Vanden Berghe T, Parthoens E, D'Herde K, Vandenabeele P. Methods for distinguishing apoptotic from necrotic cells and measuring their clearance. *Meth. Enzymol.* 2008;442:307–341.
57. Vanden Berghe T, Vanlangenakker N, Parthoens E, Deckers W, Devos M, Festjens N, et al. Necroptosis, necrosis and secondary necrosis converge on similar cellular disintegration features. *Cell Death & Differentiation.* 2010 Jun.;17(6):922–930.
58. Sawai H, Domae N. Discrimination between primary necrosis and apoptosis by necrostatin-1 in Annexin V-positive/propidium iodide-negative cells. *Biochem. Biophys. Res. Commun.* 2011 Aug.;411(3):569–573.
59. Zhang J, Sun B, Huang Y, Kouadir M, Zhou X, Wang Y, et al. IFN- $\gamma$  promotes THP-1 cell apoptosis during early infection with *Mycobacterium bovis* by activating different apoptotic signaling. *FEMS Immunol. Med. Microbiol.* 2010 Dec.;60(3):191–198.
60. Baritaud M, Cabon L, Delavallée L, Galán-Malo P, Gilles M-E, Brunelle-Navas M-N, et al. AIF-mediated caspase-independent necroptosis requires ATM and DNA-PK-induced histone H2AX Ser139 phosphorylation. *Cell Death Dis.* 2012;3:e390.
61. Robinson N, McComb S, Mulligan R, Dudani R, Krishnan L, Sad S. Type I interferon induces necroptosis in macrophages during infection with *Salmonella enterica* serovar Typhimurium. *Nat. Immunol.* 2012 Oct.;13(10):954–962.
62. Vandenabeele P, Declercq W, Van Herreweghe F, Vanden Berghe T. The role of the kinases RIP1 and RIP3 in TNF-induced necrosis. *Sci Signal.* 2010;3(115):re4.

63. Sun L, Wang H, Wang Z, He S, Chen S, Liao D, et al. Mixed Lineage Kinase Domain-like Protein Mediates Necrosis Signaling Downstream of RIP3 Kinase. *Cell*. Elsevier Inc.; 2012 Jan. 20;148(1-2):213–227.
64. He S, Wang L, Miao L, Wang T, Du F, Zhao L, et al. Receptor interacting protein kinase-3 determines cellular necrotic response to TNF-alpha. *Cell*. 2009 Jun. 12;137(6):1100–1111.
65. Chan FK-M, Baehrecke EH. RIP3 finds partners in crime. *Cell*. 2012 Jan. 20;148(1-2):17–18.
66. Wang Z, Jiang H, Chen S, Du F, Wang X. The mitochondrial phosphatase PGAM5 functions at the convergence point of multiple necrotic death pathways. *Cell*. 2012 Jan. 20;148(1-2):228–243.
67. Chen X, Li W, Ren J, Huang D, He W-T, Song Y, et al. Translocation of mixed lineage kinase domain-like protein to plasma membrane leads to necrotic cell death. *Cell Res*. 2014 Jan.;24(1):105–121.
68. Wang H, Sun L, Su L, Rizo J, Liu L, Wang L-F, et al. Mixed Lineage Kinase Domain-like Protein MLKL Causes Necrotic Membrane Disruption upon Phosphorylation by RIP3. *Mol. Cell*. Elsevier Inc.; 2014 Apr. 10;54(1):133–146.
69. Labbé K, Saleh M. Pyroptosis: A Caspase-1-Dependent Programmed Cell Death and a Barrier to Infection - Springer. *The Inflammasomes*. 2011.
70. Broz P, Monack D. PLOS Pathogens: Noncanonical Inflammasomes: Caspase-11 Activation and Effector Mechanisms. *PLoS Pathog*. 2013.
71. Broz P, Moltke von J, Jones JW, Vance RE, Monack DM. Differential requirement for Caspase-1 autoproteolysis in pathogen-induced cell death and cytokine processing. *Cell Host & Microbe*. 2010 Dec. 16;8(6):471–483.
72. Willingham SB, Bergstralh DT, O'Connor W, Morrison AC, Taxman DJ, Duncan JA, et al. Microbial Pathogen-Induced Necrotic Cell Death Mediated by the Inflammasome Components CIAS1/Cryopyrin/NLRP3 and ASC. *Cell Host & Microbe*. 2007 Sep.;2(3):147–159.
73. Duncan JA, Gao X, Huang MT-H, O'Connor BP, Thomas CE, Willingham SB, et al. *Neisseria gonorrhoeae* Activates the Proteinase Cathepsin B to Mediate the Signaling Activities of the NLRP3 and ASC-Containing Inflammasome. 2009.
74. Newman ZL, Leppla SH, Moayeri M. CA-074Me protection against anthrax lethal toxin. *Infect. Immun*. 2009 Oct.;77(10):4327–4336.
75. Shao W, Yeretssian G, Doiron K, Hussain SN, Saleh M. The caspase-1 digestome identifies the glycolysis pathway as a target during infection and septic shock. *J. Biol. Chem*. 2007 Dec. 14;282(50):36321–36329.

76. Fink SL, Cookson BT. Caspase-1-dependent pore formation during pyroptosis leads to osmotic lysis of infected host macrophages. *Cell Microbiol.* 2006 Nov.;8(11):1812–1825.
77. Kayagaki N, Warming S, Lamkanfi M, Vande Walle L, Louie S, Dong J, et al. Non-canonical inflammasome activation targets caspase-11. *Nature.* 2011 Nov. 3;479(7371):117–121.
78. Rathinam VAK, Vanaja SK, Waggoner L, Sokolovska A, Becker C, Stuart LM, et al. TRIF licenses caspase-11-dependent NLRP3 inflammasome activation by gram-negative bacteria. *Cell.* 2012 Aug. 3;150(3):606–619.
79. Broz P, Ruby T, Belhocine K, Bouley DM, Kayagaki N, Dixit VM, et al. Caspase-11 increases susceptibility to *Salmonella* infection in the absence of caspase-1. *Nature.* 2012 Oct. 11;490(7419):288–291.
80. Aachoui Y, Leaf IA, Hagar JA, Fontana MF, Campos CG, Zak DE, et al. Caspase-11 Protects Against Bacteria That Escape the Vacuole. *Science.* 2013 Feb. 21;339(6122):975–978.
81. Case CL, Kohler LJ, Lima JB, Strowig T, de Zoete MR, Flavell RA, et al. Caspase-11 stimulates rapid flagellin-independent pyroptosis in response to *Legionella pneumophila*. 2013.
82. Casson CN, Copenhaver AM, Zwack EE, Nguyen HT, Strowig T, Javdan B, et al. Caspase-11 activation in response to bacterial secretion systems that access the host cytosol. *PLoS Pathog.* 2013 Jun.;9(6):e1003400.
83. Yu S-W, Wang H, Poitras MF, Coombs C, Bowers WJ, Federoff HJ, et al. Mediation of poly(ADP-ribose) polymerase-1-dependent cell death by apoptosis-inducing factor. *Science.* 2002 Jul. 12;297(5579):259–263.
84. Yu S-W, Andrabi SA, Wang H, Kim NS, Poirier GG, Dawson TM, et al. Apoptosis-inducing factor mediates poly(ADP-ribose) (PAR) polymer-induced cell death. *Proc. Natl. Acad. Sci. U.S.A.* 2006 Nov. 28;103(48):18314–18319.
85. Andrabi SA, Kim NS, Yu SW, Wang H, Koh DW, Sasaki M, et al. Poly(ADP-ribose) (PAR) polymer is a death signal. *Proceedings of the National Academy of Sciences.* 2006 Nov. 28;103(48):18308–18313.
86. Moubarak RS, Yuste VJ, Artus C, Bouharrou A, Greer PA, Menissier-de Murcia J, et al. Sequential activation of poly(ADP-ribose) polymerase 1, calpains, and Bax is essential in apoptosis-inducing factor-mediated programmed necrosis. *Mol. Cell. Biol.* 2007 Jul.;27(13):4844–4862.
87. Wang Y, Dawson VL, Dawson TM. Poly(ADP-ribose) signals to mitochondrial AIF: a key event in parthanatos. *Exp. Neurol.* 2009 Aug.;218(2):193–202.

88. Javle M, Curtin NJ. The role of PARP in DNA repair and its therapeutic exploitation. *Br J Cancer*. Nature Publishing Group; 2011 Oct. 11;105(8):1114–1122.
89. Virág L, Robaszkiewicz A, Rodriguez-Vargas JM, Oliver FJ. Poly(ADP-ribose) signaling in cell death. *Mol. Aspects Med*. 2013 Dec.;34(6):1153–1167.
90. Delavallée L, Cabon L, Galán-Malo P, Lorenzo HK, Susin SA. AIF-mediated caspase-independent necroptosis: a new chance for targeted therapeutics. *IUBMB Life*. 2011 Apr.;63(4):221–232.
91. Lu J-R, Lu W-W, Lai J-Z, Tsai F-L, Wu S-H, Lin C-W, et al. Calcium flux and calpain-mediated activation of the apoptosis-inducing factor contribute to enterovirus 71-induced apoptosis. *J. Gen. Virol*. 2013 Jul.;94(Pt 7):1477–1485.
92. Yuste VJ, Moubarak RS, Delettre C, Bras M, Sancho P, Robert N, et al. Cysteine protease inhibition prevents mitochondrial apoptosis-inducing factor (AIF) release. *Cell Death & Differentiation*. 2005 Jun. 3;12(11):1445–1448.
93. Alano CC, Swanson RA. Players in the PARP-1 cell-death pathway: JNK1 joins the cast. *Trends Biochem. Sci*. 2006 Jun.;31(6):309–311.
94. Xu Y, Huang S, Liu ZG, Han J. Poly(ADP-ribose) Polymerase-1 Signaling to Mitochondria in Necrotic Cell Death Requires RIP1/TRAF2-mediated JNK1 Activation. *Journal of Biological Chemistry*. 2006 Mar. 24;281(13):8788–8795.
95. Molloy A, Laochumroonvorapong P, Kaplan G. Apoptosis, but not necrosis, of infected monocytes is coupled with killing of intracellular bacillus Calmette-Guerin. *J. Exp. Med*. Rockefeller Univ Press; 1994;180(4):1499–1509.
96. Duan L, Gan H, Golan DE, Remold HG. Critical role of mitochondrial damage in determining outcome of macrophage infection with *Mycobacterium tuberculosis*. *J. Immunol*. 2002 Nov. 1;169(9):5181–5187.
97. Fratazzi C, Arbeit RD, Carini C, Balcewicz-Sablinska MK, Keane J, Kornfeld H, et al. Macrophage apoptosis in mycobacterial infections. *J. Leukoc. Biol*. 1999 Nov.;66(5):763–764.
98. Park JS. Virulent clinical isolates of *Mycobacterium tuberculosis* grow rapidly and induce cellular necrosis but minimal apoptosis in murine macrophages. *J. Leukoc. Biol*. 2005 Oct. 4;79(1):80–86.
99. Pan H, Yan B-S, Rojas M, Shebzukhov YV, Zhou H, Kobzik L, et al. Ipr1 gene mediates innate immunity to tuberculosis. *Nat. Cell Biol*. Nature Publishing Group; 2005 Apr. 7;434(7034):767–772.
100. Behar SM, Divangahi M, Remold HG. Evasion of innate immunity by *Mycobacterium tuberculosis*: is death an exit strategy? *Nat. Rev. Microbiol*. 2010

Sep.;8(9):668–674.

101. Bafica A, Scanga CA, Serhan C, Machado F, White S, Sher A, et al. Host control of *Mycobacterium tuberculosis* is regulated by 5-lipoxygenase-dependent lipoxin production. *J. Clin. Invest.* 2005 Jun. 1;115(6):1601–1606.
102. Divangahi M, Chen M, Gan H, Desjardins D, Hickman TT, Lee DM, et al. *Mycobacterium tuberculosis* evades macrophage defenses by inhibiting plasma membrane repair. *Nat. Immunol.* 2009 Aug.;10(8):899–906.
103. Tobin DM, Roca FJ, Oh SF, McFarland R, Vickery TW, Ray JP, et al. Host Genotype-Specific Therapies Can Optimize the Inflammatory Response to *Mycobacterial Infections*. *Cell.* Elsevier Inc.; 2012 Feb. 3;148(3):434–446.
104. Chen M, Gan H, Remold HG. A Mechanism of Virulence: Virulent *Mycobacterium tuberculosis* Strain H37Rv, but Not Attenuated H37Ra, Causes Significant Mitochondrial Inner Membrane Disruption in Macrophages Leading to Necrosis. 2006.
105. Chen M, Divangahi M, Gan H, Shin DSJ, Hong S, Lee DM, et al. Lipid mediators in innate immunity against tuberculosis: opposing roles of PGE2 and LXA4 in the induction of macrophage death. *Journal of Experimental Medicine.* 2008 Nov. 24;205(12):2791–2801.
106. Gan H, Lee J, Ren F, Chen M, Kornfeld H, Remold HG. *Mycobacterium tuberculosis* blocks crosslinking of annexin-1 and apoptotic envelope formation on infected macrophages to maintain virulence. *Nat. Immunol.* 2008 Oct.;9(10):1189–1197.
107. Lee J, Remold HG, Jeong MH, Kornfeld H. Macrophage Apoptosis in Response to High Intracellular Burden of *Mycobacterium tuberculosis* Is Mediated by a Novel Caspase-Independent Pathway. 2006.
108. Lee J, Repasy T, Papavinasasundaram K, Sasseti C, Kornfeld H. *Mycobacterium tuberculosis* induces an atypical cell death mode to escape from infected macrophages. *PLoS ONE.* 2011;6(3):e18367.
109. Welin A, Eklund D, Stendahl O, Lerm M. Human macrophages infected with a high burden of ESAT-6-expressing *M. tuberculosis* undergo caspase-1- and cathepsin B-independent necrosis. *PLoS ONE.* 2011;6(5):e20302.
110. Keller C, Mellouk N, Danckaert A, Simeone R, Brosch R, Enninga J, et al. Single Cell Measurements of Vacuolar Rupture Caused by Intracellular Pathogens. *JoVE.* MyJoVE Corporation; 2013;(76).
111. Rahman A, Sobia P, Gupta N, Kaer LV, Das G. *Mycobacterium tuberculosis* subverts the TLR-2-MyD88 pathway to facilitate its translocation into the cytosol. *PLoS ONE.* 2014;9(1):e86886.

112. Hsu T, Hingley-Wilson SM, Chen B, Chen M, Dai AZ, Morin PM, et al. The primary mechanism of attenuation of bacillus Calmette-Guerin is a loss of secreted lytic function required for invasion of lung interstitial tissue. *Proceedings of the National Academy of Sciences*. 2003 Oct. 14;100(21):12420–12425.
113. de Jonge MI, Pehau-Arnaudet G, Fretz MM, Romain F, Bottai D, Brodin P, et al. ESAT-6 from *Mycobacterium tuberculosis* Dissociates from Its Putative Chaperone CFP-10 under Acidic Conditions and Exhibits Membrane-Lysing Activity. *J. Bacteriol.* 2007 Aug. 1;189(16):6028–6034.
114. Smith J, Manoranjan J, Pan M, Bohsali A, Xu J, Liu J, et al. Evidence for Pore Formation in Host Cell Membranes by ESX-1-Secreted ESAT-6 and Its Role in *Mycobacterium marinum* Escape from the Vacuole. *Infect. Immun.* 2008 Nov. 17;76(12):5478–5487.
115. Kaku T, Kawamura I, Uchiyama R, Kurenuma T, Mitsuyama M. RD1 region in mycobacterial genome is involved in the induction of necrosis in infected RAW264 cells via mitochondrial membrane damage and ATP depletion. *FEMS Microbiol. Lett.* 2007 Sep.;274(2):189–195.
116. Abdallah AM, Bestebroer J, Savage NDL, de Punder K, van Zon M, Wilson L, et al. Mycobacterial secretion systems ESX-1 and ESX-5 play distinct roles in host cell death and inflammasome activation. *The Journal of Immunology*. 2011 Nov. 1;187(9):4744–4753.
117. Derrick SC, Morris SL. The ESAT6 protein of *Mycobacterium tuberculosis* induces apoptosis of macrophages by activating caspase expression. *Cell Microbiol.* 2007 Jun.;9(6):1547–1555.
118. Choi H-H, Shin D-M, Kang G, Kim KH, Park JB, Hur GM, et al. Endoplasmic reticulum stress response is involved in *Mycobacterium tuberculosis* protein ESAT-6-mediated apoptosis. *FEBS Letters*. 2010 Jun. 3;584(11):2445–2454.
119. Tundup S, Mohareer K, Hasnain SE. *Mycobacterium tuberculosis* PE25/PPE41 protein complex induces necrosis in macrophages: Role in virulence and disease reactivation? *FEBS Open Bio. Federation of European Biochemical Societies*; 2014;4(C):822–828.
120. Cadieux N, Parra M, Cohen H, Maric D, Morris SL, Brennan MJ. Induction of cell death after localization to the host cell mitochondria by the *Mycobacterium tuberculosis* PE\_PGRS33 protein. *Microbiology (Reading, Engl.)*. 2011 Mar.;157(Pt 3):793–804.
121. Assis PA, Espíndola MS, Paula-Silva FW, Rios WM, Pereira PA, Leão SC, et al. *Mycobacterium tuberculosis* expressing phospholipase C subverts PGE2 synthesis and induces necrosis in alveolar macrophages. *BMC Microbiol. BioMed Central Ltd*; 2014;14(1):128.

122. Danilchanka O, Sun J, Pavlenok M, Maueröder C, Speer A, Siroy A, et al. An outer membrane channel protein of *Mycobacterium tuberculosis* with exotoxin activity. *Proc. Natl. Acad. Sci. U.S.A.* 2014 Apr. 21.
123. Danelishvili L, Everman JL, McNamara MJ, Bermudez LE. Inhibition of the Plasma-Membrane-Associated Serine Protease Cathepsin G by *Mycobacterium tuberculosis* Rv3364c Suppresses Caspase-1 and Pyroptosis in Macrophages. *Frontiers in Microbiology.* 2011;2:281.
124. Velmurugan K, Chen B, Miller JL, Azogue S, Gurses S, Hsu T, et al. *Mycobacterium tuberculosis* nuoG is a virulence gene that inhibits apoptosis of infected host cells. *PLoS Pathog.* 2007 Jul.;3(7):e110.
125. Riccardi C, Nicoletti I. Analysis of apoptosis by propidium iodide staining and flow cytometry. *Nat Protoc.* 2006 Nov.;1(3):1458–1461.
126. Sohn H, Kim J-S, Shin SJ, Kim K, Won C-J, Kim WS, et al. Targeting of *Mycobacterium tuberculosis* heparin-binding hemagglutinin to mitochondria in macrophages. *PLoS Pathog.* 2011 Dec.;7(12):e1002435.
127. Miller JL, Velmurugan K, Cowan MJ, Briken V. The type I NADH dehydrogenase of *Mycobacterium tuberculosis* counters phagosomal NOX2 activity to inhibit TNF- $\alpha$ -mediated host cell apoptosis. *PLoS Pathog.* 2010 Apr.;6(4):e1000864.
128. Degterev A, Hitomi J, Gemscheid M, Ch'en IL, Korkina O, Teng X, et al. Identification of RIP1 kinase as a specific cellular target of necrostatins. *Nat. Chem. Biol.* 2008 May;4(5):313–321.
129. He S, Liang Y, Shao F, Wang X. Toll-like receptors activate programmed necrosis in macrophages through a receptor-interacting kinase-3-mediated pathway. *Proc. Natl. Acad. Sci. U.S.A.* 2011 Dec. 13;108(50):20054–20059.
130. Alano CC, Ying W, Swanson RA. Poly(ADP-ribose) polymerase-1-mediated cell death in astrocytes requires NAD<sup>+</sup> depletion and mitochondrial permeability transition. *J. Biol. Chem.* 2004 Apr. 30;279(18):18895–18902.
131. Suzuki T, Franchi L, Toma C, Ashida H, Ogawa M, Yoshikawa Y, et al. Differential Regulation of Caspase-1 Activation, Pyroptosis, and Autophagy via Ipaf and ASC in *Shigella*-Infected Macrophages. *PLoS Pathog. Public Library of Science*; 2007 Aug. 10;3(8):e111.
132. Di Paolo NC, Doronin K, Baldwin LK, Papayannopoulou T, Shayakhmetov DM. The Transcription Factor IRF3 Triggers “Defensive Suicide” Necrosis in Response to Viral and Bacterial Pathogens. *Cell Reports.* 2013 Jun.;3(6):1840–1846.
133. Schriener SE, Linford NJ, Martin GM, Treuting P, Ogburn CE, Emond M, et al. Extension of murine life span by overexpression of catalase targeted to mitochondria. *Science.* 2005 Jun. 24;308(5730):1909–1911.

134. Vega-Manriquez X, Lopez-Vidal Y, Moran J, Adams LG, Gutierrez-Pabello JA. Apoptosis-Inducing Factor Participation in Bovine Macrophage Mycobacterium bovis-Induced Caspase-Independent Cell Death. *Infect. Immun.* 2007 Feb. 21;75(3):1223–1228.
135. Carneiro LAM, Travassos LH, Soares F, Tattoli I, Magalhaes JG, Bozza MT, et al. Shigella Induces Mitochondrial Dysfunction and Cell Death in Nonmyeloid Cells. *Cell Host & Microbe.* Elsevier Ltd; 2009 Feb. 19;5(2):123–136.
136. Crowle A, Douvas G, May M. Chlorpromazine: a drug potentially useful for treating mycobacterial infections. *Chemotherapy.* Karger Publishers; 1992;38(6):410–419.
137. Dheenadhayalan V, Delogu G, Brennan MJ. Expression of the PE\_PGRS 33 protein in Mycobacterium smegmatis triggers necrosis in macrophages and enhanced mycobacterial survival. *Microbes and Infection.* 2006 Jan.;8(1):262–272.
138. Moreno-Altamirano MMB, Paredes-González IS, Espitia C, Santiago-Maldonado M, Hernández-Pando R, Sánchez-García FJ. Bioinformatic identification of Mycobacterium tuberculosis proteins likely to target host cell mitochondria: virulence factors? *Microb Inform Exp.* 2012;2(1):9.
139. Huang J, Brumell JH. Bacteria-autophagy interplay: a battle for survival. *Nat. Rev. Microbiol.* 2014 Feb.;12(2):101–114.
140. Codogno P, Mehrpour M, Proikas-Cezanne T. Canonical and non-canonical autophagy: variations on a common theme of self-eating? *Nat. Rev. Mol. Cell Biol.* 2012 Jan.;13(1):7–12.
141. He C, Klionsky DJ. Regulation mechanisms and signaling pathways of autophagy. *Annual review of genetics.* NIH Public Access; 2009;43:67.
142. Boyle KB, Randow F. The role of “eat-me” signals and autophagy cargo receptors in innate immunity. *Curr. Opin. Microbiol.* Elsevier Ltd; 2013 Jun. 1;16(3):339–348.
143. Shi C-S, Shenderov K, Huang N-N, Kabat J, Abu-Asab M, Fitzgerald KA, et al. Activation of autophagy by inflammatory signals limits IL-1 $\beta$  production by targeting ubiquitinated inflammasomes for destruction. *Nat. Immunol.* 2012 Mar.;13(3):255–263.
144. Shen H-M, Codogno P. Autophagic cell death: Loch Ness monster or endangered species? *Autophagy.* 2011 May 1;7(5):457–465.
145. Bradfute SB, Castillo EF, Arko-Mensah J, Chauhan S, Jiang S, Mandell M, et al. Autophagy as an immune effector against tuberculosis. *Curr. Opin. Microbiol.* 2013 Jun.;16(3):355–365.

146. Kang R, Zeh HJ, Lotze MT, Tang D. The Beclin 1 network regulates autophagy and apoptosis. *Cell Death & Differentiation*. 2011 Feb. 11;18(4):571–580.
147. Mizushima N, Yoshimori T. How to interpret LC3 immunoblotting. *Autophagy*. 2007 Oct.;3(6):542–545.
148. Mizushima N, Yoshimori T, Levine B. ScienceDirect.com - Cell - Methods in Mammalian Autophagy Research. *Cell*. 2010.
149. Mostowy S. Autophagy and bacterial clearance: a not so clear picture. *Cell Microbiol*. 2012 Dec. 2;15(3):395–402.
150. Watson RO, Manzanillo PS, Cox JS. Extracellular *M. tuberculosis* DNA Targets Bacteria for Autophagy by Activating the Host DNA-Sensing Pathway. *Cell*. 2012 Aug. 17;150(4):803–815.
151. Manzanillo PS, Ayres JS, Watson RO, Collins AC, Souza G, Rae CS, et al. The ubiquitin ligase parkin mediates resistance to intracellular pathogens. *Nature*. 2013 Sep. 26;501(7468):512–516.
152. Esclatine A, Chaumorcet M, Codogno P. Macroautophagy signaling and regulation. *Curr. Top. Microbiol. Immunol*. 2009;335:33–70.
153. Yang J, Carra S, Zhu W-G, Kampinga HH. The Regulation of the Autophagic Network and Its Implications for Human Disease. *Int. J. Biol. Sci*. 9(10):1121–1133.
154. Wei Y, Sinha S, Levine B. Dual role of JNK1-mediated phosphorylation of Bcl-2 in autophagy and apoptosis regulation. *Autophagy*. 2008 Oct.;4(7):949–951.
155. Pietrocola F, Izzo V, Niso-Santano M, Vacchelli E, Galluzzi L, Maiuri MC, et al. Regulation of autophagy by stress-responsive transcription factors. *Seminars in Cancer Biology*. Elsevier Ltd; 2013 Oct. 1;23(5):310–322.
156. Seok S, Fu T, Choi S-E, Li Y, Zhu R, Kumar S, et al. Transcriptional regulation of autophagy by an FXR-CREB axis. *Nature*. 2014 Dec. 4;516(7529):108–111.
157. Chauhan S, Goodwin JG, Chauhan S, Manyam G, Wang J, Kamat AM, et al. ZKSCAN3 Is a Master Transcriptional Repressor of Autophagy. *Mol. Cell*. Elsevier Inc.; 2013 Apr. 11;50(1):16–28.
158. Dutta RK, Kathania M, Raje M, Majumdar S. IL-6 inhibits IFN- $\gamma$  induced autophagy in *Mycobacterium tuberculosis* H37Rv infected macrophages. *Int. J. Biochem. Cell Biol*. 2012 Jun.;44(6):942–954.
159. Harris J, De Haro SA, Master SS, Keane J, Roberts EA, Delgado M, et al. T helper 2 cytokines inhibit autophagic control of intracellular *Mycobacterium tuberculosis*. *Immunity*. 2007 Sep.;27(3):505–517.

160. Yuk J-M, Shin D-M, Lee H-M, Yang C-S, Jin HS, Kim K-K, et al. Vitamin D3 induces autophagy in human monocytes/macrophages via cathelicidin. *Cell Host & Microbe*. Elsevier; 2009;6(3):231–243.
161. Gutierrez MG, Master SS, Singh SB, Taylor GA, Colombo MI, Deretic V. Autophagy is a defense mechanism inhibiting BCG and Mycobacterium tuberculosis survival in infected macrophages. *Cell*. 2004 Dec. 17;119(6):753–766.
162. Singh SB, Davis AS, Taylor GA, Deretic V. Human IRGM induces autophagy to eliminate intracellular mycobacteria. *Science*. 2006 Sep. 8;313(5792):1438–1441.
163. Matsuzawa T, Kim B-H, Shenoy AR, Kamitani S, Miyake M, Macmicking JD. IFN- $\gamma$  Elicits Macrophage Autophagy via the p38 MAPK Signaling Pathway. *J. Immunol*. 2012 Jul. 15;189(2):813–818.
164. Deretic MPJA-MMPERSMMAMNDWOSJSBBJ-ABTHTJV, Arko-Mensah J, Ponpuak M, Roberts E, Master S, Mandell MA, et al. TBK-1 Promotes Autophagy-Mediated Antimicrobial Defense by Controlling Autophagosome Maturation. *Immunity*. Elsevier Inc.; 2012 Aug. 24;37(2):223–234.
165. Biswas D, Qureshi OS, Lee W-Y, Croudace JE, Mura M, Lammas DA. ATP-induced autophagy is associated with rapid killing of intracellular mycobacteria within human monocytes/macrophages. *BMC Immunol*. 2008;9:35.
166. Xu Y, Jagannath C, Liu X-D, Sharafkhaneh A, Kolodziejaska KE, Eissa NT. Toll-like receptor 4 is a sensor for autophagy associated with innate immunity. *Immunity*. 2007 Jul.;27(1):135–144.
167. Zullo AJ, Lee S. Mycobacterial induction of autophagy varies by species and occurs independently of mammalian target of rapamycin inhibition. *Journal of Biological Chemistry*. 2012 Apr. 13;287(16):12668–12678.
168. Seto S, Tsujimura K, Horii T, Koide Y. Autophagy Adaptor Protein p62/SQSTM1 and Autophagy-Related Gene Atg5 Mediate Autophagosome Formation in Response to Mycobacterium tuberculosis Infection in Dendritic Cells. *PLoS ONE*. Public Library of Science; 2013 Dec. 23;8(12):e86017.
169. Kim J-J, Lee H-M, Shin D-M, Kim W, Yuk J-M, Jin HS, et al. Host Cell Autophagy Activated by Antibiotics Is Required for Their Effective Antimycobacterial Drug Action. *Cell Host & Microbe*. Elsevier Inc.; 2012 May 17;11(5):457–468.
170. Alonso S, Pethe K, Russell DG, Purdy GE. Lysosomal killing of Mycobacterium mediated by ubiquitin-derived peptides is enhanced by autophagy. *Proc. Natl. Acad. Sci. U.S.A.* 2007 Apr. 3;104(14):6031–6036.
171. Sonawane A, Santos JC, Mishra BB, Jena P, Progida C, Sorensen OE, et al. Cathelicidin is involved in the intracellular killing of mycobacteria in macrophages.

Cell Microbiol. 2011 Aug. 11;13(10):1601–1617.

172. Castillo EF, Dekonenko A, Arko-Mensah J, Mandell MA, Dupont N, Jiang S, et al. Autophagy protects against active tuberculosis by suppressing bacterial burden and inflammation. *Proc. Natl. Acad. Sci. U.S.A.* 2012 Nov. 13;109(46):E3168–76.
173. Jagannath C, Lindsey DR, Dhandayuthapani S, Xu Y, Hunter RL, Eissa NT. Autophagy enhances the efficacy of BCG vaccine by increasing peptide presentation in mouse dendritic cells. *Nat. Med.* 2009 Mar.;15(3):267–276.
174. Manzanillo PS, Shiloh MU, Portnoy DA, Cox JS. Mycobacterium tuberculosis activates the DNA-dependent cytosolic surveillance pathway within macrophages. *Cell Host & Microbe.* 2012 May 17;11(5):469–480.
175. Shin D-M, Yuk J-M, Lee H-M, Lee S-H, Son JW, Harding CV, et al. Mycobacterial lipoprotein activates autophagy via TLR2/1/CD14 and a functional vitamin D receptor signalling. *Cell Microbiol.* 2010 Jun. 18;12(11):1648–1665.
176. Kim KH, An DR, Song J, Yoon JY, Kim HS, Yoon HJ, et al. Mycobacterium tuberculosis Eis protein initiates suppression of host immune responses by acetylation of DUSP16/MKP-7.
177. Shin D-M, Jeon B-Y, Lee H-M, Jin HS, Yuk J-M, Song C-H, et al. Mycobacterium tuberculosis eis regulates autophagy, inflammation, and cell death through redox-dependent signaling. *PLoS Pathog.* 2010;6(12):e1001230.
178. Shui W, Petzold CJ, Redding A, Liu J, Pitcher A, Sheu L, et al. Organelle membrane proteomics reveals differential influence of mycobacterial lipoglycans on macrophage phagosome maturation and autophagosome accumulation. *J. Proteome Res.* 2011 Jan. 7;10(1):339–348.
179. Romagnoli A, Etna MP, Giacomini E, Pardini M, Remoli ME, Corazzari M, et al. ESX-1 dependent impairment of autophagic flux by Mycobacterium tuberculosis in human dendritic cells. *Autophagy.* 2012 Sep. 1;8(9):17–16.
180. Wang J, Yang K, Zhou L, Minhaowu, Wu Y, Zhu M, et al. MicroRNA-155 promotes autophagy to eliminate intracellular mycobacteria by targeting Rheb. *PLoS Pathog.* 2013;9(10):e1003697.
181. van der Vaart M, Korbee CJ, Lamers GEM, Tengeler AC, Hosseini R, Haks MC, et al. The DNA Damage-Regulated Autophagy Modulator DRAM1 Links Mycobacterial Recognition via TLR-MYD88 to Autophagic Defense. *CHOM.* Elsevier; 2014 Jun. 11;15(6):753–767.
182. Seto S, Tsujimura K, Koide Y. Coronin-1a inhibits autophagosome formation around Mycobacterium tuberculosis-containing phagosomes and assists mycobacterial survival in macrophages. *Cell Microbiol.* 2012 May;14(5):710–727.

183. Singh V, Jamwal S, Jain R, Verma P, Gokhale R, Rao KVS. Mycobacterium tuberculosis-Driven Targeted Recalibration of Macrophage Lipid Homeostasis Promotes the Foamy Phenotype. *Cell Host & Microbe*. 2012 Nov.;12(5):669–681.
184. Eng KE, Panas MD, Hedestam GBK, McInerney GM. A novel quantitative flow cytometry-based assay for autophagy. *Autophagy*. 2010 Jul. 1;6(5).
185. Shintani T, Klionsky DJ. Cargo proteins facilitate the formation of transport vesicles in the cytoplasm to vacuole targeting pathway. *J. Biol. Chem*. 2004 Jul. 16;279(29):29889–29894.
186. Dahl JL, Wei J, Moulder JW, Laal S, Friedman RL. Subcellular localization of the intracellular survival-enhancing Eis protein of Mycobacterium tuberculosis. *Infect. Immun*. 2001 Jul.;69(7):4295–4302.
187. Samuel LP, Song C-H, Wei J, Roberts EA, Dahl JL, Barry CE, et al. Expression, production and release of the Eis protein by Mycobacterium tuberculosis during infection of macrophages and its effect on cytokine secretion. *Microbiology (Reading, Engl.)*. 2007 Feb.;153(Pt 2):529–540.
188. Shrivastava S, Bhanja Chowdhury J, Steele R, Ray R, Ray RB. Hepatitis C virus upregulates Beclin1 for induction of autophagy and activates mTOR signaling. *J. Virol*. 2012 Aug.;86(16):8705–8712.
189. Beswick RW, Ambrose HE, Wagner SD. Nocodazole, a microtubule depolymerising agent, induces apoptosis of chronic lymphocytic leukaemia cells associated with changes in Bcl-2 phosphorylation and expression. *Leukemia research*. Elsevier; 2006;30(4):427–436.
190. Wang RC, Wei Y, An Z, Zou Z, Xiao G, Bhagat G, et al. Akt-mediated regulation of autophagy and tumorigenesis through Beclin 1 phosphorylation. *Science*. 2012 Nov. 16;338(6109):956–959.
191. Jo H, Mondal S, Tan D, Nagata E, Takizawa S, Sharma AK, et al. Small molecule-induced cytosolic activation of protein kinase Akt rescues ischemia-elicited neuronal death. *Proc. Natl. Acad. Sci. U.S.A.* 2012 Jun. 26;109(26):10581–10586.
192. Maiuri MC, Zalckvar E, Kimchi A, Kroemer G. Self-eating and self-killing: crosstalk between autophagy and apoptosis. *Nat. Rev. Mol. Cell Biol*. 2007 Sep.;8(9):741–752.
193. Owen KA, Meyer CB, Bouton AH, Casanova JE. Activation of focal adhesion kinase by Salmonella suppresses autophagy via an Akt/mTOR signaling pathway and promotes bacterial survival in macrophages. *PLoS Pathog*. 2014 Jun.;10(6):e1004159.
194. Muniz-Feliciano L, Van Grol J, Portillo J-AC, Liew L, Liu B, Carlin CR, et al. Toxoplasma gondii-Induced Activation of EGFR Prevents Autophagy Protein-

- Mediated Killing of the Parasite. *PLoS Pathog.* Public Library of Science; 2013 Dec. 19;9(12):e1003809.
195. Wei Y, Pattingre S, Sinha S, Bassik M, Levine B. JNK1-mediated phosphorylation of Bcl-2 regulates starvation-induced autophagy. *Mol. Cell.* 2008 Jun. 20;30(6):678–688.
  196. Siddiqui MA, Malathi K. RNase L induces autophagy via c-Jun N-terminal kinase and double-stranded RNA-dependent protein kinase signaling pathways. *Journal of Biological Chemistry.* 2012 Dec. 21;287(52):43651–43664.
  197. Kamata H, Honda S-I, Maeda S, Chang L, Hirata H, Karin M. Reactive Oxygen Species Promote TNF $\alpha$ -Induced Death and Sustained JNK Activation by Inhibiting MAP Kinase Phosphatases. *Cell.* 2005 Mar.;120(5):649–661.
  198. Scherz-Shouval R, Shvets E, Fass E, Shorer H, Gil L, Elazar Z. Reactive oxygen species are essential for autophagy and specifically regulate the activity of Atg4. *EMBO J.* 2007 Mar. 8;26(7):1749–1760.
  199. Kongara S, Karantza V. The interplay between autophagy and ROS in tumorigenesis. *Front. Oncol. Frontiers;* 2012;2.
  200. Richetta C, Grégoire IP, Verlhac P, Azocar O, Baguet J, Flacher M, et al. Sustained autophagy contributes to measles virus infectivity. *PLoS Pathog.* 2013;9(9):e1003599.
  201. Wang Y, Kim N, Li X, Greer P. Calpain activation is not required for AIF translocation in PARP-1-dependent cell death (parthanatos) - Wang - 2009 - *Journal of Neurochemistry - Wiley Online Library.* Journal of .... 2009.
  202. Behr MA, Schurr E. Cell biology: A table for two. *Nature.* 2013 Sep. 4;501(7468):498–499.
  203. Kleinnijenhuis J, Oosting M, Plantinga TS, van der Meer JWM, Joosten LAB, Crevel RV, et al. Autophagy modulates the Mycobacterium tuberculosis-induced cytokine response. *Immunology.* 2011 Nov.;134(3):341–348.
  204. Foreman-Wykert AK, Miller JF. Hypervirulence and pathogen fitness. *Trends Microbiol.* 2003 Mar.;11(3):105–108.
  205. Mouslim C, Hilbert F, Huang H, Groisman EA. Conflicting needs for a Salmonella hypervirulence gene in host and non-host environments. *Molecular Microbiology.* 2002 Aug.;45(4):1019–1027.
  206. Parwati I, van Crevel R, van Soolingen D. Possible underlying mechanisms for successful emergence of the Mycobacterium tuberculosis Beijing genotype strains. *The Lancet Infectious Diseases.* Elsevier; 2010 Feb. 1;10(2):103–111.

207. Manca C, Tsenova L, Bergtold A, Freeman S, Tovey M, Musser JM, et al. Virulence of a Mycobacterium tuberculosis clinical isolate in mice is determined by failure to induce Th1 type immunity and is associated with induction of IFN-alpha/beta. *Proc. Natl. Acad. Sci. U.S.A.* 2001 May 8;98(10):5752–5757.
208. Manca C, Tsenova L, Freeman S, Barczak AK, Tovey M, Murray PJ, et al. Hypervirulent M. tuberculosis W/Beijing strains upregulate type I IFNs and increase expression of negative regulators of the Jak-Stat pathway. *J. Interferon Cytokine Res.* 2005 Nov.;25(11):694–701.
209. Reed MB, Domenech P, Manca C, Su H, Barczak AK, Kreiswirth BN, et al. A glycolipid of hypervirulent tuberculosis strains that inhibits the innate immune response. *Nature.* 2004 Sep. 2;431(7004):84–87.
210. Reed MB, Gagneux S, DeRiemer K, Small PM, Barry CE. The W-Beijing lineage of Mycobacterium tuberculosis overproduces triglycerides and has the DosR dormancy regulon constitutively upregulated. *J. Bacteriol.* 2007 Apr.;189(7):2583–2589.
211. Amaral EP, Ribeiro SCM, Lanes VR, Almeida FM, de Andrade MRM, Bomfim CCB, et al. Pulmonary Infection with Hypervirulent Mycobacteria Reveals a Crucial Role for the P2X7 Receptor in Aggressive Forms of Tuberculosis. *PLoS Pathog.* 2014 Jul.;10(7):e1004188.
212. Lima P, Sidders B, Morici L, Reader R, Senaratne R, Casali N, et al. Enhanced mortality despite control of lung infection in mice aerogenically infected with a Mycobacterium tuberculosis mce1 operon mutant. *Microbes Infect.* 2007 Sep.;9(11):1285–1290.
213. Shimono N, Morici L, Casali N, Cantrell S, Sidders B, Ehrt S, et al. Hypervirulent mutant of Mycobacterium tuberculosis resulting from disruption of the mce1 operon. *Proc. Natl. Acad. Sci. U.S.A.* 2003 Dec. 23;100(26):15918–15923.
214. Cantrell SA, Leavell MD, Marjanovic O, Iavarone AT, Leary JA, Riley LW. Free mycolic acid accumulation in the cell wall of the mce1 operon mutant strain of Mycobacterium tuberculosis. *J. Microbiol.* 2013 Oct.;51(5):619–626.
215. Casali N, White AM, Riley LW. Regulation of the Mycobacterium tuberculosis mce1 operon. *J. Bacteriol.* 2006 Jan.;188(2):441–449.
216. Uchida Y, Casali N, White A, Morici L, Kendall LV, Riley LW. Accelerated immunopathological response of mice infected with Mycobacterium tuberculosis disrupted in the mce1 operon negative transcriptional regulator. *Cell Microbiol.* 2007 May;9(5):1275–1283.
217. Casali N. Hypervirulent Mycobacterium tuberculosis. *Mycobacterium genomics and molecular biology.* 2009;:19–34.

218. Hu Y, Movahedzadeh F, Stoker NG, Coates ARM. Deletion of the Mycobacterium tuberculosis alpha-crystallin-like hspX gene causes increased bacterial growth in vivo. *Infect. Immun.* 2006 Feb.;74(2):861–868.
219. Bokum ten AMC, Movahedzadeh F, Frita R, Bancroft GJ, Stoker NG. The case for hypervirulence through gene deletion in Mycobacterium tuberculosis. *Trends Microbiol.* 2008 Sep.;16(9):436–441.
220. Papavinasasundaram KG, Chan B, Chung J-H, Colston MJ, Davis EO, Av-Gay Y. Deletion of the Mycobacterium tuberculosis pknH gene confers a higher bacillary load during the chronic phase of infection in BALB/c mice. *J. Bacteriol.* 2005 Aug.;187(16):5751–5760.
221. Kumar D, Palaniyandi K, Challu VK, Kumar P, Narayanan S. PknE, a serine/threonine protein kinase from Mycobacterium tuberculosis has a role in adaptive responses. *Arch. Microbiol.* 2013 Jan.;195(1):75–80.
222. Jayakumar D, Jacobs WR, Narayanan S. Protein kinase E of Mycobacterium tuberculosis has a role in the nitric oxide stress response and apoptosis in a human macrophage model of infection. *Cell Microbiol.* 2008 Feb.;10(2):365–374.
223. Gopaldaswamy R, Narayanan S, Chen B, Jacobs WR, Av-Gay Y. The serine/threonine protein kinase PknI controls the growth of Mycobacterium tuberculosis upon infection. *FEMS Microbiol. Lett.* 2009 Jun.;295(1):23–29.
224. Anna L Hampton. Progression of Ulcerative Dermatitis Lesions in C57BL/6Cr1 Mice and the Development of a Scoring System for Dermatitis Lesions. *Journal of the American Association for Laboratory Animal Science : JAALAS.* American Association for Laboratory Animal Science; 2012 Sep. 1;51(5):586.
225. Dorhoi A, Iannaccone M, Farinacci M, Faé KC, Schreiber J, Moura-Alves P, et al. MicroRNA-223 controls susceptibility to tuberculosis by regulating lung neutrophil recruitment. *J. Clin. Invest.* 2013 Oct. 1;123(11):4836–4848.
226. Mishra BB, Rathinam VAK, Martens GW, Martinot AJ, Kornfeld H, Fitzgerald KA, et al. Nitric oxide controls the immunopathology of tuberculosis by inhibiting NLRP3 inflammasome-dependent processing of IL-1 $\beta$ . *Nat. Immunol.* 2013 Jan.;14(1):52–60.
227. Taylor JL, Hattle JM, Dreitz SA, Troudt JM, Izzo LS, Basaraba RJ, et al. Role for Matrix Metalloproteinase 9 in Granuloma Formation during Pulmonary Mycobacterium tuberculosis Infection. *Infect. Immun.* 2006 Oct. 20;74(11):6135–6144.
228. Friedrich N, Hagedorn M, Soldati-Favre D, Soldati T. Prison break: pathogens' strategies to egress from host cells. *Microbiol. Mol. Biol. Rev.* 2012 Dec.;76(4):707–720.

229. Fredlund J, Enninga J. Cytoplasmic access by intracellular bacterial pathogens. *Trends Microbiol.* 2014 Mar.;22(3):128–137.
230. Molmeret M, Jones S, Santic M, Habyarimana F, Esteban MTG, Kwaik YA. Temporal and spatial trigger of post-exponential virulence-associated regulatory cascades by *Legionella pneumophila* after bacterial escape into the host cell cytosol. *Environ. Microbiol.* 2010 Mar.;12(3):704–715.
231. Tattoli I, Sorbara MT, Vuckovic D, Ling A, Soares F, Carneiro LAM, et al. Amino acid starvation induced by invasive bacterial pathogens triggers an innate host defense program. *Cell Host & Microbe.* 2012 Jun. 14;11(6):563–575.
232. Knodler LA, Nair V, Steele-Mortimer O. Quantitative assessment of cytosolic *Salmonella* in epithelial cells. *PLoS ONE.* 2014;9(1):e84681.
233. Collins CA, De Mazière A, van Dijk S, Carlsson F, Klumperman J, Brown EJ. Atg5-independent sequestration of ubiquitinated mycobacteria. *PLoS Pathog.* 2009 May;5(5):e1000430.
234. Higa N, Toma C, Koizumi Y, Nakasone N, Nohara T, Masumoto J, et al. *Vibrio parahaemolyticus* effector proteins suppress inflammasome activation by interfering with host autophagy signaling. *PLoS Pathog.* 2013 Jan.;9(1):e1003142.
235. Xu G, Shi Y. Apoptosis signaling pathways and lymphocyte homeostasis. *Cell Res.* Nature Publishing Group; 2007 Sep.;17(9):759–771.